

STATUS OF THESIS

Title of thesis

MODELLING AND CONTROL OF MULTI-FINGERED
ROBOT HAND USING INTELLIGENT TECHNIQUES

I WAN FAIZURA BINTI WAN TARMIZI

hereby allow my thesis to be placed at the Information Resource Center (IRC) of Universiti Teknologi PETRONAS (UTP) with the following conditions:

1. The thesis becomes the property of UTP.
2. The IRC of UTP may make copies of the thesis for academic purposes only.
3. This thesis is classified as

Confidential

Non-confidential

If this thesis is confidential, please state the reason:

The contents of the thesis will remain confidential for _____ years.

Remarks on disclosure:

Endorsed by

Signature of Author

Signature of Supervisor

Permanent address:
No 7186, Jalan Tati,
Kg, Panchor, Teluk Kalong,
24000 Kemaman,
Terengganu Darul Iman.

Date: _____

Date: _____

UNIVERSITI TEKNOLOGI PETRONAS

“MODELLING AND CONTROL OF MULTI-FINGERED ROBOT HAND USING
INTELLIGENT TECHNIQUES”

by

WAN FAIZURA BINTI WAN TARMIZI

The undersigned certify that they have read, and recommend to The Postgraduate Studies Programme for acceptance this thesis for the fulfillment of the requirements for the degree of Master of Science in Electrical and Electronics Engineering.

Signature: _____

Main Supervisor: Assoc. Prof. Dr. Irraivan Elamvazuthi

Signature: _____

Head of Department: Assoc. Prof. Dr. Rosdiazli B Ibrahim

Date: _____

UNIVERSITI TEKNOLOGI PETRONAS
MODELLING AND CONTROL OF MULTI-FINGERED ROBOT HAND USING
INTELLIGENT TECHNIQUES

by

WAN FAIZURA BINTI WAN TARMIZI

A Thesis

Submitted to the Scholl of Graduate Studies

as a Requirement for the Degree of

MASTER OF SCIENCE

ELECTRICAL & ELECTRONIC ENGINEERING

UNIVERSITI TEKNOLOGI PETRONAS

BANDAR SERI ISKANDAR

PERAK

March 2014

DECLARATION OF THESIS

Title of thesis

MODELLING AND CONTROL OF MULTI-FINGERED
ROBOT HAND USING INTELLIGENT TECHNIQUES

I WAN FAIZURA BINTI WAN TARMIZI

hereby declare that the thesis is based on my original work except for quotations and citations which have been duly acknowledged. I also declare that it has not been previously or concurrently submitted for any other degree at UTP or other institutions.

Witnessed by

Signature of Author

Signature of Supervisor

Permanent address:
No 7186, Jalan Tati,
Kg. Panchor, Teluk Kalong,
24000 Kemaman,
Terengganu Darul Iman.

Date: _____

Date: _____

*Special dedication to my beloved husband, father, mother,
brother, friends, sisters and teachers who taught me the
meaning of success.*

ACKNOWLEDGEMENT

First of all, I would like to thank ALLAH, the Almighty God for his blessings and innumerable gifts that have been granted on me to complete this work.

I would like to thanks to my supervisor Assoc. Prof. Dr. Irraivan Elamvazuthi and Assoc. Prof. Dr. Mumtaj Begam on their support, encouragement and guidance given during my studies to complete this research.

I also would like to express my appreciation and gratitude to my beloved husband for a lot of help, support and encouragement to me and also, didn't forget to the friends which are Razif Rashid, Wan Amir Faiz, Muhd Azmi Adly, Lindasalwa, Adnan Baloch and others for a lot of help and give constructive ideas.

Also, Not to forget to thanks to the UTP that has been providing the best learning facilities for students to do a research while also providing allowances to students through the GA scheme to support themselves while in the UTP.

Wan Faizura Binti Wan Tarmizi

March 2014

ABSTRACT

Research and development of robust multi-fingered robot hand (MFRH) have been going on for more than three decades. Yet few can be found in an industrial application. The difficulties stem from many factors, one of which is that the lack of general and effective control techniques for the manipulation of robot hand.

In this research, a MFRH with five fingers has been proposed with intelligent control algorithms. Initially, mathematical modeling for the proposed MFRH has been derived to find the Forward Kinematic, Inverse Kinematic, Jacobian, Dynamics and the plant model. Thereafter, simulation of the MFRH using PID controller, Fuzzy Logic Controller, Fuzzy-PID controller and PID-PSO controller has been carried out to gauge the system performance based parameters such rise time, settling time and percent overshoot.

Proportional-Integral-Derivative (PID) controllers are the predominant types of feedback control. PID controller is widely used in industry due to their simplicity and easy to tuning. For controller tuning, the PID parameters can be tuned by any conventional method in order to assure a good reference signal to the closed loop system.

Also, it was found that Fuzzy Logic Controller (FLC) provides better tuning of the system response compared with the conventional PID controller. Fuzzy controllers are successful applied to non-linear system because of their knowledge based nonlinear structural characteristics. Where the combination of the fuzzy and PID are much better than stand-alone PID and Fuzzy controllers.

In addition, the research findings from the Particle Swarm Optimization (PSO) technique facilitate the researcher to obtain better outcomes. Particle swarm optimization or PSO is a group of individuals known as particles or intelligent agents that search for space flight. The applicability of various methods in this study has produced to find the better system response in term of step response, settling time and steady state error.

ABSTRAK

Penyelidikan dan pembangunan Pelbagai Tangan Robot atau MFRH telah berlangsung selama lebih dari tiga dekad. Namun tidak boleh ditemui dalam aplikasi industri. Kesukarannya yang berpunca daripada banyak factor, salah satunya adalah kurangnya kawalan algoritma umum dan efisien untuk manipulasi tangan robot.

Dalam kajian ini, MFRH dicadangkan mempunyai lima jari dengan menggunakan algoritma kawalan pintar. Pada awalnya, pemodelan matematik bertujuan MFRH untuk mendapatkan Forward Kinematic, Inverse Kinematic, Jacobian, Dynamic dan Plant Model. Selepas itu, simulasi MFRH menggunakan Kawalan PID, Fuzzy Logic Controller (FLC), Fuzzy-PID dan PID-PSO untuk mengukur prestasi sistem berdasarkan parameter yang terdiri daripada masa naik, masa selesai, dan lebihan peratus.

Kawalan PID merupakan sejenis dominan kawalan maklum balas. PID digunakan secara meluas dalam industri kerana kesederhanaan dan mudah untuk penalaan (tuning), Untuk penalaan kawalan, parameter PID yang dicari daripada kaedah konvensional adalah untuk memastikan isyarat rujukan yang baik dengan sistem loop tertutup yang diperolehi dengan menapis isyarat tepat langkah set-point.

Begitu juga, Pengawal Logik Kabur (FLC) menghasilkan sistem respons penalaan (tuning) yang baik berbanding dengan kawalan PID konvensional. Pengawal kabur berjaya digunakan untuk sistem non-linear kerana pengetahuan mereka berdasarkan ciri-ciri struktur linear. Pengawal hybrid adalah gabungan PID dan Fuzzy di mana ia telah memperoleh hasil yang lebih baik berbanding dengan kawalan sendiri daripada PID dan Fuzzy.

Di samping itu, penemuan kajian daripada teknik Particle Swarm Optimization (PSO) memudahkan penyelidikan untuk mendapatkan keputusan yang lebih baik. Zarah sekumpulan pengoptimuman atau PSO adalah sekumpulan individu yang dikenali sebagai zarah atau agen pintar yang mencari penerbangan angkasa. Pelbagai kaedah boleh digunakan dalam kajian ini untuk menghasikan system respon yang baik.

In compliance with the terms of the Copyright Act 1987 and the IP Policy of the university, the copyright of this thesis has been reassigned by the author to the legal entity of the university,

Institute of Technology PETRONAS Sdn Bhd.

Due acknowledgement shall always be made of the use of any material contained in, or derived from, this thesis.

© WAN FAIZURA BINTI WAN TARMZI, 2014

Institute of Technology PETRONAS Sdn Bhd

All rights reserved.

TABLE OF CONTENTS

STATUS OF THESIS	i
APPROVAL OF THESIS	ii
TITLE PAGE	iii
DECLARATION OF THESIS	iv
ACKNOWLEDGEMENT	vi
ABSTRACT.....	vii
ABSTRAK.....	viii
TABLE OF CONTENTS.....	x
LIST OF FIGURES	xii
LIST OF TABLES	xv
LIST OF ABBREVIATIONS.....	xvi
NOMENCLATURE	xvii
CHAPTER 1 INTRODUCTION	1
1.1 Introduction	1
1.2 Problem Statement	3
1.3 Research Objectives	3
1.4 Research Scope	4
1.5 Outline of Thesis	4
CHAPTER 2 LITERATURE REVIEW	5
2.1 Overview of Multi-Fingered Robot Hand.....	5
2.1.1 Mechanical Design	6
2.1.1.1 Motor Configuration	6
2.1.1.2 Pneumatic Configuration	7
2.1.1.3 Air muscle Configuration	8
2.1.1.4 Ultrasonic Motor & Elastic Elements Configuration.....	8
2.1.2 Sensing for MFRH	9
2.1.2.1 Touch Sensing.....	10
2.1.2.2 Tactile Sensing.....	10
2.1.2.3 Slip	11

2.1.3 Control Technique for MFRH	11
2.1.3.1 Conventional Controller.....	11
2.1.3.2 Modern Controller	12
2.2 Critical Analysis of Review on MFRH.....	15
2.3 Summary	17
CHAPTER 3 METHDOLOGY	19
3.1 Modeling of a MFRH.....	19
3.1.1 CAD MODEL OF MFRH	19
3.1.2 KINEMATIC AND DYNAMIC MODEL.....	22
3.2 Motor Level Control of MFRH.....	23
3.3 Position Control of MFRH.....	28
3.3.1 PID Controller	28
3.3.1.1 Ziegler Nichlos Method	29
3.3.2 Fuzzy Logic Controller.....	30
3.3.2.1 Two Memberships Function	31
3.3.2.2 Three Memberships Function	32
3.3.2.3 Five Membership Function	33
3.3.2.4 Seven Membership Function	34
3.3.3 Fuzzy-PID Controller	37
3.3.4 PSO-PID Controller.....	37
3.3.4.1 PSO Algorithm.....	38
3.3.4.2 PSO Parameter	41
3.4 Summary	43
CHAPTER 4 RESULTS & DISCUSSION	45
4.1 Results of Joint 1	45
4.2 Results of Joint 2.....	48
.....	48
4.3 Results of Joint 3.....	50
4.4 Discussion	53
4.5 Summary	55
CHAPTER 5 CONCLUSION.....	57

5.1 Critical Evaluation of Achievements	57
5.2 Discussion	59
5.3 Suggestions for Further Work.....	59
5.4 Concluding Remarks	60
REFERENCES	61
LIST OF PUBLICATIONS	69
APPENDIX A	
ADDITIONAL INFO OF MFRH.....	71
APPENDIX B	
CAD MODEL DESIGN	87
APPENDIX C	
MATHEMATICAL MODELING.....	91
APPENDIX D	
MATLAB CODES.....	107
APPENDIX E	
TECHNICAL SPECIFICATION OF DC SERVOMOTOR	111
APPENDIX F	
SYSTEM PERFORMANCE METRIC	116
APPENDIX G	
ADDITIONAL RESULTS	117
GLOSSARY	123

LIST OF FIGURES

Figure 2.1: Robonaut Hand [24]	7
Figure 2.2: Utah/MIT [25]	7
Figure 2.3: Shadow Hand [26].....	8
Figure 2.4: Ikuo Robot Hand [28].....	9
Figure 2.5: Grip the Ball	10
Figure 2.6: Hold the Book	10
Figure 2.7: Grasp the Rod.....	11
Figure 3.1: Structure of Human Hand [64].....	20
Figure 3.2: CAD Model	20
Figure 3.3: View of MFRH Design	21
Figure 3.4: Length Size of MFRH Design.....	22
Figure 3.5: MFRH Kinematic Model.....	22
Figure 3.6: Electrical Circuit of DC motor [66]	23
Figure 3.7: PID Controller	28
Figure 3.8: PID Controller Block Diagram.....	29
Figure 3.9: Time response of Ziegler Nichols method	29
Figure 3.10: Fuzzy Logic Controller Block Diagram.....	30
Figure 3.11: Input of Two Memberships Function.....	31
Figure 3.12: Output of Two Memberships Function	31
Figure 3.13: Input and Output of Three Memberships Function.....	32
Figure 3.14: Input of Five Memberships Function	33
Figure 3.15: Input and Output of Seven Memberships Function.....	35
Figure 3.16: Fuzzy-PID Controller Block Diagram	37
Figure 3.17: PSO-PID Controller Block Diagram.....	38
Figure 3.18: Flowchart of PSO [74]	40
Figure 4.1: Step Response of Joint 1 using PID	45
Figure 4.2: Step Response of Joint 1 using Fuzzy.....	46
Figure 4.3: Step Response of Joint 1 using Fuzzy-PID	46

Figure 4.4: Step Response of Joint 1 using PSO-PID.....	46
Figure 4.5: Step Response of Joint 1 using PSO-PID, Fuzzy-PID, Fuzzy and PID	47
Figure 4.6: Step Response of Joint 2 using PID	48
Figure 4.7: Step Response of Joint 2 using Fuzzy	48
Figure 4.8: Step Response of Joint 2 using Fuzzy-PID	49
Figure 4.9: Step Response of Joint 2 using PSO-PID.....	49
Figure 4.10: Step Response of Joint 2 using PSO-PID, Fuzzy-PID, Fuzzy and PID ..	49
Figure 4.11: Step Response of Joint 3 using PID	51
Figure 4.12: Step Response of Joint 3 using Fuzzy	51
Figure 4.13: Step Response of Joint 3 using Fuzzy-PID	51
Figure 4.14: Step Response of Joint 3 using PSO-PID.....	52
Figure 4.15: Step Response of Joint 3 using PSO-PID, Fuzzy-PID, Fuzzy and PID ..	52
Figure 4.16: Joint Control System of 1 Finger [65].....	54
Figure 4.17: Control System for MFRH.....	55

LIST OF TABLES

Table 2.1: Types of Control Techniques.....	15
Table 3.1: Multi-Fingered Robot Hand Model Parameter.....	21
Table 3.2: Parameters of DC servomotor	27
Table 3.3: Description of Equation Symbol	29
Table 3.4: Parameter of Ziegler Nichols Method	30
Table 3.5: Fuzzy Rules of Two Memberships Function.....	31
Table 3.6: Fuzzy Rules of Three Memberships Function.....	32
Table 3.7: Fuzzy Rules of Five Memberships Function	33
Table 3.8: Fuzzy Rules of Seven Memberships Function	35
Table 3.9: Parameter 1 of PSO	41
Table 3.10: Parameter 2 of PSO	41
Table 3.11: Parameter 3 of PSO	42
Table 3.12: Parameter 4 of PSO	42
Table 3.13: Parameter 5 of PSO	42
Table 4.1: Results of Joint 1 using PSO-PID, Fuzzy PID, Fuzzy and PID	47
Table 4.2: Results of Joint 2 using PID, Fuzzy, Fuzzy PID and PSO-PID	50
Table 4.3: Results of Joint 3 using PID, Fuzzy, Fuzzy PID and PSO-PID	52
Table 4.4: Comparative Analysis with Past Researcher	53

LIST OF ABBREVIATIONS

CAD	Computer Aided Design
CAN	Controller Area Network
C-C	Cohen-Coon
DC	Direct Current
DIP	Distal Interphalangeal
DLR	Deutsches Zentrum für Luft-undRaumfahrt
DOF	Degree of Freedom
EMF	Electromotive Force
ELU	Elumotion
EVA	Extravehicular Activity
GPL	General Public License
MCP	Metacapophalangeal
MFRH	Multi-Fingered Robot Hand
MIT	Massachusetts Institute of Technology
NASA	National Aeronautics and Space Administration
PIP	Proximal Interphalangeal
PID	Proportional Derivative Integral
PSO	Particle Swarm Optimization
PVDF	Polyvinylidene Fluoride
W-J-C	Wang-Juang-Chan
Z-N	Ziegler Nichols

NOMENCLATURE

K_i	Integral Gain
K_p	Proportional Gain
K_t	Torque constant
L	Electric inductance / Lagrangian
l_1	Link 1
l_2	Link 2
l_3	Link 3
M	Mass
m	meter
m_1	mass 1
m_2	mass 2
m_3	mass 3
mm	Millimeter
Nm^3	Newton Meter
R	Electric resistance
S	Sin
T_p	Peak Time
T_r	Rise Time
T_s	Settling Time
V	Velocity
$Y(t)$	Controller's Output

CHAPTER 1

INTRODUCTION

The term ‘Robot Hand’ is described as device that can mimic the movements of a human hand in operation. This thesis focuses on modeling and control of Multi-Fingered Robot Hand (MFRH).

This chapter begins some facts about general industrial robot. Then, it will be discussed about MFRH specifically. This is followed by a discussion on limitations of the current control methods of MFRH and the motivations behind the research described in this thesis. Later the objectives of this research are presented and end the chapter by giving the outline of the rest of the thesis.

1.1 Introduction

The word ‘robot’ was introduced in 1921 by the Czech playwright Karel Capek in his satirical play R. U. R. (Rossum’s Universal Robots), where he depicted robots as machines which resembled people but worked tirelessly [1]. However, the work leading up to today’s robots began only after World War where remotely controlled mechanical manipulators were developed. Since then, it has seen tremendous surge of activity in robotics, both in terms of research and technological maturation, from the simple pick and place and painting and welding robots, to more sophisticated assembly robots for inserting integrated circuit chips onto printed circuit boards, to mobile carts for parts handling and delivery. Increasingly, attempts have been made to devise multi-fingered hands for research use which are somewhere between teleoperation, prosthesis, and dexterous end-effectors. These hands truly represent our dual point of view in terms of jumping back and forth from an anthropomorphic point of view (mimicking our own hands) to the point of view of intelligent end-effectors (for endowing our robots with greater dexterity) [2].

A robot hand is described as device that can mimic the movements of a human hand in operation. The function of the robot hand is to grasp, move, and rotate an object. It is to help humans carry out a variety of tasks such as industrial operation for nuclear power plant, underwater and space station and in hospital, the robot hand assisted surgery in organ removal for transplant situations.

The robot hand can be divided into three categories; mechanical gripper, special purpose hand and universal hand [3]. A multi-fingered robot hand (MFRH) falls under the category of special purpose hand. The universal hand can be divided into two types; built in actuator and external actuator [3], [4]. The built-in actuator type of robot hand generates the motion of fingers by using motors installed inside the finger on the palm. For example, the dexterous hand for WENDY [4] and DLR II Hand [5]. This type of robot hand has advantage that the hand can be used with various types of robot arms because the robot hand has independent structure. On other hand, there are disadvantages. The most serious one is the limitation on size. Most of this type of robot hand has equal to or less than four fingers. Even, those with five fingers are not equal with human hand because they have less number of joints or DOF [6].

On the other hand, the external actuator type makes the structures of their fingers simple and light by using wire or belt driven mechanism. For example, Utah/ M.I.T Hand [7], Robonaut Hand [8], and the Shadow Hand [9] are classified as this type. The advantages of this type; first, when setting the high power actuator like air pressure actuator, the output force became very large and second, the structural limitation of the finger part becomes smaller, so the design of mechanism with large number of DOF become possible. For example, the shadow hand has 21 DOF with equal to human hand but the hand must be connected to external actuator mechanically, so it becomes difficult to be used with various robot arms. At the end, the movable area of hand is limited and the result in poor flexibility [6]. Generally, the technologies which are important to improve and develop dexterity of MFRH are the followings [3]:

- *Mechanical designs of hands*

Hands are designed for tasks and are composed of fingers, the number of which are larger than or equal to two. Each finger has several degrees of freedom. Each finger is

actuated by electrical motors, pneumatic or air muscles associated with the degrees of freedom.

- *Sensor technology*

Sensors are attached to hands in order to gather information about hand links and interacted environments.

- *Control techniques*

Control techniques are to determine the position and velocity of the joints of fingers for desired tasks.

1.2 Problem Statement

The literature review conducted during the course of this research has shown that there has been a significant amount of work in the field on MFRH. MFRH are driven by variety of mechanisms such as motor, pneumatic, air muscle with different finger configurations. The literature review shows that for MFRH, overall, both the conventional controller such as PID and modern controllers such as Fuzzy, Neural Network, Genetic Algorithm, etc. have several limitations such high overshoot, longer settling time, not consistent based on system response. The present research is therefore directed at finding a solution to improve the system performance for the control techniques based on analysis of system performance in terms of settling time and overshoot of MFRH.

1.3 Research Objectives

The main objective of this research is to develop a suitable control technique for MFRH. In this respect, the control technique of MFRH should be able to provide improved results with the least complexity and development time. Accordingly, the research has been scoped to meet specific objectives as the following:

- to develop a control techniques such as PID, Fuzzy, Fuzzy-PID and PSO-PID for position control;
- to improve system performance in terms of settling time and overshoot;
- to compare the system performance of the control techniques

A multi-faceted approach was implemented in the form of thorough literature review, extensive modeling and simulation work to achieve the above objectives.

1.4 Research Scope

The control technique is limited to PID, Fuzzy, Fuzzy-PID and PSO-PID for position control where the system performance is measured in terms of settling time and overshoot based on the system response.

1.5 Outline of Thesis

This thesis is comprised of five chapters:

An overview of various interdisciplinary fields in robotic industries such as mechanical design, sensing and control techniques is discussed in chapter 2. In addition, the related works on control techniques that have been implemented by previous researchers are provided. Thereafter, a critical analysis of the related work is presented.

Chapter 3 discusses the modeling of MFRH, motor level control, proposed control techniques such as PID, Fuzzy, Fuzzy-PID and PSO-PID for position control of MFRH.

The results obtained for all the simulation work is provided in Chapter 4. In this chapter, the results in graphical and table form are presented with detail discussions on the outcome.

Finally, the summary of the undertaken research and contributions of the research is presented in Chapter 5. Possible future work is also outlined.

CHAPTER 2

LITERATURE REVIEW

Over the last few decades, there has been considerable research in robotics. Various robotics systems such as manipulator arms, humanoid, Multi-Fingered Robot Hand (MFRH) and etc. have been developed. As outlined in chapter 1, the MFRH can be further improved in terms of its control techniques. However, in order to provide a complete picture of MFRH, in this chapter, the mechanical design, sensing and control techniques are reviewed. Since the subject area is vast, only those works are reviewed which are of greatest significance and interest to our research. First, the available MFRH designs in terms of mechanical design are discussed. Then, current technologies and techniques are reviewed in terms of sensing and control technique. Next, the related work is provided. Then, the critical analysis of the related work is provided.

2.1 Overview of Multi-Fingered Robot Hand

Currently, the robotic hand is one of the major research topics in the category of object manipulation. The researchers have been designing various robotic hands that have a high degree of freedom (DOF) to improve the manipulability [10]-[13]. Many large companies are actively investing in the development of this type of robots because it gives many advantages and benefits to mankind [14]-[19]. Many studies have been conducted to enhance building of robots, in terms of quality performance on human environment as artificial intelligence, mobility, object manipulation and interaction [20], [21]. There is no denial that the robot hand is useful to humans. Robot Hand is not only designed for human services, but it is also designed for industrial use of dangerous activities [22]. In this research, multi-fingered robot hand can be discussed in term of mechanical design, sensing and control techniques.

2.1.1 Mechanical Design

Most of developed robot today is anthropomorphic or non-anthropomorphic design. An anthropomorphic robot is called as humanoid robot which design is based on human body and allows it to work with the tool or human environment. Normally non-anthropomorphic robots are used for dexterous work and industrial activity. The mechanical design of a robot hand can be discussed in terms of motor, pneumatic, air muscle, ultrasonic motor with elastic element design configurations.

2.1.1.1 Motor Configuration

One of robotic hand that uses motor is Robonaut hand [23] as shown in Figure 2.1. The hand was created by the Robotic Systems Technology Branch at NASA Johnson Space Center (JSC) in Houston, Texas. It is highly anthropomorphic robot hand because the design is fully regarding similarly like human hand. Robonaut hand is designed based on motor configuration that are fourteen *brushless motor* and *electronic drive*, *two-DOF wrist*, and *five fingers, twelve DOF hand*. The hands into dexterous work set for the manipulation and grasping a set that is used to maintain a stable grasp. The hand also has a total of fourteen DOFs, and consists of a forearm, a two DOF wrist, and a twelve DOF hand complete with position, velocity, and force sensors. The latest version of Robonaut hand is R2. The hand [24] has been designed to use the EVA space in the most convenient size and is able to fit the astronaut's hand. Hands of Robonaut can handle tools such as EVA Tether hook and it can enter into all parts required. Design of a combination of wrist pitch and yaw, it meets a suitable glove for the human hand.

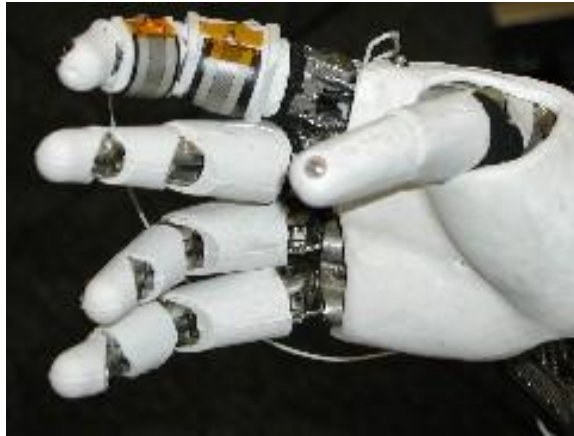


Figure 2.1: Robonaut Hand [24]

2.1.1.2 *Pneumatic Configuration*

Utah/MIT [25] hand was designed by the Center for Engineering Design at the University of Utah in conjunction with the Artificial Intelligence Laboratory at MIT. Utah/MIT Hand is based on pneumatic design like shown in Figure 2.2. It has four fingers and employs a pulley based on *tendon drive*. It has three modular four fingers mounted parallel to the palm plane with a non-anthropomorphic thumb orientation. The drive system involves 32 individual pneumatic actuators with apposing tendons for each joint.

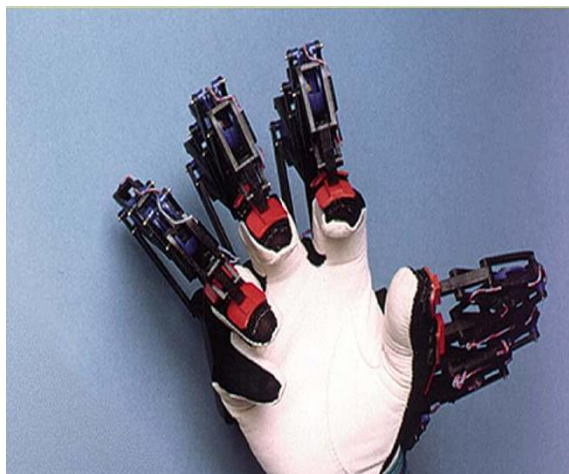


Figure 2.2: Utah/MIT [25]

2.1.1.3 Air muscle Configuration

Shadow Hand [26] was designed by Shadow Robot Company based on air muscle configuration like shown in Figure 2.3. The robot hand is designed with the size and shape like human hand which able to grip the small to medium sized objects and performs correctness tasks. The Shadow Dexterous Hand is highly anthropomorphic design and an advanced humanoid robot hand system that provides 24 movements to reproduce as closely as possible the degrees-of freedom of the human hand. It has been designed to provide comparable force output and movement sensitivity to the human hand.

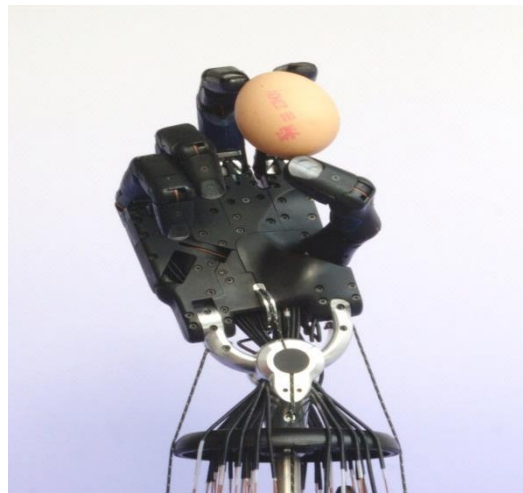


Figure 2.3: Shadow Hand [26]

The shadow robot hand system integrates all necessary control systems (software provided under GNU GPL) and documentation for research and teaching purposes. The Shadow system can be used for research in grasping, manipulation, neural control, and hazardous handling. See *Appendix A* to get more information about the Shadow Robot Hand.

2.1.1.4 Ultrasonic Motor & Elastic Elements Configuration

Another the anthropomorphic robot hand is five-fingered robot hand using ultrasonic motors and elastic elements [27] which is designed by Ikuo and Takashi as shown in Figure 2.4. The robot hand is designed based on ultrasonic motors and elastic elements configuration. The robot hand are use this method that can makes for restoring force as driving power in grasping objects, which enables the hand to

perform stable and compliant grasping motion without power supply. The ultrasonic motor has features such as high driving torque at low rotational speed, compact size and lightweight so it is suitable for the actuator of robot hand that has structural restrictions. The hand has five fingers with the number of joints is equal the number degree of freedom, which is 20 joints and 20 DOFs. It is almost equal in size to the hand of an average grown-up man.

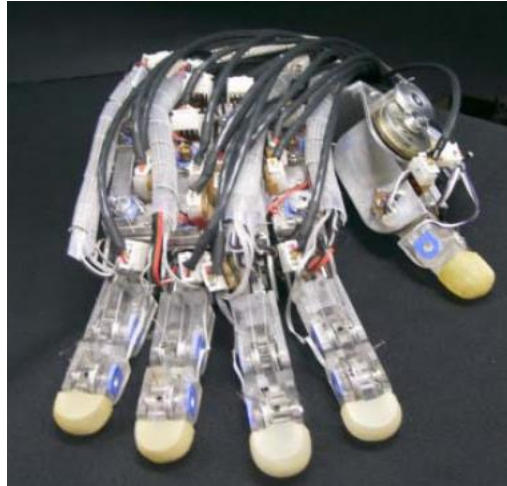


Figure 2.4: Ikuo Robot Hand [28]

2.1.2 Sensing for MFRH

The robot hands use the sensing as a tool to detect the object. The interaction of MFRH with any external objects involves several sensing technique. For detecting any object, MFRH uses the tactile sensor (*see Appendix A*). The sensor can measure the parameters of a contact between the sensor and an object. This interaction obtained is confined to a small defined region. This contrasts with a force and torque sensor that measures the total forces being applied to an object. Under sensing technique, there are three types of sensing have produced; touch sensing, tactile sensing and slip.

2.1.2.1 Touch Sensing

This is the detection and measurement of a contact force at a defined point. A touch sensor can also be restricted to binary information, namely touch, and no touch [29]. MFRH get the differences the shape of the object shown in figure 2.5.

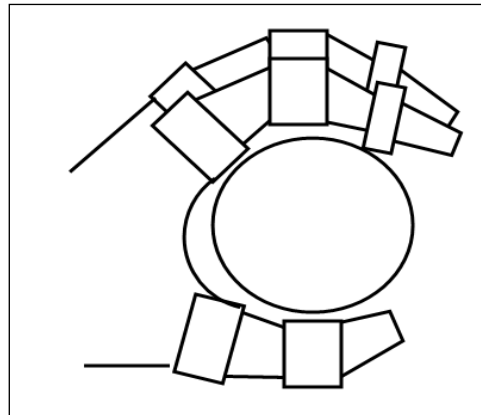


Figure 2.5: Grip the Ball

2.1.2.2 Tactile Sensing

This is the detection and measurement of the spatial distribution of forces perpendicular to a predetermined sensory area, and the subsequent interpretation of the spatial information. A tactile-sensing array can be considered to be a coordinated group of touch sensors [29]. MFRH can range the size of the object hold shown in figure 2.6.

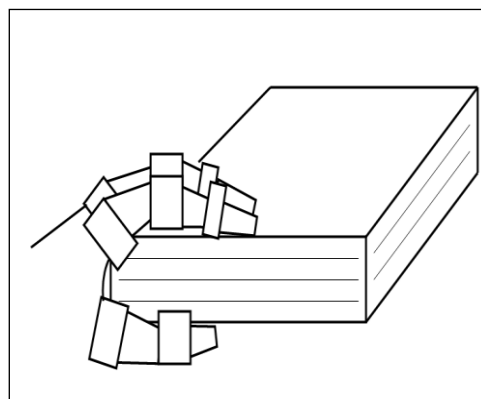


Figure 2.6: Hold the Book

2.1.2.3 Slip

This is the measurement and detection of the movement of an object relative to the sensor. This can be achieved either by a specially designed slip sensor or by the interpretation of the data from a touch sensor or a tactile array [29]. MFRH can hold and grasp the small object without dropped in figure 2.7.

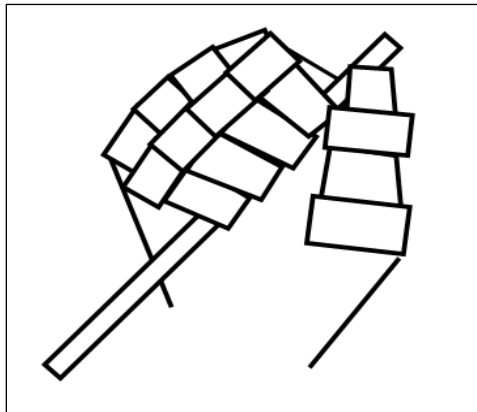


Figure 2.7: Grasp the Rod

2.1.3 Control Technique for MFRH

Controller is central to the proper functioning of MFRH. The controllers are divided into two categories; conventional and modern controller.

2.1.3.1 Conventional Controller

The conventional controller is known as Proportional–Integral–Derivative (PID) controller. PID is a generic control loop feedback mechanism (controller) widely used in industrial control systems. One of PID tuning methods is essentially called Ziegler Nichols methods. The Ziegler–Nichols method is a heuristic method of tuning a PID controller. It was developed by John G. Ziegler and Nathaniel B. Nichols. It is performed by setting the ‘I’ and ‘D’ gains to zero [30]. It means the ‘I’ and ‘D’ is referred to the value of K_i and K_d . PID controller can be improved by the tuning performance for processes with changing dynamic properties. The proposed strategies include automatic tuning PID, adaptive PID, and intelligent controllers. In process

dynamic, the controllers have recalibration to cope with little a priori knowledge and significant changes [31].

In literature, Azenha [32] has designed the PID controllers for robot manipulators that subjected to nonlinear friction at the joints. The results of the simulation are looking good for an accurate position control without the need for trial-and-error PID parameters tuning, as initially planned. PID controller also has been developed by Youngjin Choi and Wan Kyun Chung [33] in the simulation of the robot manipulator. Jose and Cervantes [34] have performed to the PID controller to stabilize robot manipulators with elastic joints. By using PID, the desired position can be achieved, even if the gravitational and elastic forces are unknown. Ming-Tzu Ho and Yi-Wei Tu [35] have improved the PID Controller Design for a Flexible-Link Manipulator. This controller uses synthesis method to guarantee robust performance in spite of uncertainty. This method does not provide single solution only, but the entire set of admissible PID gain values.

2.1.3.2 Modern Controller

There are several modern controllers such as fuzzy logic, artificial neural network, and others new controller are used in the robotic field. Amongst them, fuzzy logic controller (FLC) is now commonly used by researchers. FLC provides a good tuning of the system response of MFRH compared with conventional PID controller. Various methods of the fuzzy logic controller have been used by authors in [36]-[40]. Previously, Mehmet [36] has used a fuzzy controller modeling and simulation of an anthropomorphic robot arm with Dymola. In the trajectory control of robot manipulators, fuzzy logic control is used to match the impact of the dynamic model of the robot manipulators. Erbatur et al. [37] have carried out the simulation using fuzzy based inverse dynamic control for three degree of freedom manipulator robot Carlos Pérez [41] has produced the fuzzy controller to track an industrial robot hand during its movement. The robot hand is based on vision system to move a pan-tilt camera and keep the robot hand centered in the image every time using an adaptive fuzzy logic controlled. The purpose is to track a robot hand by a vision system while the robot is making different tasks. Steven [42] has implemented the fuzzy block method for

multi-fingered robot hand. This method is quite successful at controlling both fine and gross finger translations as well as tracking control. In 2007, S.G. Anavatti [43] has improved fuzzy logic controller with PID controller to control robot manipulator. Shi [44] also improved Fuzzy-PID to control speed of DC motor.

An artificial neural network (ANN), commonly called neural network (NN), is a mathematical model that is enthused by the structure and/or functional aspects of biological neural networks. Neural networks involve interconnection with the group of the artificial neurons and it produces the information using a connectionist approach to computation. [45]. H. Daniel Patino [46] have proposed an approach and a systematic design methodology to adaptive motion control based on neural networks (NNs) for high-performance robot manipulators, for which stability conditions and performance evaluation. In 2004, Danica developed [47] neural network for planning and intelligent control of an autonomous robot that can move safely in partially structured environment. This environment could involve any number of obstacles of arbitrary shape and size and some of them are allowed to move. Magnus Johnsson [48] designed the neural network models of haptic shape perception for robot hand. In 2008, E.A. Al-Gallaf [49] have proposed the algorithm for a four fingered robot hand using neural network where inverse hand Jacobian plays an important role in robot hand.

Genetic algorithm (GA) is a search heuristic that mimics the process of natural evolution. This heuristic is routinely used to generate useful solutions to optimization and search problems. Genetic algorithms belong to the larger class of evolutionary algorithms (EA), which generate solutions to optimization problems using techniques inspired by natural evolution, such as inheritance, mutation, selection, and crossover [50]. M. N. H. Siddique and M. O. Tokhi [51] presented genetic algorithm to flexible robot manipulator based on neural fuzzy. A genetic algorithm is used to learn the weights, biases and shape of the sigmoidal function of the neural network. In 2008, Bahaa [52] used genetic algorithm (GA) to optimize the point-to-point trajectory planning for a 3-link (redundant) robot arm. The objective function for the proposed GA is to minimizing traveling time and space, while not exceeding a maximum pre-defined torque, without collision with any obstacle in the robot workspace. In 2009,

Nahapetian [53] applied the PID gain tuning genetic algorithm and fuzzy logic for robot manipulator control.

Boubertakh [54] improved Fuzzy-PID with Ant Colony Optimization (ACO) for tuning PID controller. In order use the PID tuning method that uses a Genetic Algorithm (GA) as a main gain estimator and a fuzzy logic as a ranking basement for GA. The proposed approach is then used to tune the PID gains for different response specifications. The result of experimental work shows that better performance can be achieved with this fuzzy based GA-PID tuning relative to Ziegler-Nichols tuning and trial and error tuning. Leandro [55] has improved ACO for optimization of PID controller based on a modified continuous approach of ant colony optimization combined with a differential evolution method (MACO) for synchronization of two identical discrete chaotic systems subject the different initial condition. Regarding to [56] Ant colony optimization (ACO) is one of the swarm intelligence (SI) techniques. It is a bio-inspired optimization method that has proven its success through various combinatorial optimization problems. Using the tuning parameters of ACO is easier than conventional PID.

Particle swarm optimization (PSO) is a new variation of the algorithm used by researchers to find the optimum solution or approach optimal in a large search space. PSO algorithm is suitable for parameter optimization in continuous, multi-dimensional search space. PSO method produce high quality solutions in term step response with given the shorter computation time and tend to converge very rapidly compared with other stochastic methods compared with PID and fuzzy. In addition, it has been implemented with ease in most programming languages as the core of the program can be written in one line of code. PSO is used in the design on several modern controllers through combination of the controller like fuzzy or PID controller. Regarding to Zafer [57], fuzzy logic controller tuned by particle swarm optimization is better and more robust than the PID tuned by particle swarm optimization for robot trajectory control. However, the approach PID controller with PSO algorithm is also given concentration by authors [58]-[60]. Mahbubeh [61] and Mahmud [62] have used PID to optimize the DC motor. The PSO Algorithm uses fitness functions so that the minimum error and overshoot design is easy to be implemented. Regarding to [63], the PID combine with PSO has produced better results through optimization.

2.2 Critical Analysis of Review on MFRH

Based on discussion in section 2.1.3.2, the most relevant related work is summarised in Table 2.1.

Table 2.1: Types of Control Techniques

Author	Year	Control Technique	Application	Advantages	Disadvantages
Youngjin [34]	2003	PID	Robot Manipulator	- Easier to find the output response	- less accurate results
Carlos Perez [41]	2004	Fuzzy	Industrial Robot hand	- Improved than PID	- The result not really consistent
E.A. Al-Gallaf [49]	2008	NN	MFRH	- To produce the good mapping mechanism	- Only find the trajectory
Bahaa [52]	2008	GA	Robot arm	- to optimize the point-to-point trajectory planning	- Just focus on motion planning
Boubertakh [54]	2009	ACO	No application provided	- the best result with the lowest cost function	- Problem - where the premise parameters are fixed a priori.
Shi [44]	2011	Fuzzy-PID	DC motor	- To make a simple analysis & the result is better than PID.	-
Mahmud [62]	2011	PSO	DC motor	- the output response is better.	- Highly overshoot.

The control techniques are divided into two types; the conventional and modern controllers. Although the conventional controllers are most popular since they have been in existence for some time, however, the modern controllers such as Fuzzy, Artificial Neural Network (ANN), and Genetic Algorithm (GA) and so on are increasingly being used since they offer many solutions and they are easier to use. Table 2.1 shows the types of control techniques that have been developed by other researchers. Based on these controllers, PID is a conventional controller and other controllers are modern controllers. Modern controllers are also able to provide good solution either independently or used in conjunction with conventional controller like Fuzzy with PID, Fuzzy-PID with ACO and PID with PSO.

Carlos Perez [41] used fuzzy controller to track an industrial robot hand during its movements where the system performance in terms of settling time and overshoot. E.A. Al-Gallaf [49] used neural networks to control the MFRH motion with respect to six Cartesian based coordinates where there was better trajectory mapping. Bahaa [52] used genetic algorithm to optimize point to point trajectory planning. Boubertakh [54] improved Fuzzy-PID with Ant Colony Optimization (ACO) for tuning PID controller where the best result with the lowest cost function was obtained. Shi [44] has used Fuzzy with PID to control the speed of DC motor for the automatic doors. The system was found to be more stable, smaller overshoot and faster response with 38.1% of settling time and 94.3% of overshoot. Mahmud [62] also have improved PID controller using PSO for DC motor where the output response with 38.1% of settling time and 94.3% of overshoot. The plant response produces high overshoot, but a better performance obtained with the implementation of PSO-based PID.

Overall, it can deduced that both the conventional and modern controllers have several limitations as a suitable controller for robots such as less accurate results, not consistent, high overshoot, longer settling time, etc. Therefore, this shows that more research is needed to address these shortcomings.

2.3 Summary

In this chapter, an overview of MFRH, and discussed some important aspects of MFRH such as mechanical design, sensing and control techniques are presented. By adopting and adapting the various techniques outlined above, it is possible to obtain a MFRH with improved performance in terms of settling time and overshoot based on system response.

CHAPTER 3

METHODOLOGY

In this chapter, multi-fingered robot hand will be discussed in terms of modeling of MFRH, motor level control, proposed model and position control of MFRH.

3.1 Modeling of a MFRH

The modeling of a MFRH involves the development of a CAD model and followed by dynamic analysis.

3.1.1 CAD MODEL OF MFRH

In this research, the mathematical modeling of a MFRH was based on CAD model which turn is based on human hand structure. Human hand is a very articulated structure. The high functionality of the human hand is based on the higher degrees of freedom. Human hand has 23 DOF that is provided by 17 joints [64]. If three dimensional movements are taken into consideration, degrees of freedom increase to 29 because of orientation and position variation of the hand. The joint of a multi-fingered robot hand is shown in Figure 3.1. The phalanges are the small bones that constitute the skeleton of the fingers and thumb. The nearest phalange to the hand body is called “proximal” phalange and the one at the end of the each finger is called “distal” phalange. The joints of the finger, finger, DOF owing to rotational movement and metacarpophalangeal (MCP) joint has 2 DOF owing to adduction-abduction and rotational motions. Except the thumb, the other four fingers (index, middle, ring and little fingers) have similar structure in terms of kinematics and DOF owing to rotational movement and metacarpophalangeal (MCP) joint has 2 DOF owing to adduction-abduction and rotational motions. Except the thumb, the other four fingers

(index, middle, ring and little fingers) have similar structure in terms of kinematics and dynamics features. Thumb is the most complex physical structure amongst the hand fingers and different from the fingers in that contains only two phalanges and has 5 DOF [64].

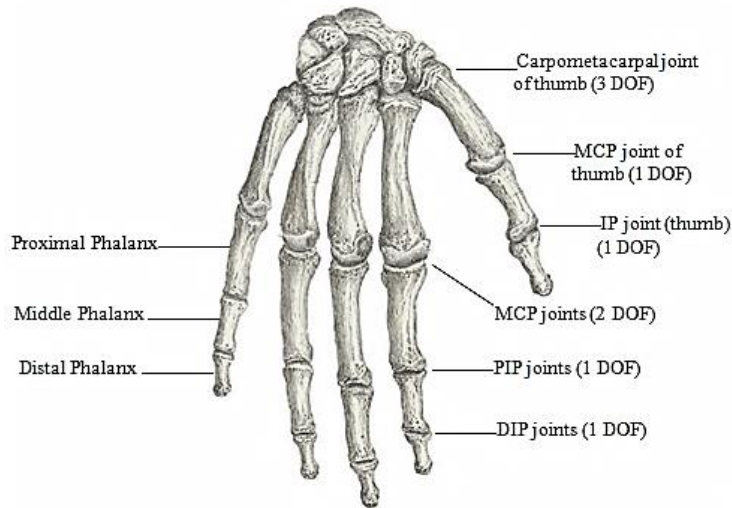


Figure 3.1: Structure of Human Hand [64]

The CAD model of the MFRH was done using the Solid Works 2010. The CAD models are shown in Figure 3.2 respectively where they consist of thumb, index, middle, ring and little fingers.

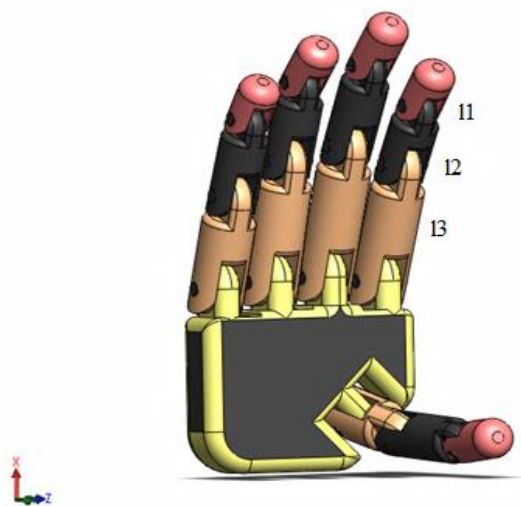


Figure 3.2: CAD Model

Each finger has 3 joints and 3 degrees of freedom (DOF). The links are named as Link 1 (I1), Link 2 (I2) and Link (I3) respectively. Each link is referred to the length size of MFRH that given in Table 3.1.

Table 3.1: Multi-Fingered Robot Hand Model Parameter

Finger	Length size			Unit
	I1	I2	I3	
Thumb	40.0	52	32.5	mm
Index	50.5	42.0	22.0	mm
Middle	60.5	42.0	24.5	mm
Ring	65.5	45.0	27.5	mm
Little	60.5	37	24	mm

The dimensions for the MFRH are based on the average size of a Malaysian male in mid-twenties. The Isometric View of CAD Model is shown in Figure 3.3 and the CAD Model with Dimensions in Figure 3.4 respectively.

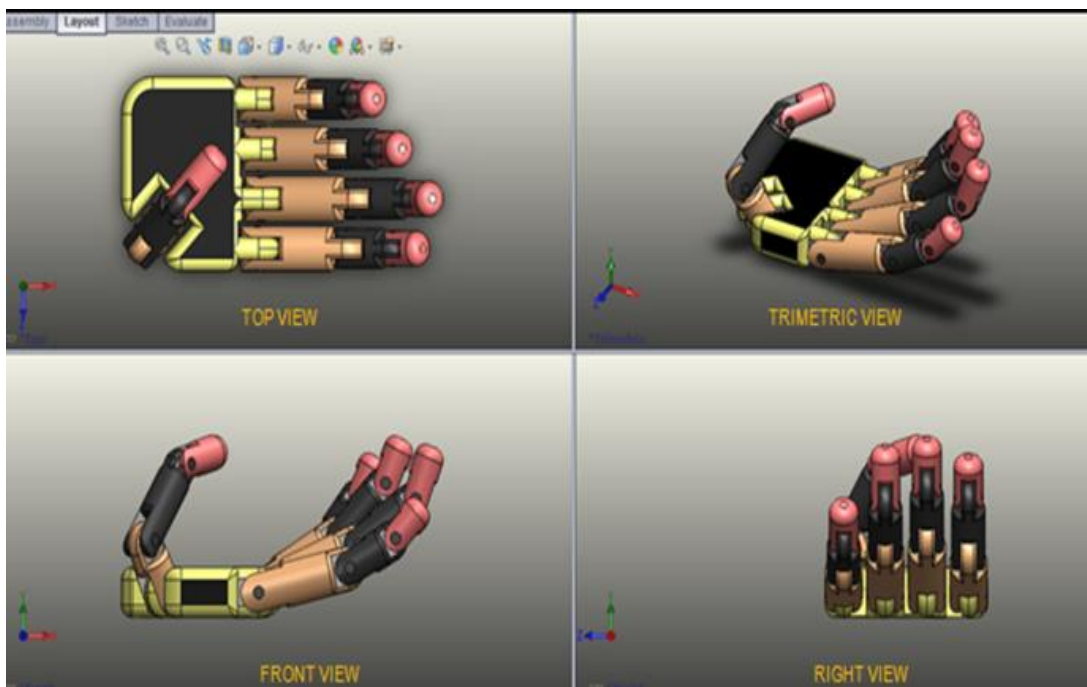


Figure 3.3: View of MFRH Design

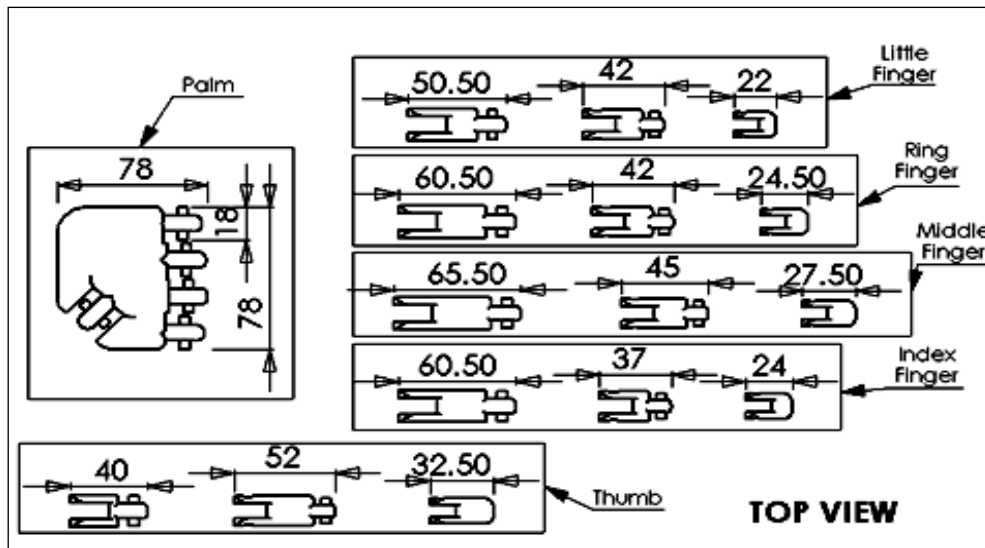


Figure 3.4: Length Size of MFRH Design

Further details of the CAD Model are given in *Appendix B*.

3.1.2 KINEMATIC AND DYNAMIC MODEL

The MFRH uses the serial robotic manipulator concept where each links are connected together at the joints and each joint is controlled by the motor that allows motion based on command from the controller. The MFRH model is shown in Figure 3.5.

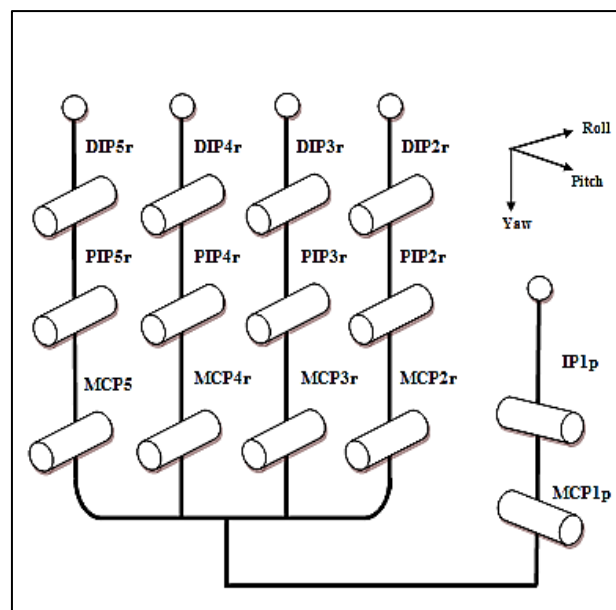


Figure 3.5: MFRH Kinematic Model

The torque of MFRH based on the given model in Figure 3.5 is derived based on kinematics and dynamic equations (see Appendix C for detail derivation). Based on Newton-Euler formula, the dynamic expression of dynamic equation is [65]:

$$\tau = M(\theta)\ddot{\theta} + V(\dot{\theta}, \ddot{\theta}) + G(\theta) \quad (3.1)$$

where $M(\theta)$ the $(n \times n)$ mass matrix of the fingers is $V(\theta, \dot{\theta})$ is $(n \times 1)$ vector of centrifugal and Coriolis term and $G(\theta)$ is $(n \times 1)$ vector gravity. Each element of $M(\theta)$ and $G(\theta)$ is a complex function which depends on θ , the position of all the joints of the fingers. Each element of $V(\dot{\theta}, \ddot{\theta})$ is a complex function of both θ and $\dot{\theta}$.

Based on the dynamic equation, Eq. (3.1), the values of torques are determined using a Matlab program that was developed. The Matlab code is shown in Appendix D. These torque values are important for selecting the suitable motor for simulation of MFRH. In this research these values are given in Table 3.2.

3.2 Motor Level Control of MFRH

A common actuator in control systems is the DC motor. It directly provides rotary motion and, coupled with wheels or drums and cables, can provide translational motion. The electric equivalent circuit of the armature and the free-body diagram of the rotor are shown in Figure 3.6.

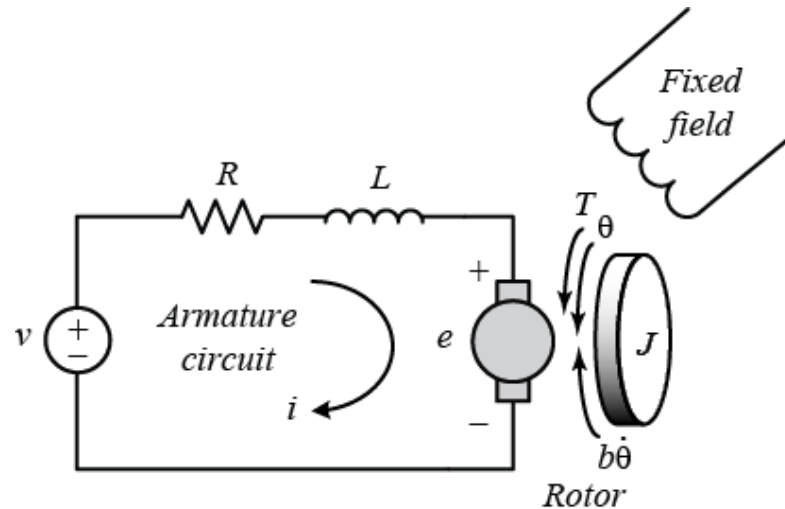


Figure 3.6: Electrical Circuit of DC motor [66]

The electrical circuit of the permanent magnet DC motor provides the following equation [67]:

$$v = R_i + L \frac{di}{dt} + k_b \frac{d\theta_m}{dt} \quad (3.2)$$

Where R is the armature resistance, L is the armature inductance, k_b is the back emf constant, $v(t)$ is the armature voltage, i is the armature current and θ_m is the rotor position, respectively.

In order to cancel the current terms, a control law is proposed as

$$v = R_i + L \frac{di}{dt} + k_b f \quad (3.3)$$

Where f is a new control input. Substituting (3.2) into (3.3) results in a linear time invariant system formed as

$$f = \frac{d\theta_m}{dt} \quad (3.4)$$

In the system obtained by (3.3), f is the input and the rotor position θ_m is the output. The system is known as an integrator that represents an uncoupled linear equation. Therefore, for tracking a desired trajectory, a linear control law is chosen as in Eq(3.5)

$$f = \dot{\theta}_{md} + k_p(\theta_{md} - \theta_m) \quad (3.5)$$

Where θ_{md} is the desired rotor position, $\dot{\theta}_{md}$ is the desired rotor velocity, and k_p is the proportional gain. Substituting (3.4) into (3.3), yields

$$\dot{\theta}_{md} - \dot{\theta}_m + k_p(\theta_{md} - \theta_m) = 0 \quad (3.6)$$

$e = \theta_{md} - \theta_m$ as the tracking error to obtain

$$\dot{e} + k_p e = 0 \quad (3.7)$$

The closed loop control system is a linear system and it is stable only if $k_p > 0$. Then $e(t) \rightarrow 0$ as $t \rightarrow \infty$, or the rotor position θ_m converges to the desired rotor position θ_{md} .

Feedbacks from the motor current and its derivative are required to implement the control law given by (3.2). In addition, the control law given by (3.3) requires the feedback of the motor position. The motor current contains all dynamical effect of manipulator transferred to the motor. This fact is concluded from the dynamic equation of a manipulator driven by DC motors [67], formulated as

$$M(\theta)\ddot{\theta} + C(\theta, \dot{\theta})\dot{\theta} + G(\theta) = k_m i \quad (3.8)$$

Where I is the armature current vector, θ is the joint variable vector, M is the completed inertia matrix, $C(\theta, \dot{\theta})\dot{\theta}$ is the centrifugal and Coriolis torque vector, $G(\theta)$ is the gravitational torque vector and k_m is the diagonal matrix of motor torque constant. The dissipative torque such as frictional and the provided load torque can be added to the left handoff (3.7) to complete the equation.

The proposed control law given by (3.2) would be advantageous in comparison with inverse dynamic control. The inverse dynamic law is defined as

$$\tau = M(\theta)a + C(\theta, \dot{\theta})\dot{\theta} + G(\theta)$$

$$\tau = k_m i \quad (3.9)$$

Where τ is the torque vector inserted to the manipulator joints and a is the input vector of the obtained system after feedback linearization as

$$a = \ddot{\theta} \quad (3.10)$$

In the proposed approach, each joint of the manipulator is driven by a permanent magnet DC motor in the control system. The inserted torque on the joint to drive the manipulator is the load torque of motor, which is considered in a dynamic equation formed as

$$T_m = J_m \ddot{\theta}_m + B_m \dot{\theta}_m + rT \quad (3.11)$$

Where T is the load torque, T_m is the motor torque, r is the gear reduction coefficient, J_m is the sum of actuator and gear inertia, and B_m is the damping coefficient. The reduction gear relates the motor position to the joint position as

$$q = r\theta_m \quad (3.12)$$

Where q is the joint position which is the joint angle for a revolute joint or the joint distance for a prismatic joint. The motor torque is proportional to the armature current as

$$T_m = \tau = k_m i \quad (3.13)$$

Where k_m is the torque coefficient. The torque coefficient is equal to the back emf constant for the permanent magnet DC motor.

$$k_m = k_b \quad (3.14)$$

This control law can transform the nonlinear system given by (3.8) to a new system shown in (3.10) which is linear and decoupled. Control law given by (3.2) is preferred as compared with the control law (3.8). Because, all feedbacks are belonging to the motor as the control strategy is the independent joint strategy. Also, the manipulator model is not required to form the control law. As a result, the control law is simple, fast, and more accurate in comparison with (3.8). The control law requires only a feedback of motor current and electrical coefficients of the motor. Moreover, the electrical signals can be measured more convenient and more precise than mechanical signals. This control law can be used for tracking control of a high-speed robot since this approach is free of manipulator model. In facts, the dynamical effects are compensated by currents of motors in high-speed applications.

The parameters of DC servomotor are as shown in Table 3.2. Details of specification of DC servomotor can be referred in *Appendix E*. In the research, the torques use dc micrometer (τ_1 : DC Micrometer 0.48 mNm series 1016...012G (column 1), τ_2 : DC Micrometer 0.48 mNm series 1016...012G (column 3), τ_3 : DC Micrometer 1.28 mNm series 1016...017S).

Table 3.2: Parameters of DC Servomotor

Parameter	Symbol	Value		
		Torque 1 =0.8307	Torque 2 = 0.6955	Torque 3 = 0.1589
Moment of inertia	J	0.12.cm2	0.05 g.cm2	0.04 g.cm2
Friction coefficient	B	0.03 mN.ms	0.03 mN.ms	0.03 mN.ms
Back EMF constant	Ke	Ke=0.806 mV/rpm	0.705 mV/rpm	0.202 mV/rpm
Torque constant	Kt	7.70 mNm/A	6.73mNm/A	1.93mNm/A
Electric resistance	R	31.6 ohm	95 ohm	8.7 ohm
Electric inductance	L	344 μH	310 μH	28 μH

Based on parameter in Table 3.2, the final transfer function of the plant model is as the following:

$$\frac{\theta(s)}{v(s)} = \frac{Ke}{(J * L)s^2 + (J * R + L * B)s + Kt^2} \quad (3.15)$$

Selection of DC servomotor for torque 1;

$$\frac{\theta(s)}{v(s)} = \frac{0.806}{41.28s^2 + 14.11s + 0.649} \quad (3.16)$$

Selection of DC servomotor for torque 2;

$$\frac{\theta(s)}{v(s)} = \frac{0.705}{15.5s^2 + 14.05s + 0.497} \quad (3.17)$$

Selection of DC servomotor for torque 3;

$$\frac{\theta(s)}{v(s)} = \frac{0.202}{1.12s^2 + 1.19s + 0.389} \quad (3.19)$$

3.3 Position Control of MFRH

In this research, Multi-fingered robot hand is carried out using three controllers. The controllers are PID, Fuzzy and Hybrid and PSO-PID controller.

3.3.1 PID Controller

PID is stand for proportional–integral–derivative controller. PID is a generic control loop feedback mechanism (controller) widely used in industrial control systems like shown in Figure 3.7. One of PID methods is essentially called Ziegler Nichols methods. The Ziegler–Nichols tuning method is a heuristic method of tuning a PID controller. It was developed by John G. Ziegler and Nathaniel B. Nichols. It is performed by setting the ‘I’ and ‘D’ gains to zero [68].

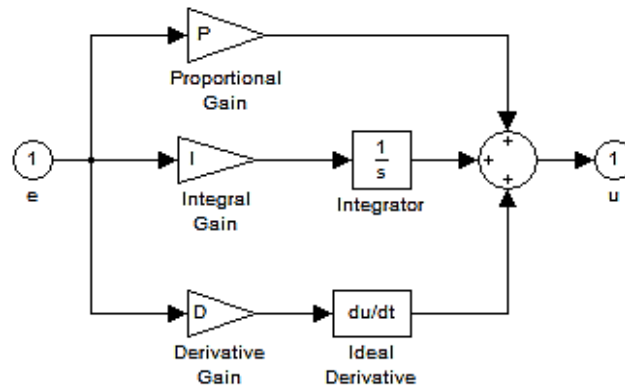


Figure 3.7: PID Controller

The equations of PID controller are represented as in equation (3.20) and (3.21):

$$y(t) = Kp \left[e(t) + Td \frac{d(e)}{d(t)} + \frac{1}{Ti} \int_0^t e(t) d(t) \right] \quad (3.20)$$

$$y(t) = \left[Kpe(t) + Kd \frac{d(e)}{d(t)} + Ki \int_0^t e(t) d(t) \right] \quad (3.21)$$

Where, Kp is the proportional gain, Ki is the integration coefficient and Kd is the derivative coefficient. Ti is integral action time and Td is referred to as derivative action time [69]. Symbols in equations 4.1 and 4.2 can be found in Table 3.3.

Table 3.3: Description of Equation Symbol

Symbol	Description
$y(t)$	Controller's Output
$e(t)$	Error Signal
Td	Derivative time constant
Ti	Integral time constant
Kp	Proportional gain
Kd	$Kp \times Td =$ Derivative gain
Ki	$Kp / Ti =$ Integral gain

The simulation of PID is carried out using PID block diagram as shown Figure 3.8.

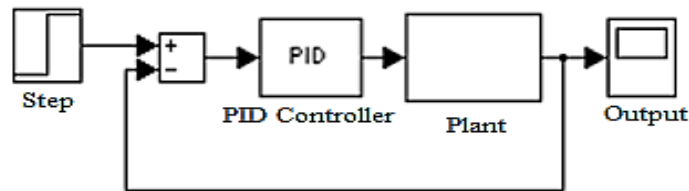


Figure 3.8: PID Controller Block Diagram

3.3.1.1 Ziegler Nichlos Method

The system response of Ziegler Nichols method is characterized by two parameters, L the delay time and T the time constant like shown in Figure 3.9. These are found by sketch a tangent to the step response at its point of inflection and noting its crossings with the time axis and the steady state value and the equation is $a = kL/T$ where, the values of k is maximum gain.

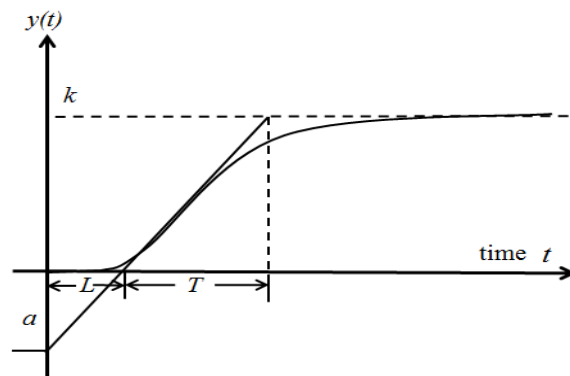


Figure 3.9: Time response of Ziegler Nichols method

By using L and a , the parameter of Ziegler Nichols Method can be used like shown in Table 3.4.

Table 3.4: Parameter of Ziegler Nichols Method

Control Type	Kp	Ti	Td
P	$\frac{1}{a}$	-	-
PI	$\frac{0.9}{a}$	$3L$	-
PID	$\frac{1.2}{a}$	$2L$	$\frac{L}{2}$

3.3.2 Fuzzy Logic Controller

The second controller is fuzzy logic controller. Fuzzy logic controller is not dependent on the mathematical model and it is widely used in robotic applications to solve various problems of uncertain and ambiguous [70]. Fuzzy controllers are successful applied to non-linear system because of their knowledge based nonlinear structural characteristics. Fuzzy logic controller is referring to the theory of fuzzy logic. It is determined as a set of mathematical principle knowledge representation of degree of membership rather than on crisp membership of classical binary logic [71]. In this research, Fuzzy logic controller has two inputs and one output: the position error, change of the error and the torque for motor. The input and output is determined by membership function of fuzzy logic. The membership functions are used consisted of two, three, five and seven membership function. The simulation has been carried out using Simulink fuzzy block diagram as shown in figure 3.10.

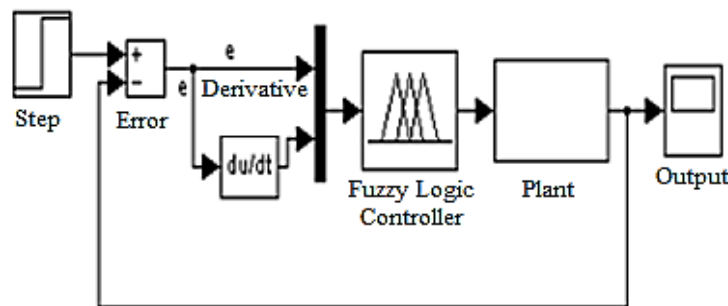


Figure 3.10: Fuzzy Logic Controller Block Diagram

3.3.2.1 Two Memberships Function

For two memberships function, the inputs are position error and change of thee error. These inputs are partitioned into two fuzzy sets: Negative (N) and Positive (P) as shown in Figure 3.11. The torque outputs of DC servomotor are portioned into three fuzzy sets: Negative (N), Zero (Z) and Positive (P) as shown in Figure 3.12.

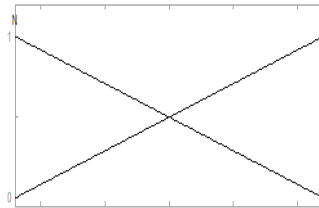


Figure 3.11: Input of Two Memberships Function

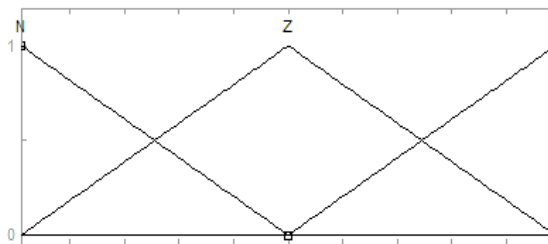


Figure 3.12: Output of Two Memberships Function

The main part of fuzzy logic controller is rule table. The total number of these rules is four. The fuzzy logic rules of two memberships function is shown in Table 3.5.

Table 3.5: Fuzzy Rules of Two Memberships Function

Output (U)		Change of the Error (de/dt)	
		N	P
Position Error (e)	N	N	Z
	P	Z	P

There are 4 rules of two membership functions have been applied:

$2 \times 2 = 4$ rules;

1. If (e is N) and (de/dt is N) then (U is N)
2. If (e is N) and (de/dt is P) then (U is Z)

3. *If (e is P) and (de/dt is N) then (U is Z)*
4. *If (e is P) and (de/dt is P) then (U is P)*

3.3.2.2 Three Memberships Function

These inputs and outputs of three memberships function are partitioned into three fuzzy sets: Negative (N), Zero (Z) and Positive (P) shown in Figure 3.13. The total number of these rules is nine. The fuzzy logic rule of three memberships function is shown in Table 3.6.

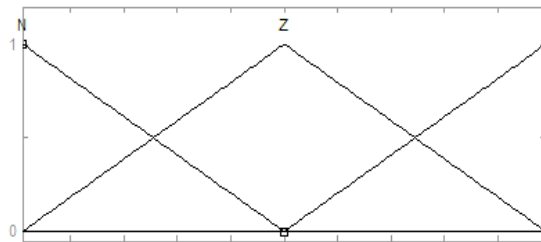


Figure 3.13: Input and Output of Three Memberships Function

Table 3.6: Fuzzy Rules of Three Memberships Function

Output (U)		Change of the Error (de/dt)		
		N	Z	P
Position Error (e)	N	N	N	Z
	Z	N	Z	P
	P	Z	P	P

There are nine rules of five membership functions have been applied:

$3 \times 3 = 9$ rules;

1. *If (e is N) and (de/dt is N) then (U is N)*
2. *If (e is N) and (de/dt is Z) then (U is N)*
3. *If (e is N) and (de/dt is P) then (U is Z)*
4. *If (e is Z) and (de/dt is N) then (U is N)*
5. *If (e is Z) and (de/dt is Z) then (U is Z)*
6. *If (e is Z) and (de/dt is P) then (U is P)*

7. If (e is P) and (de/dt is N) then (U is Z)
8. If (e is P) and (de/dt is Z) then (U is P)
9. If (e is P) and (de/dt is P) then (U is P)

3.3.2.3 Five Membership Function

These inputs and outputs of five memberships function are partitioned into three fuzzy sets: Negative Big (NB), Negative Small (NS) Zero (Z), Positive Small (PS) and Positive Big (PB) like shown in Figure 3.14. The total number of these rules is twenty five. The fuzzy logic rule of five memberships function is shown in Table 3.7.

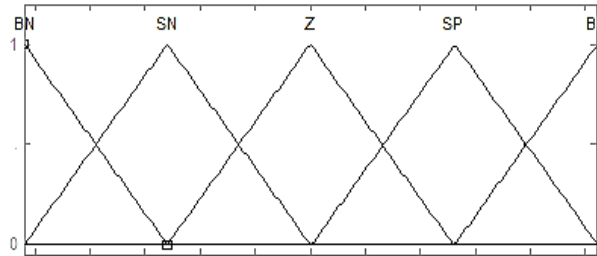


Figure 3.14: Input of Five Memberships Function

Table 3.7: Fuzzy Rules of Five Memberships Function

Output (U)		Change of the Error (de/dt)				
		NB	NS	Z	PS	PB
Position Error (e)	NB	NB	NB	NB	NS	Z
	NS	NB	NS	NS	Z	PS
	Z	NB	NS	Z	PS	PB
	PS	NS	Z	PS	PS	PB
	PB	Z	PS	PB	PB	PB

There are twenty five rules of five membership functions have been applied:

$5 \times 5 = 25$ rules;

1. If (e is NB) and (de/dt is NB) then (U is NB)
2. If (e is NB) and (de/dt is NS) then (U is NB)
3. If (e is NB) and (de/dt is Z) then (U is NB)
4. If (e is NB) and (de/dt is PS) then (U is NS)

5. *If (e is NB) and (de/dt is PB) then (U is Z)*
6. *If (e is NS) and (de/dt is NB) then (U is NB)*
7. *If (e is NS) and (de/dt is NS) then (U is NS)*
8. *If (e is NS) and (de/dt is Z) then (U is NS)*
9. *If (e is NS) and (de/dt is PS) then (U is Z)*
10. *If (e is NS) and (de/dt is PB) then (U is PS)*
11. *If (e is Z) and (de/dt is NB) then (U is NB)*
12. *If (e is Z) and (de/dt is NS) then (U is NS)*
13. *If (e is Z) and (de/dt is Z) then (U is Z)*
14. *If (e is Z) and (de/dt is PS) then (U is PS)*
15. *If (e is Z) and (de/dt is PB) then (U is PB)*
16. *If (e is PS) and (de/dt is NB) then (U is NS)*
17. *If (e is PS) and (de/dt is NS) then (U is Z)*
18. *If (e is PS) and (de/dt is Z) then (U is PS)*
19. *If (e is PS) and (de/dt is PS) then (U is PS)*
20. *If (e is PS) and (de/dt is PB) then (U is PB)*
21. *If (e is PB) and (de/dt is NB) then (U is Z)*
22. *If (e is PB) and (de/dt is NS) then (U is PS)*
23. *If (e is PB) and (de/dt is Z) then (U is PB)*
24. *If (e is PB) and (de/dt is PS) then (U is PB)*
25. *If (e is PB) and (de/dt is PB) then (U is PB)*

3.3.2.4 Seven Membership Function

Figure 3.15 shows the seven memberships function of fuzzy logic. It produces two inputs and outputs. The inputs and outputs are divided into seven fuzzy sets: Negative (NB), Negative Small (NS), Negative (N), Zero (Z), Positive Small (PS), Positive (P) and Positive Big (PB). The fuzzy rules as exposed in Table 3.8.

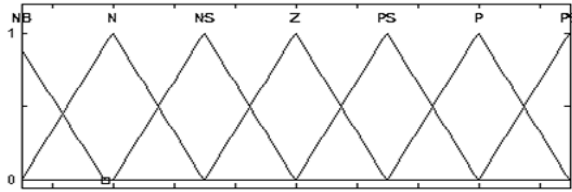


Figure 3.15: Input and Output of Seven Memberships Function

Table 3.8: Fuzzy Rules of Seven Memberships Function

Output (U)		Derivative Error (de/dt)						
		NB	N	NS	Z	PS	P	PB
Error (e)	NB	NB	NB	N	N	NS	NS	Z
	N	NB	N	N	NS	NS	Z	PS
	NS	N	N	NS	NS	Z	PS	PS
	Z	N	NS	NS	Z	PS	PS	P
	PS	NS	NS	Z	PS	PS	P	P
	P	NS	Z	PS	PS	P	P	PB
	PB	Z	PS	PS	P	P	PB	PB

There are 49 rules of seven membership functions have been applied:

$7 \times 7 = 49$ rules;

1. *If (e is NB) and (de/dt is NB) then (U is NB)*
2. *If (e is NB) and (de/dt is N) then (U is NB)*
3. *If (e is NB) and (de/dt is NS) then (U is N)*
4. *If (e is NB) and (de/dt is Z) then (U is N)*
5. *If (e is NB) and (de/dt is PS) then (U is NS)*
6. *If (e is NB) and (de/dt is P) then (U is NS)*
7. *If (e is NB) and (de/dt is PB) then (U is Z)*

8. *If (e is N) and (de/dt is NB) then (U is NB)*
9. *If (e is N) and (de/dt is N) then (U is N)*
10. *If (e is N) and (de/dt is NS) then (U is N)*
11. *If (e is N) and (de/dt is Z) then (U is NS)*
12. *If (e is N) and (de/dt is PS) then (U is NS)*
13. *If (e is N) and (de/dt is P) then (U is Z)*

14. *If (e is N) and (de/dt is PB) then (U is PS)*
15. *If (e is NS) and (de/dt is NB) then (U is N)*
16. *If (e is NS) and (de/dt is N) then (U is N)*
17. *If (e is NS) and (de/dt is NS) then (U is NS)*
18. *If (e is NS) and (de/dt is Z) then (U is NS)*
19. *If (e is NS) and (de/dt is PS) then (U is Z)*
20. *If (e is NS) and (de/dt is P) then (U is PS)*
21. *If (e is NS) and (de/dt is PB) then (U is PS)*
22. *If (e is Z) and (de/dt is NB) then (U is N)*
23. *If (e is Z) and (de/dt is N) then (U is NS)*
24. *If (e is Z) and (de/dt is NS) then (U is NS)*
25. *If (e is Z) and (de/dt is Z) then (U is Z)*
26. *If (e is Z) and (de/dt is PS) then (U is PS)*
27. *If (e is Z) and (de/dt is P) then (U is PS)*
28. *If (e is Z) and (de/dt is PB) then (U is P)*
29. *If (e is PS) and (de/dt is NB) then (U is NS)*
30. *If (e is PS) and (de/dt is N) then (U is NS)*
31. *If (e is PS) and (de/dt is NS) then (U is Z)*
32. *If (e is PS) and (de/dt is Z) then (U is PS)*
33. *If (e is PS) and (de/dt is PS) then (U is PS)*
34. *If (e is PS) and (de/dt is P) then (U is P)*
35. *If (e is PS) and (de/dt is PB) then (U is P)*
36. *If (e is P) and (de/dt is NB) then (U is NS)*
37. *If (e is P) and (de/dt is N) then (U is Z)*
38. *If (e is P) and (de/dt is NS) then (U is PS)*
39. *If (e is P) and (de/dt is Z) then (U is PS)*
40. *If (e is P) and (de/dt is PS) then (U is P)*
41. *If (e is P) and (de/dt is P) then (U is P)*
42. *If (e is P) and (de/dt is PB) then (U is PB)*
43. *If (e is PB) and (de/dt is NB) then (U is Z)*

- 44. *If (e is PB) and (de/dt is N) then (U is PS)*
- 45. *If (e is PB) and (de/dt is NS) then (U is PS)*
- 46. *If (e is PB) and (de/dt is Z) then (U is P)*
- 47. *If (e is PB) and (de/dt is PS) then (U is P)*
- 48. *If (e is PB) and (de/dt is P) then (U is PB)*
- 49. *If (e is PB) and (de/dt is PB) then (U is PB)*

3.3.3 Fuzzy-PID Controller

Fuzzy-PID controller is combination of fuzzy logic controller and PID controller. The controller has created to improve the system response of a multi-fingered robot hand. Where the combination of the fuzzy and PID are much better than stand-alone PID and Fuzzy controllers. It uses additional gain to improve rise time, settling time and steady state error as discussed in chapter 5. The Simulation of Fuzzy-PID controller was carried out using Fuzzy-PID block diagram as shown in figure 3.16.

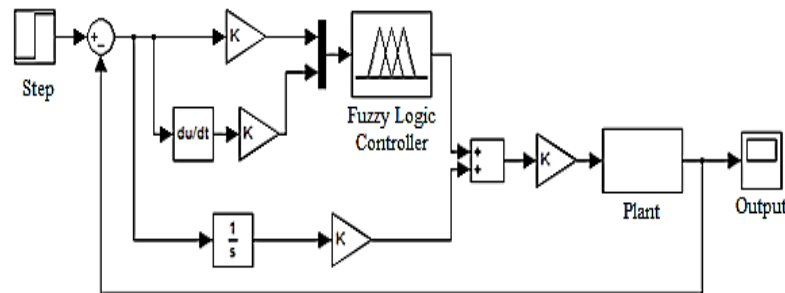


Figure 3.16: Fuzzy-PID Controller Block Diagram

3.3.4 PSO-PID Controller

PSO-PID controller is the PID controller tuned with Particle Swarm Optimization. By combination of PSO algorithm and PID controller are make a lot of results simultaneously in simulation running and the best result are selected. The system response produced in term of rise time, settling time and steady state error. Based on PSO-PID controller block diagram as shown in Figure 3.17, the simulation was carried out.

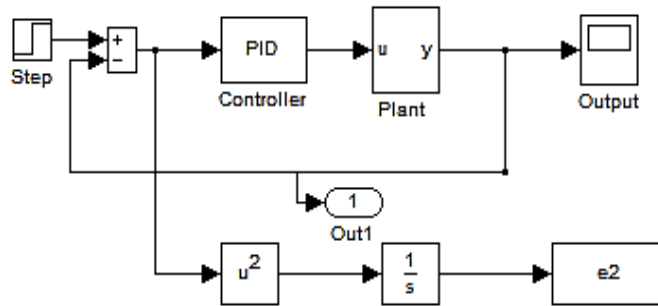


Figure 3.17: PSO-PID Controller Block Diagram

3.3.4.1 PSO Algorithm

Particle swarm optimization or PSO [72] is a group of individuals known as particles or intelligent agents that search for space flight. The problem of optimization can be solved by the particle, which is the position of a particle is influenced by the best position visited by itself (i.e., its own experience) and the position of the best particle in the whole population. The best particle is called the global the best particle. Capability can be achieved by each of these particles, it able be as near to the global optimum will be measured using the intelligence vary depending on the optimization problem.

Each particle traverses the XY coordinate within a two-dimensional search space. Its velocity is expressed by v_x and v_y (the velocity along the X-axis and Y-axis, respectively). Modification of the particles position is realized by the position and velocity information [Kennedy et al., 2001]. Each agent knows its best value obtained so far in the search (pbest) and its XY position. This information is an analogy of the personal experiences of each agent. Individual particles also have knowledge about the best value achieved by the group (gbest) among pbest. Each agent uses information relating to: its current position (x,y), its current velocities (vx,vy), distance between its current position and its pbest and the distance between its current position and the groups gbest to modify its position.

The velocity and position of each agent is modified according equation (3.23) and (3.24) respectively [73]:

$$v_i^{k+1} = v_i^k + c_1 * rand_1 * (pbest_i - s_i^k) + c_2 * rand_2 * (gbest - s_i^k) \quad (3.23)$$

$$s_i^{k+1} = s_i^k + v_i^{k+1} \quad (3.24)$$

With regards to equation (4.3):

v_i^k = current velocity of agent I at iteration k

v_i^{k+1} = new velocity of agent i at iteration k

c_1 = adjustable cognitive acceleration constants (self-confidence)

c_2 = adjustable social acceleration constant (swarm confidence)

$rand_{1,2}$ = random number between 0 and 1

s_i^k = current position of agent i at iteration k

$pbest_i$ = personal best of agent i

$gbest$ = global best of the population

For equation (4.4):

s_i^{k+1} = denotes the position of agent i at the next iteration k + 1

There are four steps of PSO and Figure 3.18 illustrates the flowchart for the PSO algorithm as the following [74]:

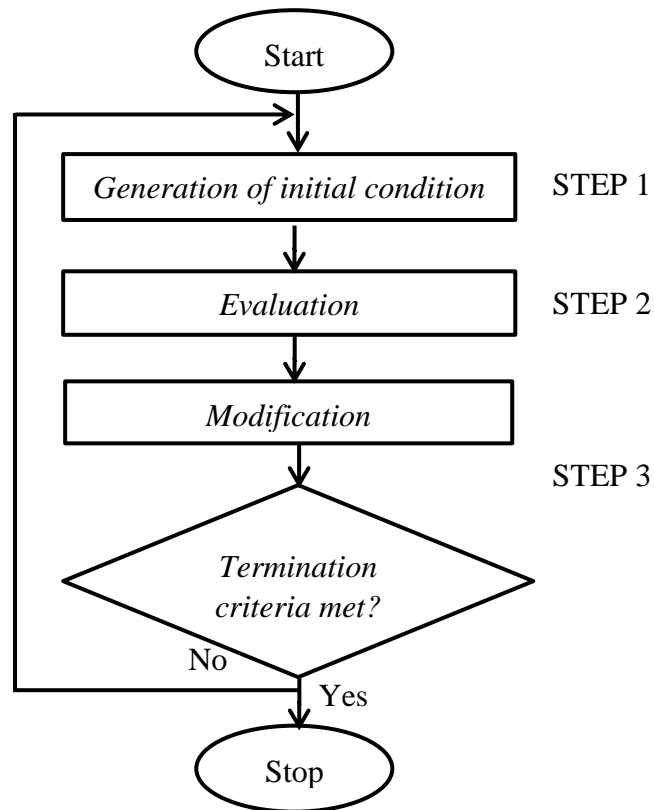


Figure 3.18: Flowchart of PSO [74]

Step 1: Generation of initial conditions of each agent.

Set the (s_{i0}) as the initial and the (v_{i0}) as the speed of each agent is randomly obtained. Each agent will set the current search point to p_{best} . G_{best} also will determine the best value of p_{best} , and the best value for the number of agents is stored.

Step 2: Evaluation of searching point of each agent

The purpose of this step is to get the best value of each agent, if the the agent is better than (p_{best}) at this time, it will be replaced with the current value. And if the the value (p_{best}) is better than (G_{best}), it will be replaced with the value (G_{best}) at this time and the value (G_{best}) this will be replaced with the best value. Then the best agent is stored.

Step 3: Modification of each searching point

By using the equation (4.3), (4.4), the value of agent will be declared to find the point.

Step 4: Checking to exit condition

In this step, several tests were carried out before the end of this process, if the it had not been reached then the process will be repeated again from step 1 and if the otherwise the process stopped.

3.3.4.2 PSO Parameter

The parameters of PSO are divided into 5 parameters. The different of parameters is regarding the values of the Size of the swarm “no of birds” (n) and Maximum number of “birds steps” (bird_step) each parameter. The simulation is to find the best of each parameter and the values. The parameters of PSO are given in the Table 3.9 to 3.13.

Table 3.9: Parameter 1 of PSO

Variable	Value	Description
n	10	Size of the swarm “ no of birds”
bird_step	10	Maximum number of “birds steps”
d	2	Dimension of the problem
c1	1.2	Velocity constant
c2	0.12	Velocity constant
w	0.9	momentum or inertia

Table 3.10: Parameter 2 of PSO

Variable	Value	Description
n	20	Size of the swarm “ no of birds”
bird_step	20	Maximum number of “birds steps”
d	2	Dimension of the problem
c1	1.2	Velocity constant
c2	0.12	Velocity constant
w	0.9	momentum or inertia

Table 3.11: Parameter 3 of PSO

Variable	Value	Description
n	30	Size of the swarm “ no of birds”
bird_step	30	Maximum number of “birds steps”
d	2	Dimension of the problem
c1	1.2	Velocity constant
c2	0.12	Velocity constant
w	0.9	momentum or inertia

Table 3.12: Parameter 4 of PSO

Variable	Value	Description
n	40	Size of the swarm “ no of birds”
bird_step	40	Maximum number of “birds steps”
d	2	Dimension of the problem
c1	1.2	Velocity constant
c2	0.12	Velocity constant
w	0.9	momentum or inertia

Table 3.13: Parameter 5 of PSO

Variable	Value	Description
n	50	Size of the swarm “ no of birds”
bird_step	50	Maximum number of “birds steps”
d	2	Dimension of the problem
c1	1.2	Velocity constant
c2	0.12	Velocity constant
w	0.9	momentum or inertia

3.4 Summary

In this chapter, a CAD design of the MFRH was developed as an input for simulation. Thereafter, the kinematic and dynamic equations were derived. Then, these equations were used for DC servomotor selection. Various control techniques such as PID, Fuzzy, Fuzzy-PID and PSO-PID were carried out. The results and discussions would be provided in the next chapter.

CHAPTER 4

RESULTS & DISCUSSION

This chapter provides the results and discussion on PID, Fuzzy, Fuzzy-PID and PSO-PID based on the parameters given in chapter 3 for three different joints, i.e.

4.1 Results of Joint 1

The results of joint 1 are presented in Figures 4.1 to 4.4 for PID, Fuzzy, Fuzzy-PID and PSO-PID respectively. Figure 4.5 shows the comparative results of PID, Fuzzy, Fuzzy-PID, PSO-PID in a single diagram. The results are based on system performance metrics such as rise time (T_r), settling time (T_s), Percent overshoot (%OS). Detail discussion on the system performance metric is given in *Appendix F*.

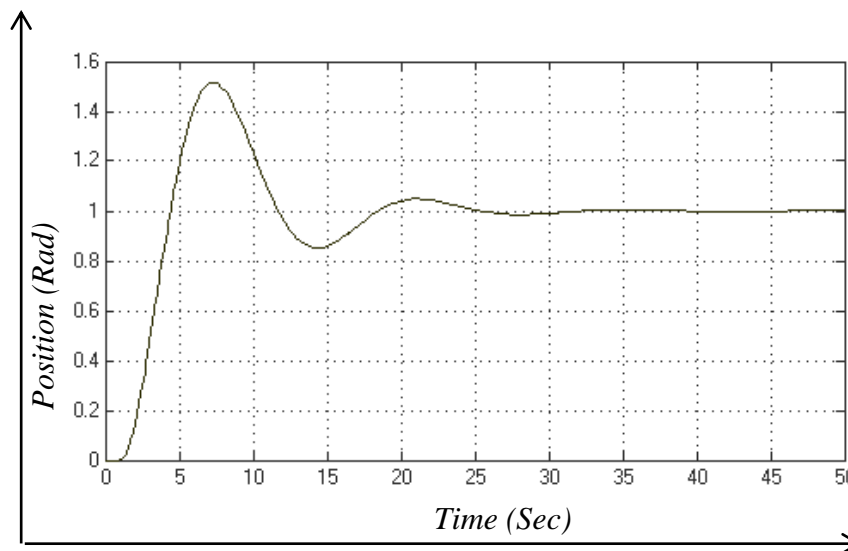


Figure 4.1: Step Response of Joint 1 using PID

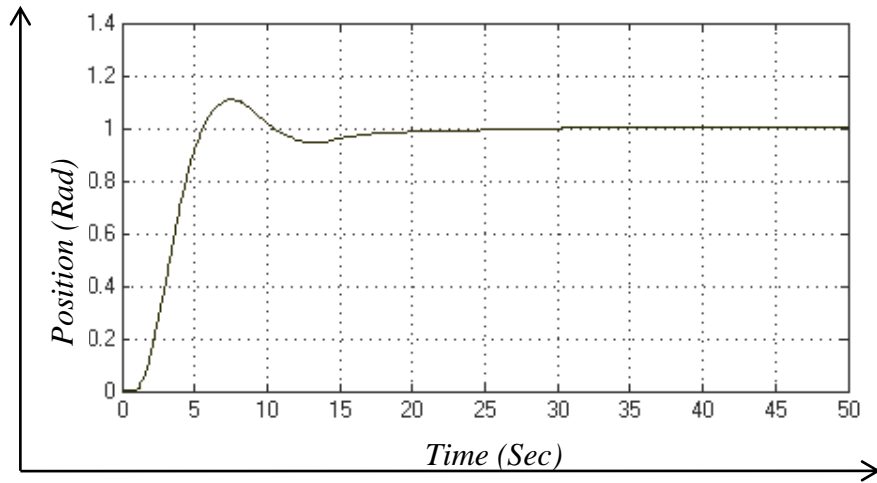


Figure 4.2: Step Response of Joint 1 using Fuzzy

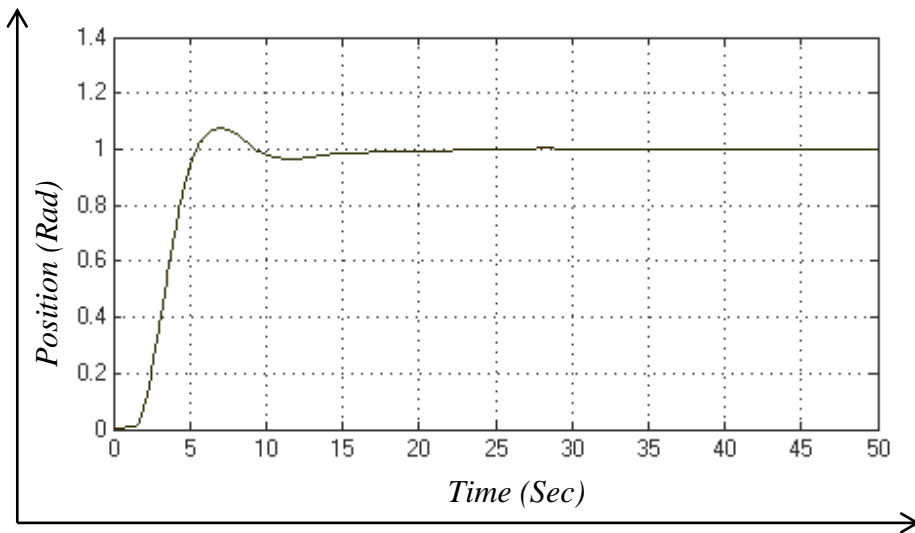


Figure 4.3: Step Response of Joint 1 using Fuzzy-PID

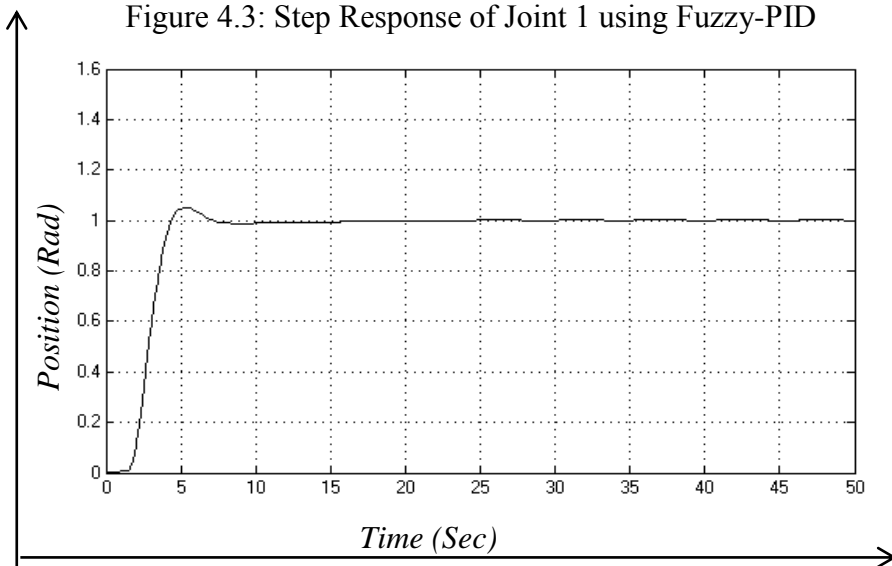


Figure 4.4: Step Response of Joint 1 using PSO-PID

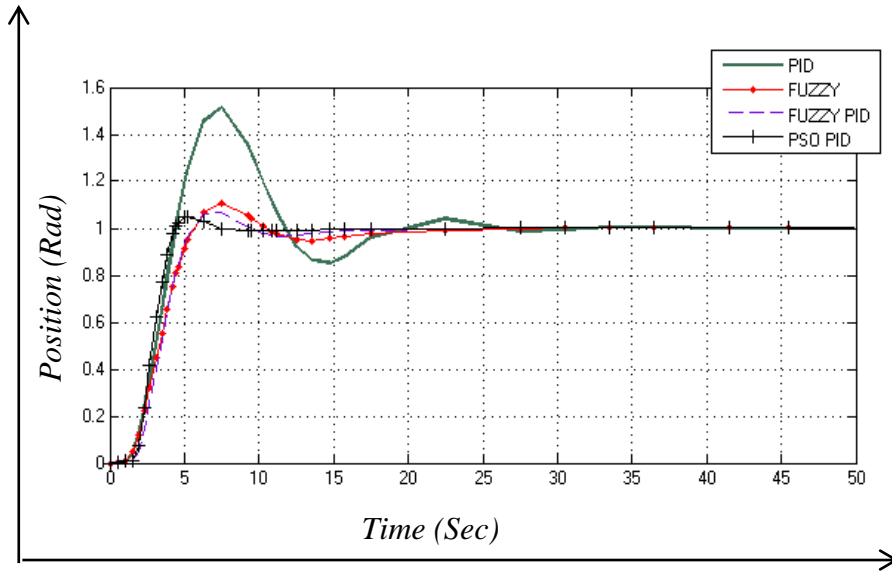


Figure 4.5: Step Response of Joint 1 using PSO-PID, Fuzzy-PID, Fuzzy and PID

The results of joint 1 as shown in Figure 4.5 for PSO-PID, Fuzzy-PID, Fuzzy and PID are given in Table 4.1.

Table 4.1: Results of Joint 1 using PSO-PID, Fuzzy-PID, Fuzzy and PID

Controller	Rise Time (T_r)	Settling Time (T_s)	Cmax	Overshoot (%OS)	Error	% (T_s) Improved	% Overshoot Improved
PSO-PID	4.7	9.6	1.07	7	0.07	60%	84.4%
Fuzzy-PID	4.8	12.5	1.08	8	0.08	43%	82.2%
Fuzzy	4.8	13.5	1.10	10	0.10	42.5%	77.7%
PID (Ref)	4.2	23.8	1.50	45	0.50	-	-

By comparing the four controllers, PSO-PID provides the best result in terms of settling time (T_s) and overshoot (%OS) are 9.6 and 7. Also the error is smallest, 0.07. This is followed by Fuzzy-PID with the settling time (T_s) and overshoot (%OS) of 12.5 and 8. Next is Fuzzy with the settling time (T_s) and overshoot (%OS) of 13.5 and 10. The percentage improvement of PSO-PID compared with PID (as a ref) is 60% for settling time (T_s) and 84.4% for percent overshoot. Fuzzy-PID improved by 43% for the settling time and 82.2% for overshoot. Then, Fuzzy improved the settling time and overshoot by 42.5% and 77.7%.

4.2 Results of Joint 2

The results of joint 2 are presented in Figures 4.6 to 4.9 for PID, Fuzzy, Fuzzy-PID, and PSO-PID respectively. Figure 4.10 shows the comparative results of PID, Fuzzy, Fuzzy-PID and PSO-PID in a single diagram.

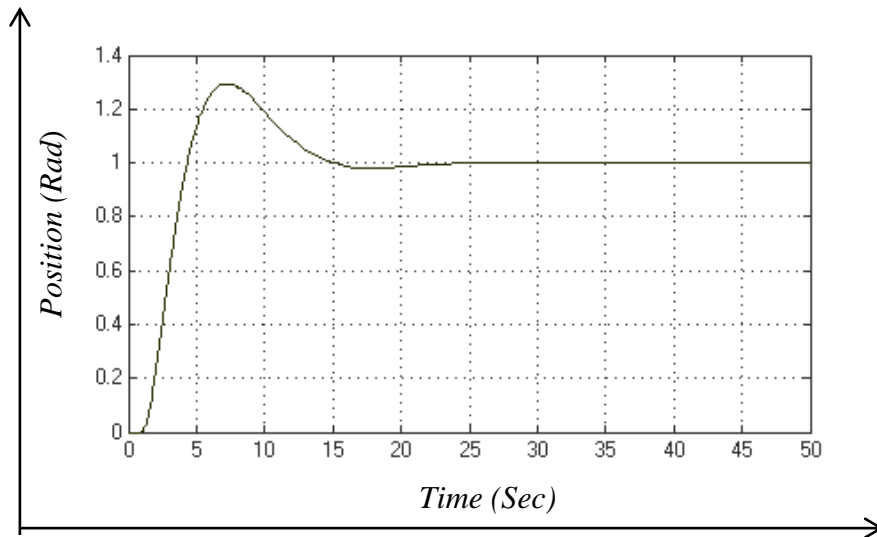


Figure 4.6: Step Response of Joint 2 using PID

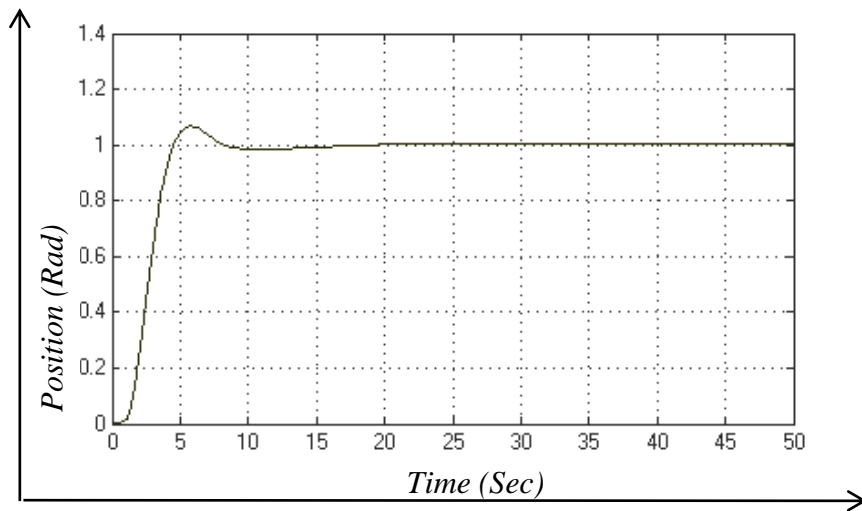


Figure 4.7: Step Response of Joint 2 using Fuzzy

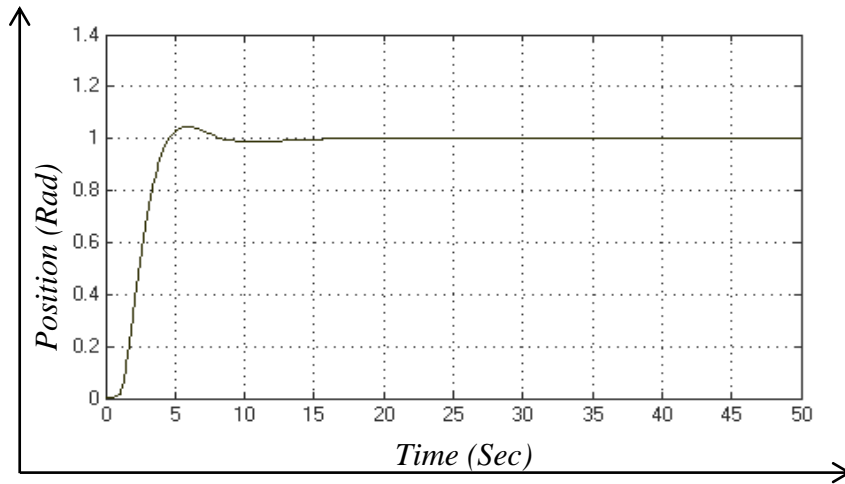


Figure 4.8: Step Response of Joint 2 using Fuzzy-PID

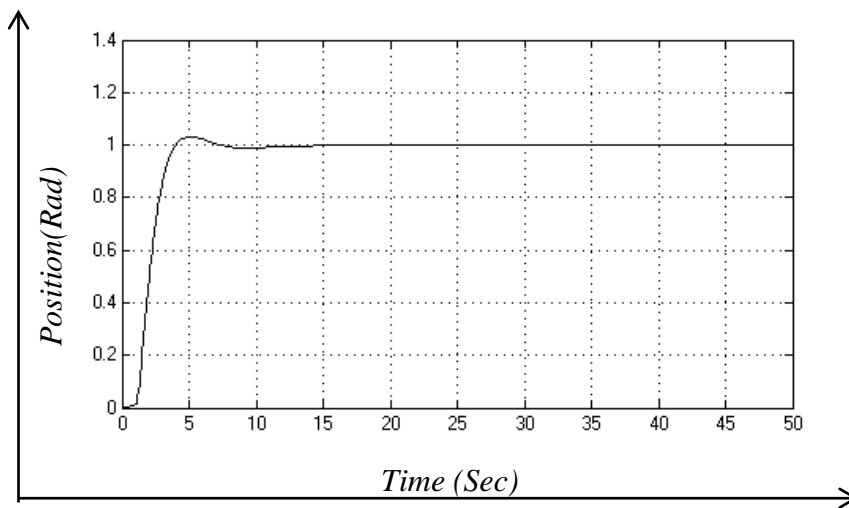


Figure 4.9: Step Response of Joint 2 using PSO-PID

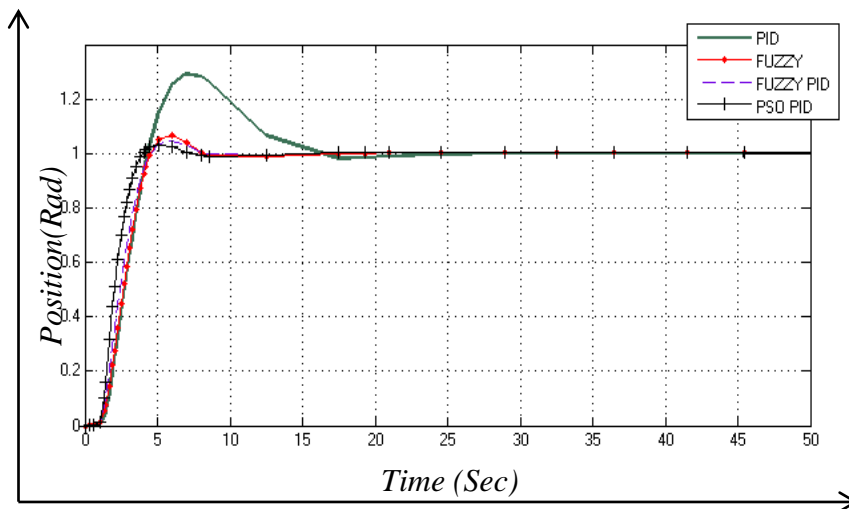


Figure 4.10: Step Response of Joint 2 using PSO-PID, Fuzzy-PID, Fuzzy and PID

The results of joint 2 as shown in Figure 4.10 for PSO-PID, Fuzzy-PID, Fuzzy and PID are given in Table 4.2.

Table 4.2: Results of Joint 2 using PSO-PID, Fuzzy-PID, Fuzzy and PID

Controller	Rise Time (T_r)	Settling Time (T_s)	Cmax	Overshoot (%)	Error	% (T_s) Improved	% Overshoot Improved
PSO-PID	2.60	7.0	1.02	2	0.02	51.7	93.3
Fuzzy-PID	3.64	7.2	1.05	5	0.05	50.3	83.3
Fuzzy	3.65	7.5	1.06	6	0.06	48.3	80.0
PID (Ref)	3.72	14.5	1.3	30	0.3	-	-

By comparing the four controllers, PSO-PID provides the best result in terms of settling time (T_s) and overshoot (%OS) are 7.0 and 2. Also the error is smallest, 0.02. This is followed by Fuzzy-PID with the settling time (T_s) and overshoot (%OS) of 7.2 and 5. Next is Fuzzy with the settling time (T_s) and overshoot (%OS) of 7.5 and 6. The percentage improvement of PSO-PID compared with PID (as a ref) is 51.7% for settling time (T_s) and 93.3% for percent overshoot. Fuzzy-PID improved by 50.3% for the settling time and 83.3% for overshoot. Then, Fuzzy improved the settling time and overshoot by 48.3% and 80%.

4.3 Results of Joint 3

The results of joint 3 are presented in Figures 4.11 to 4.14 for PID, Fuzzy, Fuzzy-PID, and PSO-PID respectively. Figure 4.15 shows the comparative results of PID, Fuzzy, Fuzzy-PID and PSO-PID in a single diagram.

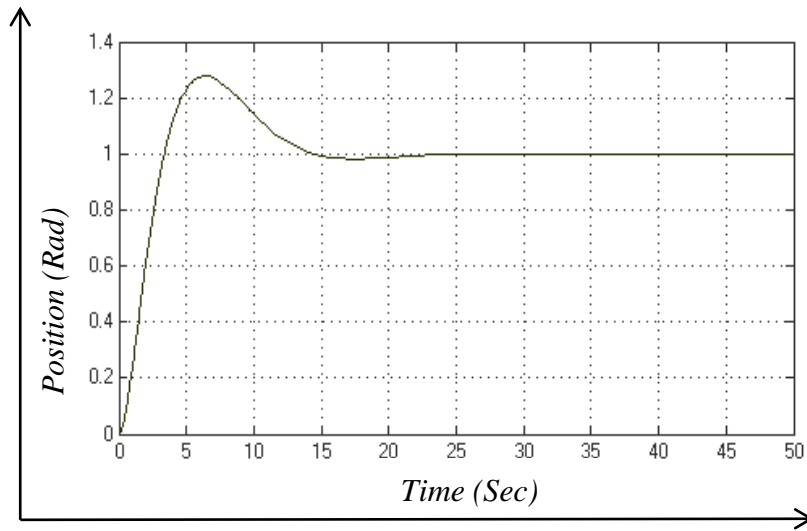


Figure 4.11: Step Response of Joint 3 using PID

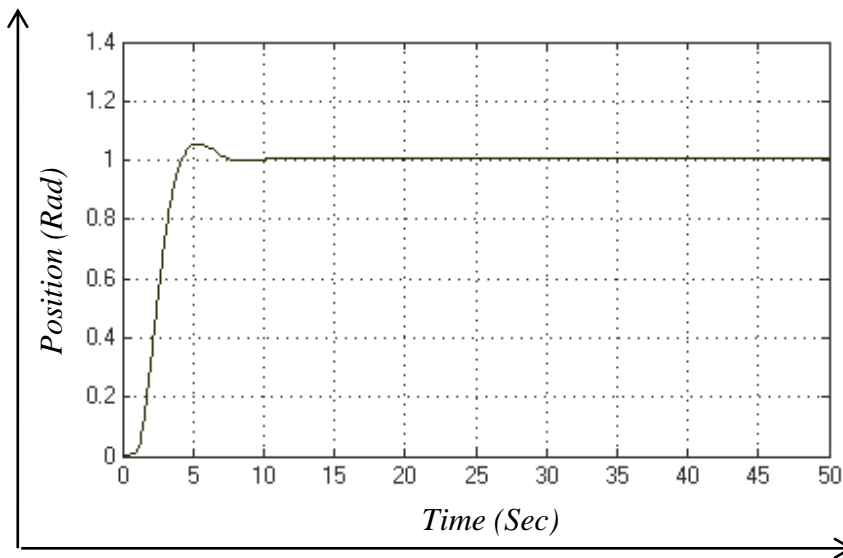


Figure 4.12: Step Response of Joint 3 using Fuzzy

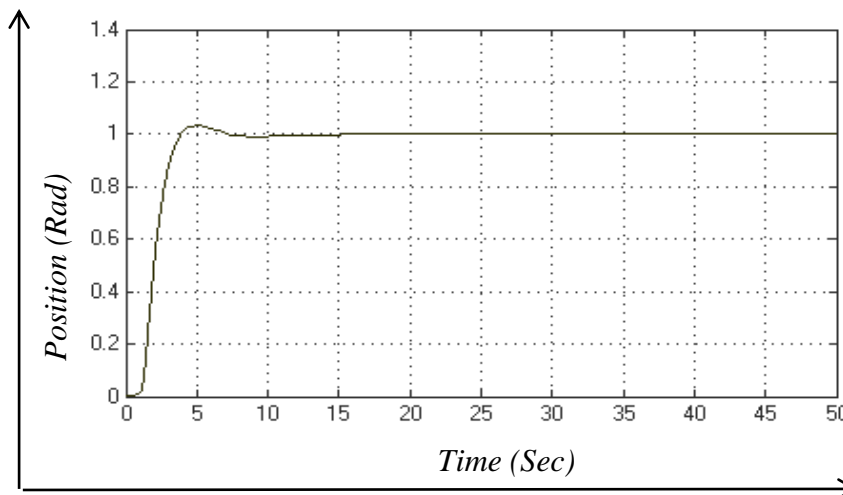


Figure 4.13: Step Response of Joint 3 using Fuzzy-PID

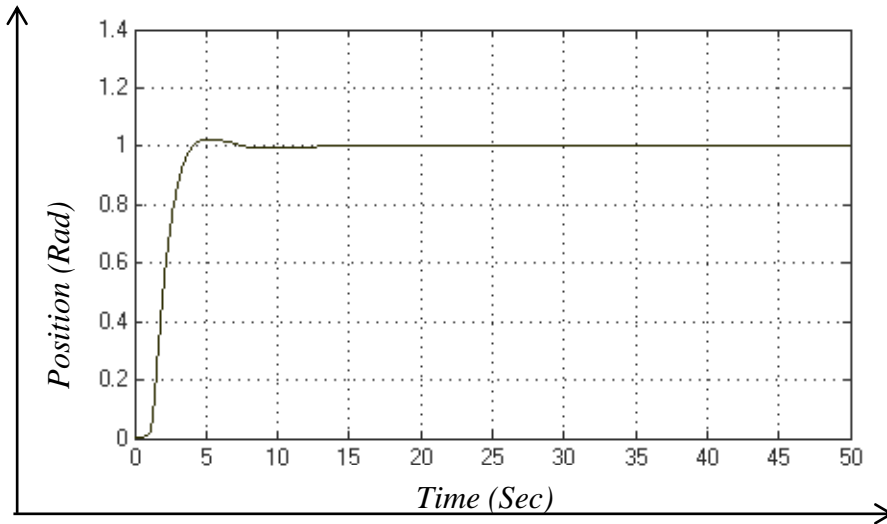


Figure 4.14: Step Response of Joint 3 using PSO-PID

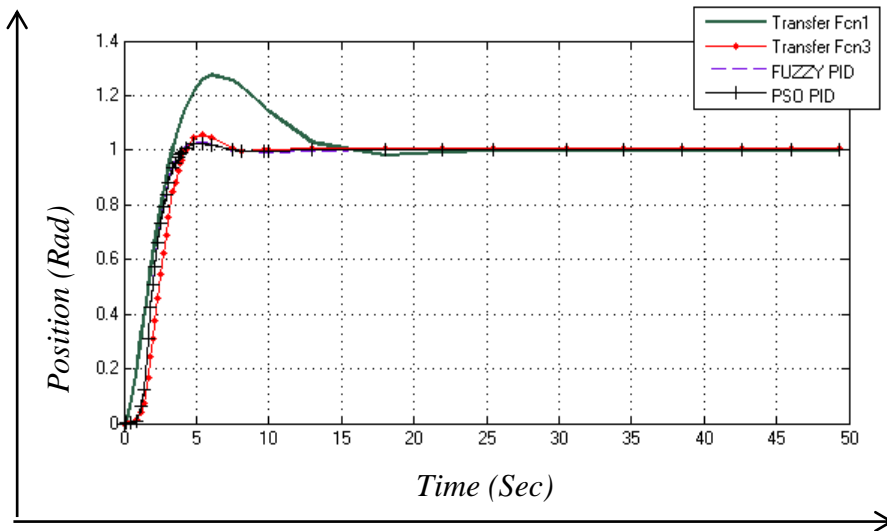


Figure 4.15: Step Response of Joint 3 using PSO-PID, Fuzzy-PID, Fuzzy and PID

The results of joint 3 as shown in Figure 4.15 for PSO-PID, Fuzzy-PID, Fuzzy and PID are given in Table 4.3.

Table 4.3: Results of Joint 3 using PSO-PID, Fuzzy-PID, Fuzzy and PID

Controller	Rise Time (T_r)	Settling Time (T_s)	Cmax	Overshoot (%)	Error	% (T_s) Improved	% Overshoot Improved
PSO-PID	3.29	5.1	1.01	1	0.01	64.1	96.4
Fuzzy-PID	3.30	5.2	1.02	2	0.02	63.4	92.8
Fuzzy	3.34	6.1	1.04	4	0.04	57	85.7
PID (Ref)	3.20	14.2	1.28	28	0.28	-	-

By comparing the four controllers, PSO-PID provides the best result in terms of settling time (T_s) and overshoot (%OS) are 5.1 and 1. Also the error is smallest, 0.01. This is followed by Fuzzy-PID with the settling time (T_s) and overshoot (%OS) of 5.2 and 2. Next is Fuzzy with the settling time (T_s) and overshoot (%OS) of 6.1 and 4. The percentage improvement of PSO-PID compared with PID (as a ref) is 64.1% for settling time (T_s) and 96.4% for percent overshoot. Fuzzy-PID improved by 63.4% for the settling time and 92.8% for overshoot. Then, Fuzzy improved the settling time and overshoot by 57% and 85.7%.

4.4 Discussion

Overall, it can be seen that for joints 1, 2 and 3, the PSO-PID provided the best results, followed by Fuzzy-PID, then Fuzzy with reference to PID in terms of settling time (T_s) and overshoot (%OS). The percentage improvement of PSO-PID compared with PID (as a ref) is and 60% for settling time (T_s) and 84.4% for percent overshoot for joint 1, percentage improvement of joint 2 is 63.4% % for settling time (T_s) and 93.3% for percent overshoot and percentage improvement of joint 3 is 64.1% for settling time (T_s) and 96.4% for percent overshoot.

Table 4.4 shows the proposed work have been compared with the past researchers.

Table 4.4: Comparative Analysis with Past Researcher

	Controller	Error	% (T_s) Improved	% Overshoot Improved
Proposed work	PSO-PID	0.01	64.1	96.4
	Fuzzy-PID	0.02	63.4	92.8
	Fuzzy	0.04	57.0	85.7
Mahmud [62]	PSO-PID	0.10	38.1	94.3
Shi [44]	Fuzzy-PID	0.01	54.8	87.5

The proposed work yielded improvement in terms of percent overshoot by 96.4 and settling time with 64.1% using PSO-PID compared to PID. Fuzzy-PID improved by 63.4% of the settling time and 92.8% of overshoot (T_s). Then, Fuzzy improved the

settling time and overshoot with 57% and 85.7%. The results by Shi[44] shows improvement of settling time and overshoot with 54.8% and 87.5 using Fuzzy-PID. Mahmud [62] also improved with 38.1% of settling time and 94.3% of overshoot. The results from the posposed work show that it is consistent with findings of Mahmud [62].

These results for joints 1, 2 and 3 shows that they could be used to control MFRH. The joint control system for 1 finger of MFRH is shown in figure 4.16.

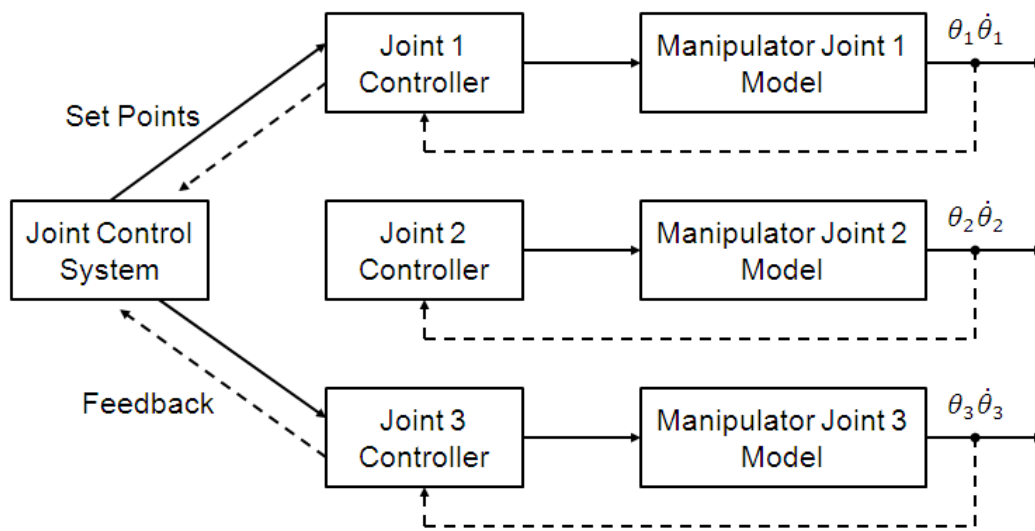


Figure 4.16: Joint Control System of 1 Finger [65]

Generally, from figure 4.16, it can be seen that the robot controller is a multi-input, multi-output (MIMO) system involving joint and end-effector locations, velocities, accelerations and force vectors. The typical robot control architecture for an n-DOF robot consists of a ‘Joint Control System’ as a master to control and synchronize n (1,2, 3) joints. This master control is responsible for sending ‘set-point’ commands to each of the joint controllers. The n joint controllers use the set point information command to each of the joint controllers. The joint controller employs a feedback of current joint position. It periodically gives feedback to the master controller.

The overall Control System for MFRH is shown in figure 4.17. This is also a MIMO system for the whole MFRH.

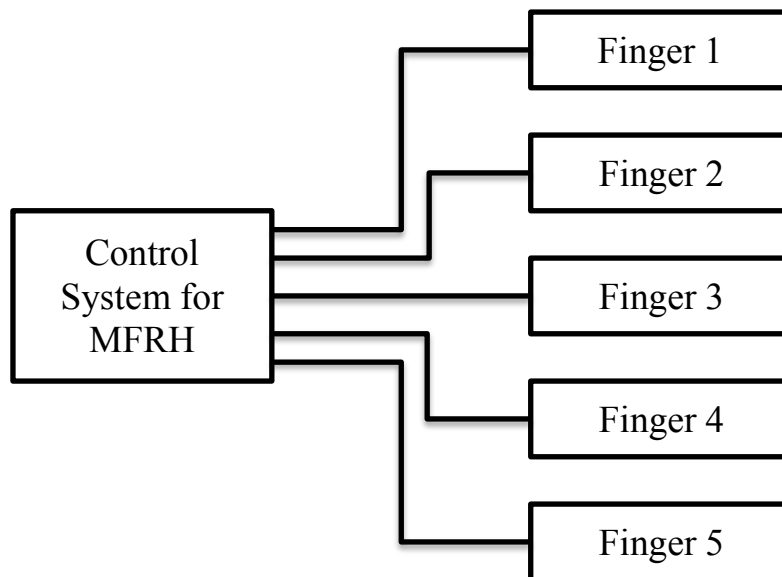


Figure 4.17: Control System for MFRH

Similar to figure 4.16, the controller in Figure 4.17 also acts as Master Controller to control and synchronize fingers 1 to 5 as a whole MFRH. It can be deduced that each finger is considered to be independent and separately controlled through the individual joints. The single-joint model is assumed to have a single input (set point) and a single output (location, velocity, etc). Hence, the n-DOF manipulator is modeled as n-independent single-input, single-output (SISO) control systems. The linear control technique for robot control is essentially an approximate method and for this a robot joint should be modeled as a linear second-order system. Servo control strategy was applied in this research where second-order linear system of the MFRH was analysed.

4.5 Summary

In this chapter, the results of control technique using PID, Fuzzy and PSO and table form are presented with detail discussions on the outcome. In chapter 5, the research summarized and the contribution made were discussed and evaluated. The outline is possible for future work.

CHAPTER 5

CONCLUSION

In this final chapter, all the material presented thus far on the modeling and control of Multi Fingered Robot Hand is brought together. First, the main achievements of the research reported in this thesis are evaluated. Initially, the research objectives are stated, then it presents the achievements on a chapter-by-chapter basis, followed by discussion of the research results, and finally, contributions with respect to the stated objectives are given. Next, some suggestions for future work are provided, and then conclude the thesis with the thoughts on the further development of Multi Fingered Robot Hand with infusion of advanced technologies.

5.1 Critical Evaluation of Achievements

In this section, it examines critically and assesses the achievements with respect to the research objectives of this thesis. First, for reader convenience, the research objectives are stated, and then it followed with the chapter-by-chapter discussion on how it met the objectives. In addition, by way of summary and to present a coherent picture, all the research is discussed in term of achievements and contributions in a single section.

5.1.1 Research Objectives

Recall from chapter 1 the current MFRH has limitations in terms of control techniques not able to meet required system performance. Specifically, derivation of equations of motion, most appropriate control techniques for position control motion were considered to be issues that need remedy. A new application of available control technique which encompasses the above aspects was identified as the potential solution to address the above issues.

Hence, the research has been focused to achieve the following crucial objectives:

- to develop a control techniques such as PID, Fuzzy, Fuzzy-PID and PSO-PID for position control;
- to improve system performance in terms of settling time and overshoot;
- to compare the system performance of the control techniques

5.1.2 Meeting the Objectives

In chapter 2, literature review of the technologies and techniques are provided for MFRH. This involved three important areas; mechanical design, sensing and control techniques. The literature review revealed published work to date shows the limitations of current control technique for MFRH. Hence, there was a need for research if one intended to improve the system performance.

In chapter 3, the modeling of MFRH, motor level control of MFRH, proposed model, position control for MFRH. The selection of DC servomotor is important in the development of position control technique of the MFRH. PID, Fuzzy Logic, and PSO are used to carry out the simulation for position control.

The results obtained for all the simulation work was provided in Chapter 4. In this chapter, the results in graphical and table form were presented with detail discussions on the outcome. The performance of the MFRH was measured based on parameters such as rise time, settling time and percent overshoot. (*See Appendix F for details*). In terms of Fuzzy Logic Controller, comparing two, three, five and seven membership functions, it was found that five membership functions produced a good response. The Fuzzy-PID Controller which a combination of PID and fuzzy logic controller showed improved performance compared to PID and Fuzzy Logic stand-alone controllers. However, the best results were obtained for PID tuned with PSO. The percentage improvement of PSO-PID compared with PID (as a ref) is and 60% for settling time (T_s) and 84.4% for percent overshoot for joint 1, percentage improvement of joint 2 is 63.4% % for settling time (T_s) and 93.3% for percent overshoot and percentage improvement of joint 3 is 64.1% for settling time (T_s) and 96.4% for percent overshoot.

5.2 Discussion

Recall that in chapter 1, the background and argued the case for introducing a new control technique to improve the performance of MFRH are placed. As the reader may remember, there are three important aspects of MFRH, i.e., mechanical design, sensing and control technique. Of these three, the control technique is the ready candidate for research since system performance need to be improved. Thus, in this thesis, the focus is on the improvement of control technique of MFRH.

To find out how others may have developed similar systems, an extensive literature review was undertaken. From the literature review, it was found that to-date, although many new technologies and techniques have emerged in the area of control techniques of MFRH, there are still limitations in some of the areas. Hence, research was necessary.

The focus of our research is the development of a Control Technique for MFRH. Thus, the research in the following areas was identified:

- to develop a control techniques such as PID, Fuzzy, Fuzzy-PID and PSO-PID for position control;
- to improve system performance in terms of settling time and overshoot;
- to compare the system performance of the control techniques

In this research, the position control technique using PID, Fuzzy Logic Controller and PSO was obtained. In addition, the research has produced promising results that could improve the performance of MRFH further.

5.3 Suggestions for Further Work

In this section, a few suggestions are presented for further research for MFRH which are involved:

- *Different Parameters*

Further work could explore the use of different set of parameters to improve further the system response of the MFRH.

- *Prototype Development*

Ultimately, a prototype needs to be developed to test the viability of the system. This will involve the development and integration of various sub-systems such as the mechanical design, sensing and control techniques.

5.4 Concluding Remarks

The work reported in this thesis has made a worthwhile contribution to ‘knowledge base’ in the field of robotics industry, particularly, MFRH through the results obtained, as summarized above.

REFERENCES

- [1] Murray, R.M, Li, Z and Sastry, S.S., A Mathematical Introduction to Robotic Manipulation, *CRC Press*, 1994.
- [2] Thayer, N and Priya, S, Design and Implementation of a Dexterous Anthropomorphic Robotic Typing (DART) Hand, *J. of Smart Mater*, vol. 20, no. 3, 035010 , pp. 1-12, 2011.
- [3] Kazuo Tanie: “Design of Robot Hands”, Industrial Robotics, Ed, S. y. Nof, John Wiley & Sons, pp.112-137, 1982.
- [4] Toshio Morita, Hiroyasu Iwata, Shingeki Sugano, “Human Symbiotic Robot Design based on Division and Unification of Functional Requirements”, *Proc. of the 2000 IEEE Int. Conf. on Robot. and Auto.*, vol. 3, pp. 2229-2234, 2000.
- [5] J. Butterfass, M.Grebenstein, H. Lieu, G. Hirzinger, “DLR-Hand II: Next Generation of Dexterous Robot Hand”, *Proc. of the 2001 IEEE Int. Conf. on Robot. and Auto.*, vol. 1, pp. 109-114, 2001.
- [6] Ikuo Yamano, Kenjiro Takemura and Takashi Maeno, “Development of Five – Fingered Robot Hand using Ultrasonic Motors and Elastic Elements”, *Proc. of the 2003 IEEE/RSJ Int. Conf. on Robots and Syst.*, vol.3, pp.2648-2653, Oct. 2003.
- [7] S.C. Jacobsen, E.K. Inversen, D.F. Knutti, R. T. Johnson and K.B. Biggers, “Design of the Utah/MIT Dexterous Hand, *Proc. of the 1986 IEEE Int. Conf. on Robot. and Auto.*, vol.3, pp 1520-1532, Apr. 1986.
- [8] C.S. Lovchic, M.A. Diftler: The Robonaut Hand: A Dexterous Robot Hand for Space, *Proc. of 1999 IEEE Int. Conf. on Robot. and Auto.*, pp. 907-912, 1999

- [9] Shadow Robot Company, <http://www.shadow.org.uk/product/newhand.sthtml>.
- [10] C.S. Lovchik, M.A.Diftler, "The Robonaut Hand : A Dexterous Robot Hand for Space", *Proc. of the 1999 IEEE Int. Conf. on Robot. & Auto., Detroit, Michigan*, pp. 907-912, 1999.
- [11] J.Butterfass, G.Hirzinger, S.Knoch, H.Liu, "DLR's Multisensory Articulated Hand. I. Hard- And Software Architecture", *Proc. of the 1998 IEEE Int. Conf. on Robot. & Auto., Leuven, Belgium*, pp. 2081 – 2086.
- [12] N.Fukaya, S.Toyama, T.Asfour, R.Dillmann, Design of the TUAT/Karlsruhe humanoid hand", *Proc. of the 2000 IEEE/RSJ Int. Conf. on Intel. Robots and Syst., Takamatsu, Japan*, pp. 1754 – 175, 2000.
- [13] L.R.Lin, H.P.Huang, "Integrating Fuzzy Control of the Dexterous National Taiwan University (NTU) Hand", *IEEE/ASME Trans. on Mechatronics*, Vol. 1, No. 3, Sept., 1996.
- [14] Roomba Robotic Floorvac, <http://www.roombavac.com>
- [15] Electrolux, <http://www.robotbooks.com/robot-vacuum.htm>
- [16] Samsung,http://www.samsung.com/DigitAll/GlobalExhibition/Exhibition/ppk/VC_RP30W/ppk_VC_RP30W_m01.htm
- [17] Asimo Special Site, <http://www.honda.co.jp/ASIMO>
- [18] Qrio, <http://www.sony.net/SonyInfo/QRIO>
- [19] Wakamaru,<http://www.sdia.or.jp/mhikobee/products/etc/robot.htm>
- [20] Y.Sakagami, R.Watanabe, C.Aoyama, "The Intelligent ASIMO: System Overview and Integration", *Proc. of the 2002 IEEE/RSJ Int. Conf. on Intel. Robots & Syst., EPFL, Lausanne, Switzerland*, pp. 2478-2483, 2002.

- [21] T. Ishida, Y. Kuroki, J. Yamaguchi, “Mechanical System of a Small Biped Entertainment Robot”, *Proc. of the 2002 IEEE/RSJ Int. Conf. on Intel. Robots & Syst.*, EPFL, Lausanne, Switzerland, pp.2478-2483, 2002.
- [22] Kyoung-Dae Kim, Yong K. Hwang, Won Sik Song, Manjai Lee, “Robotic Hand with Object-Manipulation and Emotion-Expression Capabilities, *Int. Conf. on Art. Reality & Telex.*, 2004.
- [23] Lovchik, C. “The robonaut hand: A dexterous robot hand for space”, *Proc. of the IEEE Int. Conf. on Robot. & Auto.*, vol. 2, pp. 907-912, (1999).
- [24] ROBONAUT, <http://robonaut.jsc.nasa.gov/>
- [25] Emily Tai, “Design of an Anthropomorphic Robotic Hand for Space Operations”, University of Maryland, pp.1-80, 2007.
- [26] Shadow Robot Company, <http://www.shadow.org.uk/product/newhand.shtml>, June 2009.
- [27] Ikuo Yamano and Takashi Maeno, Barcelona, Spain, “Five –Fingered Robot Hand using Ultrasonic Motors and Elastic Elements”, *Proc. of the 2005 IEEE Int. Conf. on Robot & Auto.*, pp. 2673-2678, April 2005.
- [28] ROBOT PORTAL, <http://mindtrans.narod.ru/hands/hands.htm>
- [29] AUTOMATION AND ROBOTICS,
<http://www.soton.ac.uk/~rmc1/robotics/artactile.htm>
- [30] WIKIPEDIA, http://en.wikipedia.org/wiki/PID_controller
- [31] Dong Hwa Kim, and Jae Hoon Cho, “Robust Tuning of PID Controller Using Bacterial-Foraging-Based Optimization”, *J. of Advanced Computational Intel.*, vol.9 No.6, pp. 669-676, 2005.

- [32] Abílio Azenha, “Automatic PID Controller Tuning for Robots with Nonlinear Friction at the Joints”, *Dept. of Elec. & Comp. Eng., Facul. of Eng., Univ of Porto, Rua Dr. Roberto Frias, 4200 – 465, Porto, Portugal*, pp.1-6, 2002.
- [33] Ming-Tzu Ho and Yi-Wei Tu, “PID Controller Design for a Flexible-Link Manipulator”, *44th IEEE Conf. on Decision. and Contr. & the European Contr. Conf.*, pp. 6841-6846, 2005.
- [34] Youngjin Choi and Wan Kyun Chung, PID “Performance Tuning Methods For A Robotic manipulator Based on ISS”, *Asian J. of Control*, vol. 5, No. 2, pp. 206-216, June 2003.
- [35] Jose Alvarez-Ramirez and Ilse Cervantes” PID Regulation of Robot Manipulators with Elastic Joints”, *Asian J. of Contr.*, vol. 5, No. 1, pp. 32-38, Mar. 2003.
- [36] Mehmet Haklidir & Isa Tasdelen, “Modeling, simulation and fuzzy control of an anthropomorphic robot arm by using Dymola”, *J. of Intel. Manu.* vol. 20, No. 2, pp.177-186, 2009.
- [37] Erbatur, K., Kaynak, O. & Rudas, I., “Fuzzy identifier based inverse dynamics control for a 3-dof articulated manipulator”, *Proc. of IEEE 23rd Int. Conf. on Indus. Electron. Contr. & Instr.*, New Orleans, USA vol. 3, pp. 1052–1056, Nov. 10–14, 1997.
- [38] Erbatur, K., Kaynak, O., & Rudas, I., “An inverse dynamics based robot control method using fuzzy identifiers”, *AIM’97, Conf.on Advances in Intel. Mecha.*, Jun. 16–20, Tokyo, Japan, 1997.
- [39] Lionel Birglen and Clement M. Gosselin, “Fuzzy Enhanced Control of an Underactuated Finger Using Tactile and Position Sensors”, *Proc. of the 2005 IEEE Int. Conf. Robot. and Auto. (ICRA)*, Apr. 18-22, 2005.
- [40] N.I Glossas and N.A Aspragathos, “Fuzzy logic grasp control using tactile sensors”, *Mecha. J. of Elsevier*, vol. 11, no.7, pp. 899-920, Oct. 2001.

- [41] Carlos Pérez, Oscar Reinoso, M. Asunción Vicente “Robot hand visual tracking using an adaptive fuzzy logic controller”, *WSCG POSTERS proc.*, Feb. 2-6, 2004.
- [42] Steven M. Spano & Nicholas Bourbakis, “Implementation of a Multi-Fingered Robotic Hand Using a Method of Fuzzy Blocks”, *Proc. of the IEEE Int. Joint Symposia on Intel. & Syst.*, pp. 262-267, 1998.
- [43] S. G. Anavatti and S. A. Salman, “Fuzzy + PID Controller for Robot Manipulator”, *Int.Conf. on Comp. Intel. for Modelling Contr. and Auto.& Int. Conf. On Intel. Agents, Web Techno. and Inter. Commerce (CIMCA-IAWTIC'06)*, 2006.
- [44] Aiping Shi, Maoli Yan, Jiangyong Li, Weixing Xu, Yunyang Shi, “The Research of FUZZY PID Control Application in DC Motor of Automatic Doors”, “*International Conference on Electrical and Control Engineering (ICECE)*, 2011.
- [45] WIKEPEDIA, http://en.wikipedia.org/Neural_networks.
- [46] H. Daniel Patiño, “Neural Networks for Advanced Control of Robot Manipulators”, *IEEE Trans.on Neural Networks*, vol.13, no. 2, pp. 343 – 354, Mar 2002.
- [47] Danica Janglová, “Neural Networks in Mobile Robot Motion”, Janglová, D. / Neural Networks in Mobile Robot Motion, *Int. J. of Advanced Robot. Syst.*, ISSN 1729-8806 vol. 1, no. 1, pp. 15-22, 2004.
- [48] Magnus Johnsson and Christian Balkenius, “Neural network models of haptic shape perception”, *J. of Robotic & Autonomous Syst.* 55, pp.720–727, 2007.
- [49] E.A. Al-Gallaf, “Neural Networks for Multi-Finger Robot Hand Control”, *JKAU: Eng. Sci.*, Vol. 19 No. 1, pp.19-42, 2008.
- [50] WIKEPEDIA, http://en.wikipedia.org/Genetic_Algorithm.
- [51] M. N. H. Siddique and M. O. Tokhi J, “GA-based Neural Fuzzy Control of Flexible-link Manipulators”, *Proc. of the 2002 Int. Conf. on Contr. App.*, 2002.

- [52] Bahaa Ibraheem Kazem, Ali Ibrahim Mahdi, Ali Talib Oudah, “Motion Planning for a Robot Arm by Using Genetic Algorithm”, *Jordan J. of Mechanical. and Indus. Eng.*, Vol. 2, No, pp. 131-136, Sep. 2008.
- [53] N. Nahapetian, M.R. Jahed Motlagh, M. Analoui F, “PID Gain Tuning using Genetic Algorithms and Fuzzy Logic For Robot Manipulator Control”, *Int. Conf. on Advanced Comp. Contr.*, pp. 346-350, 2008.
- [54] Hamid Boubertakh, Mohamed Tadjine, Pierre-Yves Glorennec and Salim Labiod, “Tuning Fuzzy PID Controllers using Ant Colony Optimization”, *17th Mediterranean Conf.on Contr. & Auto. Makedonia Palace*, Thessaloniki, Greece June 24 - 26, 2009.
- [55] Leandro dos Santos Coelho and Diego Luis de Andrade Bernert, “A modified ant colony optimization algorithm based on differential evolution for chaotic synchronization”, *J. of Expert Syst. with App.*, vol. 37, pp. 4198–4203, 2010.
- [56] WIKEPEDIA,http://en.wikipedia.org/wiki/Ant_colony_optimization_algorithms
- [57] Zafer, A Fuzzy Logic Controller tuned with PSO for 2 DOF robot trajectory control, *J. of Expert Syst. with App.*, vol. 38, pp. 1017–1031, 2011.
- [58] B. Nagaraj, P. Vijayakumar “A Comparative Study Of Pid Controller Tuning using GA, EP, PSO AND ACO”, *J. of Auto., Mobile Robotics & Intel. Systems*, Vol. 5, No. 2, pp. 42-48, 2011.
- [59] Mehdi Nasri, Hossein Nezamabadi-pour, and Malihe Maghfoori, “A PSO-Based Optimum Design of PID Controller for a Linear Brushless DC Motor”, *Proc. of World Academy of Science, Eng. and Techno*, pp. 211-215 vol. 26, 2007.
- [60] S.M.GirirajKumar, Deepak Jayaraj and Anoop.R.Kishan “PSO based tuning of a PID controller for a High”, *Int. J. of Comp. App. (0975 - 8887)*, vol. 1, No. 19, pp. 12-18 2010.

- [61] Mahbubeh Moghadas, Mohammad Reza Dastranj, Nemat Changizi, M Odjata Rouhani, "PID Control of DC motor using Particle swarm Optimization (PSO) Algorithm", *The J. of Math. & Comp. Science*, vol .1, no.4, pp. 386-391, 2010.
- [62] Mahmud Iwan Solihin, Lee Fook Tack and Moey Leap Kean, "Tuning of PID Controller Using Particle Swarm Optimization (PSO)", *Proceeding of the International Conference on Advanced Science, Engineering and Information Technology*, 2011.
- [63] Boumediène Allaoua, Brahim Gasbaoui And Brahim Mebarki, "Setting Up PID DC Motor Speed Control Alteration Parameters Using Particle Swarm Optimization Strategy", *Leonardo Electron. J. of Practices and Technologies*, ISSN 1583-1078, no. 14, pp. 19-32, Jan-Jun 2009.
- [64] Bundhoo, V., Park, E. J., "Design of an Artificial Muscle Actuated Finger towards Biomimetic Prosthetic Hands", *12th Int. Conf. on Advanced Robot. ICAR Seattle*, pp. 368-375, Jul 18-20, 2005.
- [65] <http://ctms.engin.umich.edu/CTMS/index.php?example=MotorSpeed§ion=SystemModeling>
- [66] M.W. Spong, "Motion Control of Robot Manipulators", in *Handbook of Control*, W. Lavine, editor, *CRS Press*, pp. 1339-1350, 1996.
- [67] Mohammad Mehdi Fadeh, "On the Voltage-Based Control of Robot Manipulators", *Int. Journal of Control, Automation and Systems*, vol.6 no.5, pp.702-712, October 2008.
- [68] WIKEPEDIA, http://en.wikipedia.org/wiki/PID_controller
- [69] Y. Yavin, "Control of a Three-Link Manipulator with a Constraint on the Velocity of its End-Effector", *Elsevier J. of Comp. and Math. with App.*, vol.40, no. 10–11, pp. 1263–1273, Nov–Dec 2000.

- [70] Asim Ali Khan, Sant Longowal, Longowal and Nishkam Rapal and Guru Nanak, “Fuzzy PID Controller: Design, Tuning and Comparison with Conventional PID Controller”, *Proc. of the 2006 IEEE Int. Conf. on Eng. of Intel. Syst.*, 2006.
- [71] Michael Negnevistsky, “Artificial Intelligent: A Guide to Intelligent Systems”, *Addison Wesley*, Second Edition, 2005, ch. 4, sec. 4.1, pp. 87-89.
- [72] WIKEPEDIA, http://en.wikipedia.org/wiki/Particle_swarm_optimization.
- [73] S.M.GirirajKumar, Deepak Jayaraj, Anoop.R.Kishan, “PSO based tuning of a PID controller for a High performance drilling machine”, *Int. J. of Comp. App.*, pp. 12-18, vol. 1, no.19, 2010.
- [74] Nelendran Pillay, “A Particle Swarm Optimization Approach For Tuning Of SISO PID Control Loops”, *Dept. Elect. & Electronic, Durban Uni. Technology*. pp. 1-182, 2008.
- [75] Elumotion Ltd, <http://www.elumotion.com/>
- [76] Byungjune Choi, Sanghun Lee and Hyouk Ryeol Choi and Sungchul Kan, “Development of Anthropomorphic Robot Hand with Tactile Sensor: SKKU Hand II”, *Proc. of the 2006 IEEE/RSJ Int. Conf. on Intel. Robots and Syst*, pp. 253-270, Oct. 9 - 15, 2006.
- [77] Institute Robotic and Mechatronics,
<http://www.dlr.de/rm/en/desktopdefault.aspx/tabid-3761/>
- [78] Kenji KANEKO, Kensuke HARADA, and Fumio KANEHIRO, “Development of Multi-fingered Hand for Life-size Humanoid Robots”, *Proc. of the IEEE Int. Conf. on Robot. & Auto.*, 10-14 April 2006.
- [79] Man Zhilong, *Robotic for Computer Engineering Student*, *Prentice Hall*, Singapore, ch. 2, sec. 2.3, pp. 41-45, 2004.

LIST OF PUBLICATIONS

- [1] Wan Faizura Wan Tarmizi, and Irraivan Elamvazuthi and Mumtaj Begam, “Development of Multi-Fingered Robot Hand: A proposal”, *National Postgraduate Conference on Engineering, Science and Technology (NPC2009)*, Tronoh, Malaysia, March 23-24, 2009.
- [2] Wan Faizura Binti Wan Tarmizi, Irraivan Elamvazuthi and Mumtaj Begam, “Mathematical Modeling of a Multi-fingered Robot Hand (MFRH)”, *2nd International Conference and Workshop on Basic and Applied Sciences & Regional Annual Fundamental Science Seminar 2009 (ICORAFSS 2009)*, Johor Bahru, Malaysia, June 2-4, 2009.
- [3] Wan Faizura Binti Wan Tarmizi, Irraivan Elamvazuthi and Mumtaj Begam, “Kinematic and Dynamic Modeling of a Multi-Fingered Robot Hand”, *International Journal of Basic & Applied Sciences IJBAS 2009*, vol. 9. No. 10, pp. 89-96, ISSN 2077-1223, 2009.
- [4] Wan Faizura Binti Wan Tarmizi, M. Azmi Adly Bin Abd. Majid @ Razi, Wan Amirfaiz Bin Wan Daud, Irraivan Elamvazuthi and Mumtaj Begam, “Modeling and Simulation of a Multi-Fingered Robot Hand”, *International Conference on Intelligent and Advanced Systems (ICIAS 2010)*, Kuala Lumpur, Malaysia.15-17 June, 2010.
- [5] Wan Faizura Wan Tarmizi, I. Elamvazuthi and K.M. Begam, W. Amirfaiz and M. Azmi Adly, “Hybrid Controller for Multi-Fingered Robot Hand”, *International Conference on Robotic Automation System (ICORAS 2011)*, Kemaman, Terengganu, Malaysia, May 23-24, 2011.

APPENDIX A
ADDITIONAL INFO OF MFRH

A-1 MFRH using Motor Design

The Barrett hand [25] is also non-anthropomorphic manipulator with considerable grasp capabilities. Barrett hand is also in motor design. The advantages of Barrett hand is to factory usage, highly programmable, three fingered, eight-axis and reconfigurable “grasper”. The Barrett hand has three articulated fingers as shown in Figure A-1 and a palm which act in concert to trap the target object firmly and securely within a grasp consisting of seven coordinated contact vectors — one from the palm plate and one from each link of each finger. Each finger of Barrett hand is controlled one of three servomotors. Each of the three finger motors must drive two joint axes.



Figure A-1: Barrett Hand [28]

Another robotic hand design using motor is Salisbury hand [25] as shown in Figure A-2. It was developed by Kenneth Salisbury as part of his doctoral desertion. Unlike Robonaut hand, Salisbury does not use an anthropomorphic design. The hand in its place consists of three configured with one in opposition, providing a stable spherical grasp. The hand also has three DOF and is actuated by Teflon-coated cable driven by remotely located servomotor. Salisbury hand is consisted with tendon sensors, motor position, encoder and six fingertip force torque sensors for tactile

sensor operations. The purpose of designing this robot is making more grasp types possible. Thus, the distal joint of each finger has a wider range of motion than the human joint to help compensate for the fewer total degrees of freedom.

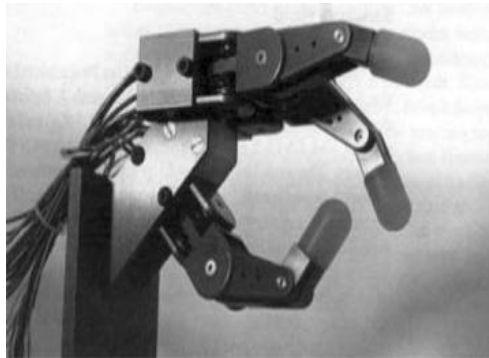


Figure A-2: Salisbury Hand [25]

The DLR (Deutsches Zentrum für Luft-undRaumfahrt) II Hand is an anthropomorphic dexterous grasping and manipulation system and design use motor as shown in Figure A-3. The hand was designed by Grebenstein et al. [61] at Institute of Robotics and Mechatronics. It is divided into four identical fingers with each finger having four joints and three degree of freedom. One of the fingers has an additional degree of freedom connected with the palm to adjust stability of the grasp. This robot has a complete integration of actuation systems consisting of sensors and electronics in the hands that can lead to maximum flexibility and enables easy interfacing with other robots.

The aim of this robot was designed is to produces fine manipulation to give improvement of the grasping performance in case of precision and power-grasp. Hence, the design of the Hand II was and fine-manipulation requires a large area junction range of motion and opposition of thumb and ring finger. Therefore, the design of Hand II also has an additional minor degree of freedom which enables to use the hand in two different alignments. This system uses a slow motion type of degree of freedom to decrease weight and complexity. It only use one brushed dc motor using a spindle to control the motion of the first and fourth finger.



Figure A-3: DLR II Hand [28]

Although the designs and actions, such as human hands, but the robot hand must first identify the objects that are not known for its reaction to either hold or grasp. As an example of actions the robot hand is opened and closed the door and drawer, the device operation and use of tools. Thus, the human hand is a source of reference in designing of the DLR anthropomorphic robot as a universal dexterous grasping and manipulation tool for service robotics.

Figure A-4 shows an anthropomorphic robot based on motor design is Elu2-Hand [75]. This robot was developed by Elumotion Ltd. The robot is human-scale anthropomorphic robot hand can reach a real hand movement at speeds similar to humans. This makes it ideal Elu2-hand to interact with people and also many kinds of tools and objects in our environment is designed around the ergonomics of human hands. The Elu2-hand has nine degrees of freedom servo-driven in the volume of the hand. Hands reached actuations of life as much through movement-related, such as cover your hands and flexible combination of books. Although originally designed to meet the design Elu2-Hand compact means may be installed on many different robot arms.

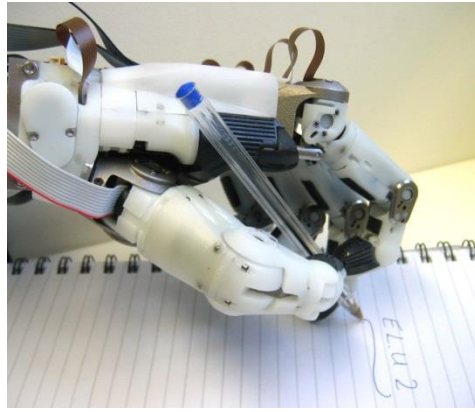


Figure A-4: Elu2-Hand [75]

The Elu2-Hand [75] has been planned for power, precision and reliability of the use of plastic-metal hybrid construction for light weight combined with strength and endurance. Elu2 hands have large areas that support pad line soft hands to manipulate objects, and in his interaction with people; pads also provide a potential for tactile sensing. Efficient delivery of back-Drivable finger allows the use of motor-current to indicate the joint torque. Besides, every degree of freedom has the potential for ultra-reliable non-contact sensing the absolute limit switches provide redundancy and additional positions for important security applications. The powerful and compact Elu2-Hand has been using a lot of possibilities start from research to medical applications.

Among the anthropomorphic robot hand is SKKU Hand II [76] is shown in Figure A-5. The driving circuits of SKKU Hand II are embedded, and it can interact with others using CAN protocol. It has a miniaturized tactile sensor related to the robot hand. The robot is designed with the motor base. It is driven by a DC motor built-in fingertip tactile sensor which can detect contact normal force. The slip of tactile sensor is consisting of two organic materials polyvinylidene fluoride (PVDF) is known as the piezoelectric polymer, and the pressure variable resistor ink. The robot uses a motor control board of the PIC 16f458 to check the condition of the motor in real time.

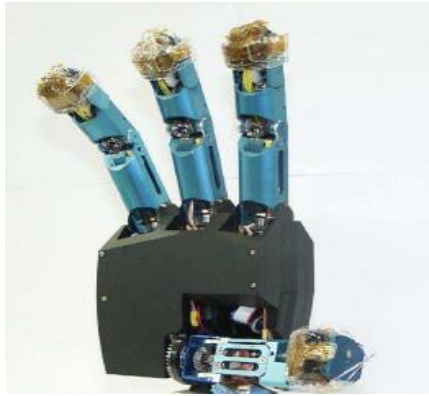


Figure A-5: SKKU Hand II [28]

MAI-hand [77] is an anthropomorphic robot that designed using motor as shown in Figure A-6. It was designed and built at the Institute of Industrial and Control Engineering (IOC) at the Polytechnic University of Catalonia (UPC). The hand has four fingers with 16 degree of freedom that forms part of an integrated system for the experimentation and testing of object grasping and manipulation strategies. The control system of MA-I consists 16 position control loops, independently controlling each of the 16 DC motors. The advantage of this hand is easy coupling decoupling with any robot arm. For future work related with MA-I are teleoperation using a sensorized globe with haptic capabilities, teleoperation using a graphic simulator of the hand-arm ensemble and inclusion of vision feedback in the teleoperation.

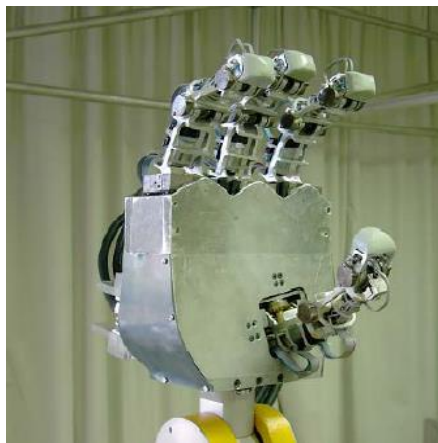


Figure A-6: Robotic Hand MA-I [77]

One of the advanced anthropomorphic robotic hands is development of a multi-fingered robot hand can be attached to life size humanoid hand. This robot is designed based on the motor design as shown Figure A-7. The hand design is

controlled by with I/O, motor drivers, and amplifiers for 6-axes force sensors are also newly developed. The advantage of development of a multi-finger robot hand is to operate a grasped object with 3-axes translational motion and 3-axes rotational motion redundantly; at least 3 finger modules with 3 DOF are required [78]. The hand is developed by Kenji et al that have four fingers, which consists of 13 active joints and 4 linked joints. Each finger has four joint including 3 active joints and 1 linked joint. The joints are consisted of DIP, PIP and MCP joints. DIP joint works together with PIP joint. The pitch axis of MP joint of finger module enables adduction and abduction. Although the hand with five fingers is human-like, it may become bigger. Finally, the aim of this robot hand is to realize the hand with from 3 to 5 fingers.

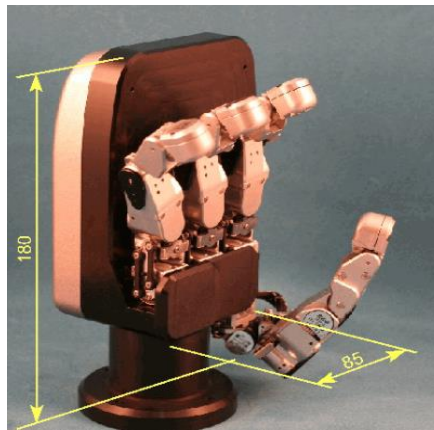


Figure A-7: Kenji Robot Hand [78]

Figure A-8 shows the non-anthropomorphic robotic hands is SSL hand [25] that has been designed four fingers for EVA application at Space System Lab. Three fingers assembled in a resisting configuration are optimized for cylindrical grasp and fought grasping finger provides additional stability.



Figure A-8: SSL Hand [25]

The hand design has four joints and three DOFs with distal and middle that joint together by indicate a four-bar linkage. The SSL Hand operates a tendon drive system in combination with passive spring return. Actuators are not incorporated into full design at the current development state.

Table A-1: Categories of Design of Robot Hand

Categories of Design	NF	ND	Type of Robot	Robot Hand
Motor design	5	12	Anthropomorphic	Robonaut Hand
Motor design	4	16	Non-anthropomorphic	Barrett Hand
Motor design	3	9	Non-anthropomorphic	Salisbury Hand
Motor design	4	12	Anthropomorphic	DLR II Hand
Motor design	5	9	Anthropomorphic	Elu-2 Hand
Motor design	4	10	Anthropomorphic	SKKU Hand II
Motor design	4	16	Non-anthropomorphic	MAI-Hand
Motor design	4	12	Anthropomorphic	Kenji Robot Hand
Air-muscle	5	21	Anthropomorphic	Shadow Hand
Prosthetic design	5	15	Anthropomorphic	Cyber Hand
Four bar linkage	5	16	Anthropomorphic	Gifu Hand III
Four bar linkage	4	12	Non-anthropomorphic	SSL Hand
Ultrasonic motor with elastic element	5	20	Anthropomorphic	Ikuo Robot Hand
Pneumatic	4	16	Anthropomorphic	Utah/MIT Hand

A-3 Example of MFRH: Shadow Robot Hand

The Shadow Dextrous Hand is an advanced humanoid robot hand system that provides 24 movements to reproduce as closely as possible the degrees-of- freedom of the human hand. It has been designed to provide comparable force output and movement sensitivity to the human hand. The model C6M Hand uses Shadow's electric "Smart Motor" actuation system, rather than the pneumatic Air Muscle actuation system of other Dextrous Hand systems. The "Smart Motor" integrates force and position control electronics, motor drive electronics, motor, gearbox, force sensing and communications into a compact unit. The Shadow Dextrous Hand is a

self-contained system – all actuation and sensing required is built into the Hand.

The Shadow Dextrous Hand system incorporates all necessary control systems (software provided under GNU GPL) and documentation for research and teaching purposes. Shadow Hand systems have been used for research in grasping, manipulation, neural control, and hazardous handling.

Dimension

The Hand has been designed to be as similar as possible to the average male hand. The fingers are all the same length, although the knuckles are staggered to give comparable fingertip locations to the human hand.

Weight

The Hand system, (Hand, sensors, and all motors) has a total weight of 4 kg.

Speed

Movement speed is dependent on safety settings in the force control system. Typically you can expect a full-range joint movement to operate at a frequency of up to 2 Hz.

Material

The entire system is built with a combination of metals and plastics.

- Forearm: Aluminium, resin shell.
- Palm: Acetyl, aluminium, polycarbonate.
- Fingers: Acetyl, aluminium, polycarbonate fingernails and polyurethane flesh.

Control and Actuation

- Power Consumption
- The C6M Dextrous Hand is designed to use motor technology.
- Electronics: 0.7 A @ 8 V. Motors: 2 A max @ 24 V.
- Separate power supplies are provided with the Hand.

Actuation

The Hand is driven by 20 Smart Motor units mounted below the wrist which provide compliant movements. Following the biologically-inspired design principle, a pair of tendons couple each Smart Motor to the corresponding joint of the Hand. Integrated electronics in the Smart Motor unit drives a high-efficiency rare-earth motor, and also manages corresponding tendon force sensors. The Smart

Motor unit is designed to ensure that the system is safe at all times. It monitors tendon forces and keeps them within defined limits, preventing the Hand from over-gripping objects. Motor temperature management prevents overheating of individual motors.

Communications

Busses

The standard interface to the Hand is a Controller Area Network (CAN) bus. The CAN interface has been tested with standard controller cards as well as the interface card supplied with the host computer. All sensor data, components, configuration and controller set points can be accessed over this bus. A simple protocol developed by Shadow is used for the communication. Code for protocol interface is supplied as part of the GNU GPL- licensed codebase only; alternate licensing is also available as an option. An embedded Ethernet interface option permits direct access to robot data and configuration by TCP/IP communication.

Robot Configuration

- The protocol used allows a variety of system-specific configuration to take place. This includes:
 - enable and disable a component of the robot, such as a group of sensors, or a single microcontroller module
 - set sensor transmission rates,
 - enable and disable joint position PID controllers individually, modify limits and set points for inner joint force PID controllers, modify set points for outer joint position PID controllers,
 - change PID controller sensor and target values, change force and position controller P,I,D gain values,
 - change operational limits such as force and temperature cutouts, reset components,
 - Track error and status indicators from the components.
- The off-board PC provides access to all of these functions via shell script, device, and file system and program code. Full documentation of the software interface and protocol is supplied.

Sensing

Position

A Hall effect sensor senses the rotation of each joint locally with typical resolution 0.2 degrees. This data is sampled by 12-bit ADCs and transmitted on the CAN bus. Data is transmitted in both calibrated and uncalibrated form. The sampling rate is configurable up to 180Hz.

Force

A separate force sensor measures the force in each of the pair of tendons driven by the Smart Motor unit. This data is captured by 12-bit ADCs and transmitted on the CAN bus, as well as being available to the Smart Motor unit for control.

Kinematics

The Dextrous Hand kinematics are as close as possible to the kinematics of the human hand as shown in Figure A-9 .

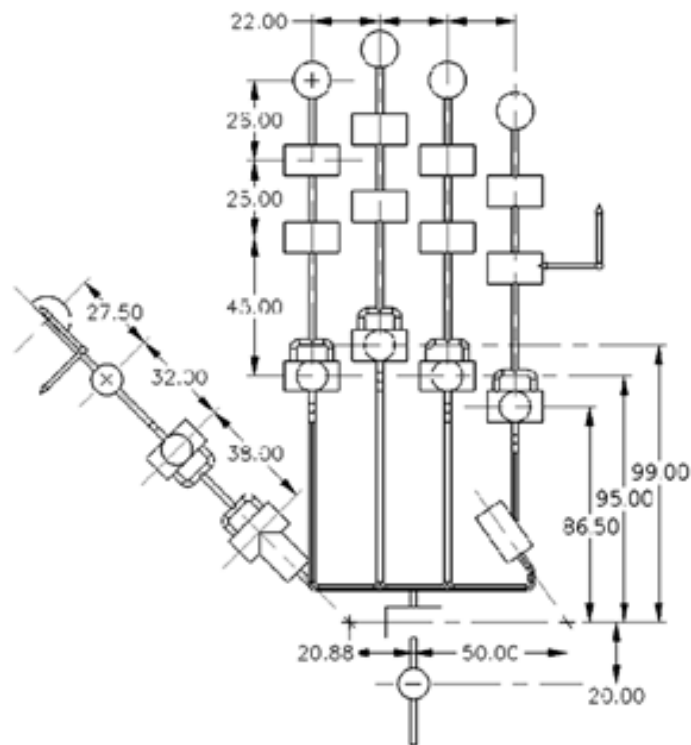


Figure A-9: Kinematic Layout of MFRH

System View

Electronics

1. Bus: Controller Area Network (CAN) bus interface to on-board electronics. Optional Ethernet on-board.
2. Palm Sensor: 7 ADCs distributed across the palm provide 26 active 12-bit sensing channels.
3. Motors: Smart Motor units integrated into the forearm incorporating per-tendon force sensing and providing timed and PID control

- *On Board View*

The Smart Motor boards implement PID control of force and position of the joints. This control can be flexibly configured to take set point and target data from a variety of sources. These controllers can be configured via the standard robot interface, and appropriate programs, scripts and graphical examples of this are provided.

- *Off-board control*

A standard x86-compatible PC running Debian GNU/Linux with the RTAI real-time system and Shadow's GPL robot code is supplied. This can be used for initial set up, evaluation and operation, as well as serving as a template for your own control system. The PC is fitted with an external CAN bus interface.

Software in the host PC provides sensor calibration and scaling, mappings from sensor names to hardware and permits easy access to all robot facilities from C code, shell scripts, or GUI.

- *Micro-controllers*

Microchip PIC18Fxx80 micros are used for embedded control throughout the robot system. The firmware is provided as source on the host PC. All microcontrollers are connected to the robot CAN bus.

- *Smart Motor nodes*

Each of the twenty Smart Motor nodes drives a motor using PWM with 1 kHz update frequency. The Smart Motor node implements two nested PID controllers. The

inner one controls tendon force, with tunable hard limits on maximum forces to provide compliance. The outer controller sets the required tendon force, and typically does this from joint position error, so it controls joint position. The PID controllers are set up in the configuration or boot phase of the system, and can be configured to operate from sensor data and from user-supplied values, permitting control of joint position, joint force, or user-supplied parameters. There is a mechanism to switch quickly between controller settings.

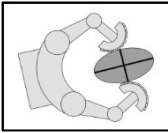
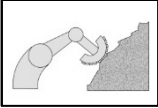
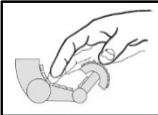
- *Hand sensor node*

The Hand Sensor Node, which is made up of a number of PCBs throughout the

A-4 Sensor for MFRH

Tactile sensing has been a component of robotics for roughly as long as vision. However, in comparison to vision, for which great strides have been made in terms of hardware and software and which is now widely used in industrial and mobile robot applications, tactile sensing always seems to be “a few years away” from widespread utility. In Nature, tactile sensing is evidently an essential survival tool. Even the simplest creatures are endowed with large numbers of mechanoreceptors for exploring and responding to various stimuli. In humans, tactile sensing is indispensable for *manipulation, exploration* and *response* as shown in Table A-2. A couple of quick thought exercises illustrate the point: When our fingers are numbed by cold we become clumsy, so that simple manipulation tasks, like unbuckling a boot, are an exercise in frustration. Our muscles, snug in our coat sleeves, are only slightly affected but our cutaneous mechanoreceptors are anesthetized. For exploration, we rapidly assimilate tactile information about material and surface properties (e.g., hardness, thermal conductivity, friction, roughness) to help us identify objects. We may have difficulty distinguishing leather from pleather™ by sight, but not by touch! The importance of tactile response, whether to a gentle touch or an impact, is seen in the damage that patients with peripheral neuropathy (e.g., as a complication of diabetes) accidentally do to themselves.

Table A-2: Uses of tactile sensing in robotics

Type of sensing	Description
	<p><i>Manipulation:</i> Grasp force control; contact locations and kinematics; stability assessment.</p>
	<p><i>Exploration:</i> Surface texture, friction and hardness; thermal properties; local features.</p>
	<p><i>Response:</i> Detection and reaction to contacts from external agents.</p>

A second set of difficulties arises from the inherently multi-modal nature of tactile sensing. In humans, there are four main types of mechanoreceptors which can be classified according to whether they are slow- or fast-adapting and whether they have large or small receptive fields. For example, when you hold your fingertips against the edge of the table you can feel the corner as a continuing effect; the receptors that are primarily responsible for the sensation are slow-adapting Meissner and Merkel corpuscles, which detect local pressure and skin-stretch. In contrast, the detection of surface scratches in the tabletop requires motion of the fingertips across the surface, which excites the fast-adapting Pacinian corpuscles. For robots to make full use tactile information a similarly multi-modal approach, often employing different transducers, is required.

Despite the challenges associated with tactile sensing, interactive and multi-modal as it is, considerable progress in sensor design and deployment has been made over the last couple of decades. Looking ahead, new fabrication techniques offer the possibility of artificial skin materials with integrated sensors and local processing for interpreting sensor signals and communicating over a common buss to reduce wiring.

Tactile sensor types

Single sensors – are most commonly force/torque sensors, dynamic sensors and thermal sensors.

1) Force/torque sensors

Force sensor is often used in combination with tactile arrays to provide information for force control. A single force/torque sensor can sense loads anywhere on the distal link of a manipulator and, not being subject to the same packaging constraints as a “skin” sensor, can generally provide more precise force measurements at higher bandwidth. If the geometry of the manipulator link is defined, and if single-point contact can be assumed (as in the case of a robot finger with a hemispherical tip contacting locally convex surfaces), then a force/torque sensor can provide information about the contact location by ratios of forces and moments in a technique called “intrinsic tactile sensing” [Salisbury, Bicchi].

2) Dynamic tactile sensors

The most common dynamic tactile sensors are small accelerometers at the fingertips or in the skin of a robotic finger. They function roughly like pacinian corpuscles in humans and have a correspondingly large receptive field so that one or two skin accelerometers suffice for an entire finger. These sensors are particularly effective for detecting the making and breaking of contact, the onset of slip and the vibrations associated with sliding over textured surfaces.

A second type of dynamic tactile sensor is the stress rate sensor. If a fingertip is sliding at a speed of a few centimeters/second over small asperities (bumps or pits) in a surface, the transient changes in stresses in the skin will be significant. A piezoelectric polymer such as PVDF that produces a charge in response to strain can be used to produce currents proportional to the rate of change of stress:

3) Thermal sensors

Thermal sensors are an important component of the human ability to identify the materials of which objects are made (think of how metal feels cool to the touch compared to wood) but little used in robotics. Human thermal sensing involves detecting thermal gradients in the skin, which correspond to both the temperature and the thermal conductivity of an object. Robotic thermal sensors have involved peltier junctions in combination with thermocouples or thermistors. Difficulties have been encountered in obtaining sufficient resolution and time response when using them to distinguish among different materials.

4) Sensor arrays

- There are various possible ways of organizing tactile sensor arrays. From a functional standpoint, the primary concerns include:

- What is being measured (e.g., surface pressure or shear tractions, deformations, local geometry)
- What is the transduction method (e.g., piezo resistive, capacitive, optical)
- What are the mounting provisions (e.g., rigid or compliant, flat or curved)
- What are the expected levels of sensor resolution, accuracy and dynamic range (e.g. point to point spacing, minimum detectable stimulus, hysteresis, frequency response).

APPENDIX B
CAD MODEL DESIGN

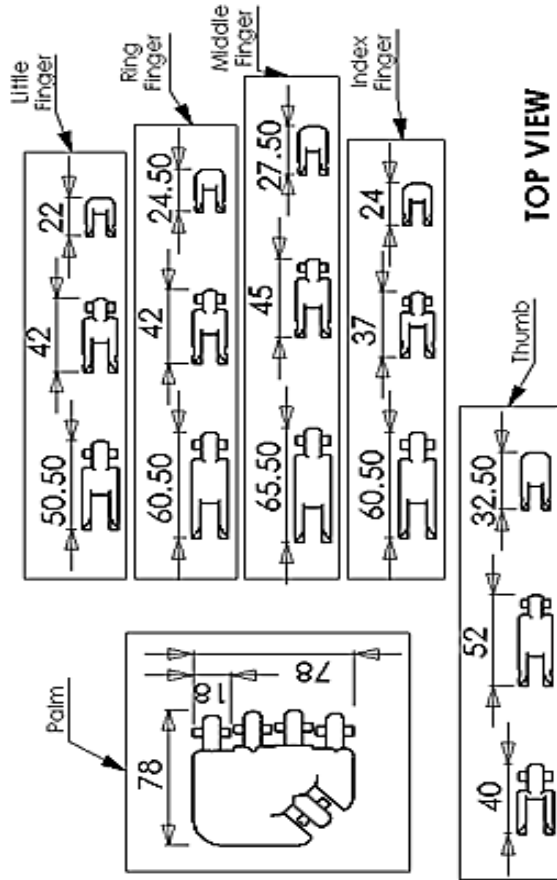


Figure B-1: Length of MFRH Design

Table B-1: Length for MFRH

Finger	Length (mm / cm)
Thumb Finger	124.5 / 12.45
Index Finger	121.0 / 12.1
Middle Finger	138.0 / 13.80
Ring Finger	127.0 / 12.7
Little Finger	114.5 / 11.45

B-1 MFRH Design View

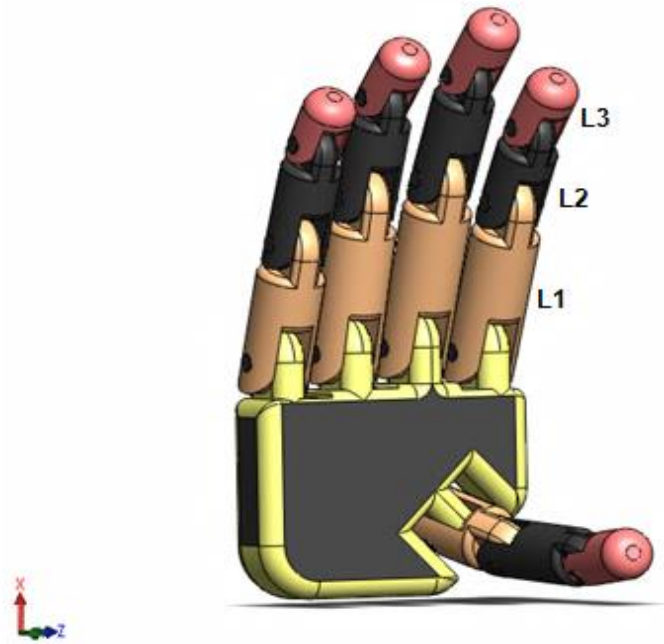


Figure B-2: CAD Model of MFRH



Figure B-3: CAD Model of MFRH View

The research focuses on one finger for simulation because others finger can come out the same method like one finger. In this research, index finger is an input to carry out the output response.

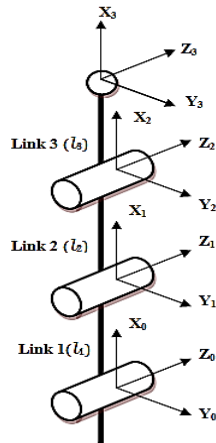


Figure B-4: Frame of an Index Finger

Table B-2: Index Finger Parameter

Variable	Value	Unit	Description
l1	0.0605	m	Link 1
l2	0.0375	m	Link 2
l3	0.0245	m	Link 3
m1	0.0100728	kg	Mass 1
m2	0.00397876	kg	Mass 2
m3	0.00208544	kg	Mass 3
g	0.981	Nm ³	Gravity

The convention that was used to locate the frame on the links is known as the D-H convention [79] which is given below:

- The z - axis of frame $\{i\}$, called z_i , is coincident with the joint i .
- The origin of frame $\{i\}$ is located where the a_i perpendicular intersects the joint i axis.
- x_i points along a_i in the direction from joint i to joint $i + 1$

Assuming that the frames have been attached to the links according to the D-H convention, the following definitions of the link parameters are valid:

- Rotate the frame $x_{i-1}y_{i-1}z_{i-1}$ about the z_{i-1} axis through an angle a_i . Translate the current frame $x_{i-1}y_{i-1}z_{i-1}$ along the current z_{i-1} axis by d_i units.
- Translate the current frame $x_{i-1}y_{i-1}z_{i-1}$ along the current x_i axis by a_i units.
- Rotate the current frame $x_{i-1}y_{i-1}z_{i-1}$ about the x_i axis through an angle a_i .

Figure B-4 show that the finger has five frames with four joints. The first frame is also known as the base frame is $x_0y_0z_0$ and the subsequent frames are assigned as per the figure starting with $x_1y_1z_1$ and ending with $x_3y_3z_3$. The forward kinematic solution of a finger will be assigned using homogenous matrix.

APPENDIX C

MATHEMATICAL MODELING

C1. Forward Kinematic

Forward Kinematic is used to determine the position and orientation of MFRH to determine the position and orientation of the robot hand relative to the robot base coordinate system. The derivation of forward kinematic equation based on Table 3.3.

Table C1: Parameter for One Finger

i	θ_i	d_i	a_{i-1}	α_{i-1}
1	θ_1	0	0	0
2	θ_2	0	l_1 (MCP)	0
3	θ_3	0	l_2 (PIP)	0
4	0	0	l_3 (DIP)	0

The derivation of forward kinematic equation based on Table 3.3 is as follows:

$$H_{i-1}^i = \begin{bmatrix} c\theta_i & -s\theta_i & 0 & a_{i-1} \\ s\theta_i c\alpha_{i-1} & c\theta_i c\alpha_{i-1} & s\alpha_{i-1} & s\alpha_{i-1} d_i \\ s\theta_i s\alpha_{i-1} & c\theta_i s\alpha_{i-1} & c\alpha_{i-1} & c\alpha_{i-1} d_i \\ 0 & 0 & 0 & 1 \end{bmatrix} \quad (C.1)$$

$$H_0^1 = \begin{bmatrix} C_1 & -S_1 & 0 & 0 \\ S_1 & C_1 & 0 & 0 \\ 0 & 0 & 1 & 0 \\ 0 & 0 & 0 & 1 \end{bmatrix} \quad (C.2)$$

$$H_1^2 = \begin{bmatrix} C_2 & -S_2 & 0 & l_1 \\ S_2 & C_2 & 0 & 0 \\ 0 & 0 & 1 & 0 \\ 0 & 0 & 0 & 1 \end{bmatrix} \quad (C.3)$$

$$H_2^3 = \begin{bmatrix} C_3 & -S_3 & 0 & l_2 \\ S_3 & C_3 & 0 & 0 \\ 0 & 0 & 1 & 0 \\ 0 & 0 & 0 & 1 \end{bmatrix} \quad (C.4)$$

And

$$H_3^4 = \begin{bmatrix} 1 & 0 & 0 & l_3 \\ 0 & 1 & 0 & 0 \\ 0 & 0 & 1 & 0 \\ 0 & 0 & 0 & 1 \end{bmatrix} \quad (C.5)$$

Hence, the forward kinematic for the fingers of robot hand are given by:

$$H_0^4 = H_0^1 H_1^2 H_2^3 H_3^4 \quad (C.6)$$

Assuming

$$\cos \theta_1 = C_1, \cos \theta_2 = C_2, \cos \theta_3 = C_3$$

$$\sin \theta_1 = S_1, \sin \theta_2 = S_2, \sin \theta_3 = S_3$$

First, find $H_0^2 = H_0^1 H_1^2$

$$\begin{aligned} H_0^2 &= \begin{bmatrix} C_1 & -S_1 & 0 & 0 \\ S_1 & C_1 & 0 & 0 \\ 0 & 0 & 1 & 0 \\ 0 & 0 & 0 & 1 \end{bmatrix} \begin{bmatrix} C_2 & -S_2 & 0 & l_1 \\ S_2 & C_2 & 0 & 0 \\ 0 & 0 & 1 & 0 \\ 0 & 0 & 0 & 1 \end{bmatrix} \\ &= \begin{bmatrix} C_1 C_2 - S_1 S_2 & -C_1 S_2 - S_1 C_2 & 0 & l_1 C_1 \\ S_1 C_2 + C_1 S_2 & -S_1 S_2 + C_1 C_2 & 0 & l_1 S_1 \\ 0 & 0 & 1 & 0 \\ 0 & 0 & 0 & 1 \end{bmatrix} \end{aligned} \quad (C.7)$$

Where,

$$\cos \theta_1 \cos \theta_2 - \sin \theta_1 \sin \theta_2 = \cos(\theta_1 + \theta_2) = C_{12} \quad (C.8)$$

$$\sin \theta_1 \cos \theta_2 + \cos \theta_1 \sin \theta_2 = \sin(\theta_1 + \theta_2) = S_{12} \quad (C.9)$$

Hence,

$$H_0^2 = \begin{bmatrix} C_{12} & -S_{12} & 0 & l_1 C_1 \\ S_{12} & C_{12} & 0 & l_1 S_1 \\ 0 & 0 & 1 & 0 \\ 0 & 0 & 0 & 1 \end{bmatrix} \quad (C.10)$$

Then, find $H_0^3 = H_0^1 H_1^2 H_2^3$

$$H_0^3 = \begin{bmatrix} C_{12} & -S_{12} & 0 & l_1 C_1 \\ S_{12} & C_{12} & 0 & l_1 S_1 \\ 0 & 0 & 1 & 0 \\ 0 & 0 & 0 & 1 \end{bmatrix} \begin{bmatrix} C_3 & -S_3 & 0 & l_2 \\ S_3 & C_3 & 0 & 0 \\ 0 & 0 & 1 & 0 \\ 0 & 0 & 0 & 1 \end{bmatrix} \quad (C.11)$$

$$= \begin{bmatrix} C_{12}C_3 - S_{12}S_3 & -C_{12}S_3 - S_{12}C_3 & 0 & l_2C_{12} + l_1C_1 \\ S_{12}C_3 + C_{12}S_3 & -S_{12}S_3 + C_{12}C_3 & 0 & l_2S_{12} + l_1S_1 \\ 0 & 0 & 1 & 0 \\ 0 & 0 & 0 & 1 \end{bmatrix} \quad (\text{C.12})$$

Assuming,

$$\text{Cos}\theta_{12}\text{Cos}\theta_3 - \text{Sin}\theta_{12}\text{Sin}\theta_3 = \text{Cos}(\theta_{12} + \theta_3) = C_{123} \quad (\text{C.13})$$

$$\text{Sin}\theta_{12}\text{Cos}\theta_3 + \text{Cos}\theta_{12}\text{Sin}\theta_3 = \text{Sin}(\theta_{12} + \theta_3) = S_{123} \quad (\text{C.14})$$

Where the eq. (C.15) and (C.16) is provided by the eq. (C.8) and (C.9) will be replaced into eq. (C.13) and (C.14),

$$\begin{aligned} \text{Cos}\theta_{12}\text{Cos}\theta_3 - \text{Sin}\theta_{12}\text{Sin}\theta_3 &= \text{Cos}(\theta_{12} + \theta_3) = C_{123} \\ &= (\text{Cos}\theta_1\text{Cos}\theta_2)\text{Cos}\theta_3 - (\text{Sin}\theta_1\text{Sin}\theta_2)\text{Sin}\theta_3 \\ &= \text{Cos}\theta_1\text{Cos}\theta_2\text{Cos}\theta_3 - \text{Sin}\theta_1\text{Sin}\theta_2\text{Sin}\theta_3 \\ &= (\text{Cos}\theta_1\text{Cos}\theta_2)\text{Cos}\theta_3 - (\text{Sin}\theta_1\text{Sin}\theta_2)\text{Sin}\theta_3 \\ &= \text{Cos}\theta_{12}\text{Cos}\theta_3 - \text{Sin}\theta_{12}\text{Sin}\theta_3 \\ &= \text{Cos}(\theta_{12} + \theta_3) = C_{123} \end{aligned} \quad (\text{C.15})$$

$$\begin{aligned} \text{Sin}\theta_{12}\text{Cos}\theta_3 + \text{Cos}\theta_{12}\text{Sin}\theta_3 &= \text{Sin}(\theta_{12} + \theta_3) = S_{123} \\ &= (\text{Sin}\theta_1\text{Sin}\theta_2)\text{Cos}\theta_3 + (\text{Cos}\theta_1\text{Cos}\theta_2)\text{Sin}\theta_3 \\ &= \text{Sin}\theta_1\text{Sin}\theta_2\text{Cos}\theta_3 + \text{Cos}\theta_1\text{Cos}\theta_2\text{Sin}\theta_3 \\ &= (\text{Sin}\theta_1\text{Sin}\theta_2)\text{Cos}\theta_3 + (\text{Cos}\theta_1\text{Cos}\theta_2)\text{Sin}\theta_3 \\ &= \text{Sin}\theta_{12}\text{Cos}\theta_3 + \text{Cos}\theta_{12}\text{Sin}\theta_3 \\ &= \text{Sin}(\theta_{12} + \theta_3) = S_{123} \end{aligned} \quad (\text{3.16})$$

Hence,

$$H_0^3 = \begin{bmatrix} C_{123} & -S_{123} & 0 & l_1C_1 + l_2C_{12} \\ S_{123} & C_{123} & 0 & l_1S_1 + l_2S_{12} \\ 0 & 0 & 1 & 0 \\ 0 & 0 & 0 & 1 \end{bmatrix} \quad (\text{3.17})$$

Finally, find

$$H_0^4 = H_0^1 H_1^2 H_2^3 H_3^4$$

$$H_0^4 = \begin{bmatrix} C_{123} & -S_{123} & 0 & l_1C_1 + l_2C_{12} \\ S_{123} & C_{123} & 0 & l_1S_1 + l_2S_{12} \\ 0 & 0 & 1 & 0 \\ 0 & 0 & 0 & 1 \end{bmatrix} \begin{bmatrix} 1 & 0 & 0 & l_3 \\ 0 & 1 & 0 & 0 \\ 0 & 0 & 1 & 0 \\ 0 & 0 & 0 & 1 \end{bmatrix}$$

$$= \begin{bmatrix} C_{123} & -S_{123} & 0 & l_1 C_1 + l_2 C_{12} + l_3 C_{123} \\ S_{123} & C_{123} & 0 & l_1 S_1 + l_2 S_{12} + l_3 C_{123} \\ 0 & 0 & 1 & 0 \\ 0 & 0 & 0 & 1 \end{bmatrix} \quad (C.18)$$

C2. Inverse Kinematic

To find the angle joint of MFRH, the equations is derived using the derivation of Inverse Kinematics [79]. Figure 3.7 is the flexion of angles of one finger where l_1 to l_3 are finger parts and θ_1 to θ_3 are the joints in-between and represents the angles.

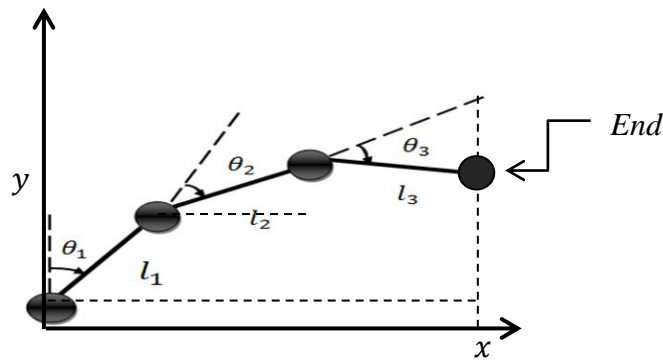


Figure C1: Flexion of Angles of One Finger

Regarding the previous forward kinematic, one finger robot has three links and provides the eq. (C.17) such as below:

$$H_0^4 = \begin{bmatrix} C_{123} & -S_{123} & 0 & l_1 C_1 + l_2 C_{12} + l_3 C_{123} \\ S_{123} & C_{123} & 0 & l_1 S_1 + l_2 S_{12} + l_3 C_{123} \\ 0 & 0 & 1 & 0 \\ 0 & 0 & 0 & 1 \end{bmatrix}$$

It means three links is referred to the three joints and for one finger and the last joint is referred to the end effector. Figure 3.3 show the flexion of angle one finger robot which are x and y provides the equation for three links where;

$$x = l_1 C_1 + l_2 C_{12} + l_3 C_{123} \quad (C.19)$$

$$y = l_1 S_1 + l_2 S_{12} + l_3 C_{123} \quad (C.20)$$

Due θ_3 cannot found directly. So, the eq. (C.19) and (C.20) will be replaced by the equation of x and y with 2 links to find the θ_2 , then followed by θ_1 and finally θ_3 .

$$x = l_1 C_1 + l_2 C_{12} \quad (C.21)$$

$$y = l_1 S_1 + l_2 S_{12} \quad (C.22)$$

It means the equation will be started with H_0^3 . Then, assume the orientation in the eq. 3.23.

$$H_0^3 = \begin{bmatrix} C_{123} & -S_{123} & 0 & l_1 C_1 + l_2 C_{12} \\ S_{123} & C_{123} & 0 & l_1 S_1 + l_2 S_{12} \\ 0 & 0 & 1 & 0 \\ 0 & 0 & 0 & 1 \end{bmatrix}$$

$$H_i^n = \begin{bmatrix} C_\phi & -S_\phi & 0 & x \\ S_\phi & C_\phi & 0 & y \\ 0 & 0 & 1 & 0 \\ 0 & 0 & 0 & 1 \end{bmatrix} \quad (C.23)$$

Based the result in homogenous forward kinematic of H_0^3 , the symbol " ϕ " is used to replace the value of "123" like exposed in the eq. (C.24) and (C.25).

$$C_\phi = C_{123} \quad (C.24)$$

$$S_\phi = S_{123} \quad (C.25)$$

First, square the eq. (C.21) and (C.22) both of side of equation x and y

$$x^2 = (l_1 C_1 + l_2 C_{12})^2 \quad (C.26)$$

$$y^2 = (l_1 S_1 + l_2 S_{12})^2 \quad (C.27)$$

And add both of equation (C.26) and (C.27),

$$x^2 + y^2 = l_1^2 C_1^2 + l_1^2 l_1 S_1^2 + l_2^2 C_{12}^2 + l_2^2 S_{12}^2 + 2l_1 l_2 (C_1 C_{12} + S_1 S_{12})$$

$$= l_1^2 C_1^2 + l_1^2 S_1^2 + l_2 C_{12}^2 + l_2 S_{12}^2 + 2l_1 l_2 [C_1 (C_1 C_2 - S_1 S_2) + l_1 l_2 (S_1 (C_1 S_2 + S_1 C_2))]$$

$$= l_1^2 C_1^2 + l_1^2 S_1^2 + l_2^2 C_{12}^2 + l_2^2 S_{12}^2 + 2l_1 l_2 [C_1^2 C_2 - C_1 S_1 S_2 + (S_1 C_1 S_2 + S_1^2 C_2)]$$

$$= l_1^2 (C_1^2 + S_1^2) + l_2^2 (C_{12}^2 + S_{12}^2) + 2l_1 l_2 [C_2 (C_1^2 + S_1^2)]$$

$$x^2 + y^2 = l_1^2 + l_2^2 + 2l_1 l_2 C_2 \quad (C.28)$$

To simplify the equation C.28, use the formula of trigonometric function below:

$$\begin{aligned} \cos \theta_i^2 + \sin \theta_i^2 &= 1 \\ i &= 1, 2, 3 \dots \end{aligned} \quad (C.29)$$

Where, $\cos \theta_1 = C_1$, $\sin \theta_1 = S_1$

$$\text{So, } C_1^2 + S_1^2 = 1 \quad (C.30)$$

Hence,

$$x^2 + y^2 = l_1^2 + l_2^2 + 2l_1l_2C_2 \quad (C.31)$$

Now, θ_2 will be found with simplified by using eq. (3.31) for find C_2 and S_2 .

$$\begin{aligned} x^2 + y^2 &= l_1^2 + l_2^2 + 2l_1l_2C_2 \\ l_1^2 + l_2^2 + 2l_1l_2C_2 &= x^2 + y^2 \\ 2l_1l_2C_2 &= x^2 + y^2 - l_1^2 - l_2^2 \\ C_2 &= \frac{x^2 + y^2 - l_1^2 - l_2^2}{2 l_1 l_2} \end{aligned} \quad (C.32)$$

To find S_2 , use the eq. (3.29)

$$\begin{aligned} \cos \theta_2^2 + \sin \theta_2^2 &= 1 \\ \text{Where, } \cos \theta_2 &= C_2, \sin \theta_2 = S_2 \\ C_2^2 + S_2^2 &= 1 \\ S_2^2 &= 1 - C_2^2 \\ S_2 &= \pm \sqrt{1 - C_2^2} \end{aligned} \quad (C.33)$$

Let $\theta_i = \arctan 2(A, B)$

$$i = 1, 2, 3 \dots \quad (C.34)$$

By using the formula from the eq. (C.34), where $A = \sin \theta_i$ and $B = \cos \theta_i$, Hence,
 $\theta_2 = \arctan 2(S_2, C_2)$

For the next step, the expression for x and y may now be solved θ_1 . In order to do so, write the eq. (C.21) and eq. (C.22).

$$x = l_1C_1 + l_2C_{12}$$

$$y = l_1S_1 + l_2S_{12}$$

By using eq. (C.8) and eq. (C.9), the value of x and y can be expanded as

$$\begin{aligned}
x &= l_1 C_1 + l_2 (C_1 C_2 - S_1 S_2) \\
&= l_1 C_1 + l_2 C_1 C_2 - l_2 S_1 S_2 \\
&= (l_1 + l_2 C_2) C_1 - (l_2 S_2) S_1
\end{aligned} \tag{C.35}$$

$$\begin{aligned}
y &= l_1 S_1 + l_2 S_1 C_2 \\
&= l_1 S_1 + l_2 S_1 C_2 + l_2 C_1 S_2 \\
&= (l_1 + l_2 C_2) S_1 + (l_2 S_2) C_1
\end{aligned} \tag{C.36}$$

The, the eq. (C.35) and (C.36) will be simplified with change the value of:

$$\begin{aligned}
l_1 + l_2 C_2 &= k_1, \text{ and } l_2 S_2 = k_2. \text{ Thus,} \\
x &= k_1 C_1 - k_2 S_1
\end{aligned} \tag{C.37}$$

$$y = k_1 S_1 + k_2 C_1 \tag{C.38}$$

Now, square the eq. (C.37) and (C.38) both of side of equation x and y above,

$$\begin{aligned}
x^2 &= k_1^2 C_1^2 + k_2^2 S_1^2 \\
x^2 &= k_1^2 S_1^2 + k_2^2 C_1^2
\end{aligned} \tag{C.39}$$

$$\begin{aligned}
x^2 + y^2 &= k_1^2 C_1^2 + k_2^2 S_1^2 + k_1^2 S_1^2 + k_2^2 C_1^2 \\
x^2 + y^2 &= k_1^2 C_1^2 + k_1^2 S_1^2 + k_2^2 C_1^2 + k_2^2 S_1^2 \\
x^2 + y^2 &= k_1^2 (C_1^2 + S_1^2) + k_2^2 (C_1^2 + S_1^2)
\end{aligned} \tag{C.40}$$

By using eq. (C.29) and (C.30), $x^2 + y^2$ will be simplified;

$$\begin{aligned}
x^2 + y^2 &= k_1^2 (1) + k_2^2 (1) \\
x^2 + y^2 &= k_1^2 + k_2^2
\end{aligned} \tag{C.41}$$

Now changing the value of $x^2 + y^2 = r^2$, Hence,

$$\begin{aligned}
r^2 &= k_1^2 + k_2^2 \\
r &= \sqrt{k_1^2 + k_2^2}
\end{aligned} \tag{C.42}$$

By using eq. (C.34) the arctan2 for k_1 and k_2 will be found where, the θ_i replaced with γ . Therefore,

$$\gamma = \arctan2(k_2, k_1) \tag{C.43}$$

$$\text{Let } k_1 = r \cos \gamma \tag{C.44}$$

$$\text{Let } k_2 = r \sin \gamma$$

Substitute equation (C.37) and (C.38) by using the eq. (C.42)

$$\begin{aligned}
 x &= k_1 C_1 - k_2 S_1 \\
 x &= r \cos \gamma C_1 - r \sin \gamma S_1 \\
 x &= r (\cos \gamma \cos \theta_1 - \sin \gamma \sin \theta_1) \\
 x/r &= \cos \gamma \cos \theta_1 - \sin \gamma \sin \theta_1
 \end{aligned} \tag{C.45}$$

$$\begin{aligned}
 y &= k_1 S_1 + k_2 C_1 \\
 y &= r \cos \gamma S_1 + r \sin \gamma C_1 \\
 y &= r (\cos \gamma S_1 + \sin \gamma C_1) \\
 y/r &= \cos \gamma \sin \theta_1 + \sin \gamma \cos \theta_1
 \end{aligned} \tag{C.46}$$

Then simplified the eq. (C.45) and eq. (C.46) by using eq. (C.8) and eq. (C.9), then applying the equation as;

$$x/r = \cos \gamma \cos \theta_1 - \sin \gamma \sin \theta_1 \tag{C.47}$$

$$x/r = \cos(\gamma + \theta_1)$$

$$y/r = \cos \gamma \sin \theta_1 + \sin \gamma \cos \theta_1 \tag{C.48}$$

$$y/r = \sin(\gamma + \theta_1)$$

$$\text{Assume that } \gamma + \theta_1 = \arctan2\left(\frac{y}{r}, \frac{x}{r}\right) = \arctan2(y, x)$$

$$\theta_1 = \arctan2(y, x) - \gamma \tag{C.49}$$

$$\text{Assume that } \gamma + \theta_1 = \arctan2\left(\frac{y}{r}, \frac{x}{r}\right) = \arctan2(y, x)$$

$$\theta_1 = \arctan2(y, x) - \gamma$$

As a result,

$$\theta_1 = \arctan2(y, x) - \arctan2(k_2, k_1) \tag{C.50}$$

Finally, Based on the eq. (C.24) and (C.25), θ_3 can be solved by using the equations for S_\emptyset and C_\emptyset : For this symbol is used \emptyset is to combine three symbol of θ_1, θ_2 and θ_3 like exposed in eq. no (C.25).

$$\theta_i = \arctan2(\arctan2(S_\emptyset, C_\emptyset)) \tag{C.51}$$

Let,

$$\emptyset = \theta_1 + \theta_2 + \theta_3 \tag{C.52}$$

Hence,

$$\begin{aligned}\theta_3 &= \phi - \theta_1 - \theta_2 \\ \theta_3 &= \arctan2(S_\phi, C_\phi) - \theta_1 - \theta_2\end{aligned}\tag{C.53}$$

C3. Jacobian

The next step is jacobian matrix. Jacobian is a relationship between joint space velocities with task space velocity.

Based on forward and inverse kinematic previous, the jacobian can be found by using the eq. (C.19), (C.20) and (C.52). First, find the velocity of the frame:

$$\begin{aligned}x &= l_1 C_1 + l_2 C_{12} + l_3 C_{123} \\ y &= l_1 S_1 + l_2 S_{12} + l_3 S_{123} \\ \phi &= \theta_1 + \theta_2 + \theta_3\end{aligned}$$

Differentiating the equation (C.19), (C.20) and (C.52)

$$\dot{x} = -l_1 S_1 \dot{\theta}_1 - l_2 S_{12} (\dot{\theta}_1 + \dot{\theta}_2) - l_3 S_{123} (\dot{\theta}_1 + \dot{\theta}_2 + \dot{\theta}_3)\tag{C.54}$$

$$\begin{aligned}\dot{x} &= -(l_1 S_1 + l_2 S_{12} + l_3 S_{123}) \dot{\theta}_1 - (l_2 S_{12} + l_3 S_{123}) \dot{\theta}_2 - (l_3 S_{123}) \dot{\theta}_3 \\ \dot{y} &= l_1 C_1 \dot{\theta}_1 + l_2 C_{12} (\dot{\theta}_1 + \dot{\theta}_2) + l_3 C_{123} (\dot{\theta}_1 + \dot{\theta}_2 + \dot{\theta}_3)\end{aligned}\tag{C.55}$$

$$\begin{aligned}\dot{y} &= (l_1 C_1 + l_2 C_{12} + l_3 C_{123}) \dot{\theta}_1 + (l_2 C_{12} + l_3 C_{123}) \dot{\theta}_2 + (l_3 C_{123}) \dot{\theta}_3 \\ \dot{\phi} &= \dot{\theta}_1 + \dot{\theta}_2 + \dot{\theta}_3\end{aligned}\tag{C.56}$$

Finally, the velocity (V) is provided by the Jacobian ($J(\theta)$) matrix:

$$V = J(\theta) \cdot \dot{\theta}$$

$$\begin{bmatrix} \dot{x} \\ \dot{y} \\ \dot{\phi} \end{bmatrix} = \begin{bmatrix} -l_1 S_1 - l_2 S_{12} - l_3 S_{123} & -l_2 S_{12} - l_3 S_{123} & -l_3 S_{123} \\ l_1 C_1 + l_2 C_{12} + l_3 C_{123} & l_2 C_{12} + l_3 C_{123} & l_3 C_{123} \\ 1 & 1 & 1 \end{bmatrix} \begin{bmatrix} \dot{\theta}_1 \\ \dot{\theta}_2 \\ \dot{\theta}_3 \end{bmatrix}$$

Hence, $J(\theta)$

$$\begin{aligned}J(\theta) &= \begin{bmatrix} -l_1 S_1 - l_2 S_{12} - l_3 S_{123} & -l_2 S_{12} - l_3 S_{123} & -l_3 S_{123} \\ l_1 C_1 + l_2 C_{12} + l_3 C_{123} & l_2 C_{12} + l_3 C_{123} & l_3 C_{123} \\ 1 & 1 & 1 \end{bmatrix} \\ DET [J(\theta)] &= \begin{vmatrix} -l_1 S_1 - l_2 S_{12} - l_3 S_{123} & -l_2 S_{12} - l_3 S_{123} & -l_3 S_{123} \\ l_1 C_1 + l_2 C_{12} + l_3 C_{123} & l_2 C_{12} + l_3 C_{123} & l_3 C_{123} \\ 1 & 1 & 1 \end{vmatrix} = 0\end{aligned}\tag{C.57}$$

The expression for the determinant of the jacobian, can be simplified using trigonometric identities to: $|J| = l_1 l_2 \sin \theta_2$. This means that Jacobian only when θ_2 is

either 0 or 180 degree. Physically, this corresponds to middle phalanx being completely extended or complex fixed.

C4.Dynamics

In dynamic part, the equations have been derived to find out the torque of MFRH. The position, velocity and acceleration of the joints ($\theta, \dot{\theta}, \ddot{\theta}$) will be assumed to be known. With this knowledge, and with knowledge of the kinematics and mass distribution information of the robot, the joint torque required to cause this motion can be calculated [64]. Based on Newton-Euler formula, the dynamic equation can be found:

Outward iterations $i: 0 \rightarrow 3$

$${}^{i+1}\omega_{i+1} = {}^{i+1}R {}^i\omega_i + \dot{\theta}_{i+1} + {}^{i+1}\hat{Z}_{i+1} \quad (C.58)$$

$${}^{i+1}\dot{\omega}_{i+1} = {}^{i+1}R {}^i\dot{\omega}_i + {}^{i+1}R {}^i\dot{\omega}_i \times \dot{\theta}_{i+1} {}^{i+1}\hat{Z}_{i+1} + \ddot{\theta}_{i+1} {}^{i+1}\hat{Z}_{i+1} \quad (C.59)$$

$${}^{i+1}\dot{v}_{i+1} = {}^{i+1}R ({}^i\dot{\omega}_i \times {}^iP_{i+1} + {}^i\omega_i \times ({}^i\omega_i \times {}^iP_{i+1})) + {}^i\dot{v}_i \quad (C.60)$$

$${}^{i+1}\dot{v}_{C_{i+1}} = {}^{i+1}R ({}^{i+1}\dot{\omega}_i \times {}^iP_{C_{i+1}} + {}^{i+1}\omega_{i+1} \times ({}^{i+1}\omega_{i+1} \times {}^{i+1}P_{i+1})) + {}^{i+1}\dot{v}_{i+1} \quad (C.61)$$

$${}^{i+1}F_{i+1} = m_{i+1} {}^{i+1}\dot{v}_{C_{i+1}} \quad (C.62)$$

$${}^{i+1}N_{i+1} = {}^{C_{i+1}}I_{i+1} {}^{i+1}\omega_{i+1} + {}^{i+1}\omega_{i+1} \times {}^{C_{i+1}}I_{i+1} {}^{i+1}\omega_{i+1} \quad (C.63)$$

Inward iterations $i: 3 \rightarrow 1$

$${}^if_i = {}^{i+1}R {}^{i+1}f_{i+1} + {}^iF_i \quad (C.64)$$

$${}^in_i = {}^iN_i + {}^{i+1}R {}^{i+1}n_{i+1} + {}^iP_{i+1} \times {}^{i+1}R {}^{i+1}f_{i+1} \quad (C.65)$$

$$\tau_i = {}^in_i^T {}^i\hat{Z}_i \quad (C.66)$$

Firstly, assume the point masses at distal end of links:

$${}^1P_{C1} = l_1 \hat{x}_1 \quad (C.67)$$

$${}^2P_{C2} = l_2 \hat{x}_2 \quad (C.68)$$

$${}^3P_{C3} = l_2 \hat{x}_2 \quad (C.69)$$

Then, the inertia tensor (I) written at the center of mass for each link is the zero:

$${}^c1I_1 = 0 \quad (C.70)$$

$${}^c2I_2 = 0 \quad (C.71)$$

$${}^c3I_3 = 0 \quad (C.72)$$

Due no force (f) acting on the end-effector, so

$$f_4 = 0 \quad (C.73)$$

$$n_4 = 0 \quad (C.74)$$

Also the base (ω) of the finger is not rotating, hence

$$\omega_0 = 0 \quad (C.75)$$

$$\dot{\omega}_0 = 0 \quad (C.76)$$

And the last, assume gravity forces;

$${}^0\dot{v}_0 = g \hat{y}_0 \quad (C.77)$$

The rotation between successive link frames is given by

$${}_{i+1}^i R = \begin{bmatrix} c_{i+1} & -s_{i+1} & 0 \\ s_{i+1} & c_{i+1} & 0 \\ 0 & 0 & 1 \end{bmatrix} \quad (C.78)$$

$${}_{i+1}^i R = \begin{bmatrix} c_{i+1} & s_{i+1} & 0 \\ -s_{i+1} & c_{i+1} & 0 \\ 0 & 0 & 1 \end{bmatrix} \quad (C.79)$$

Now, apply the eq. (3.58) through eq. (3.67) in chapter 3,

The outward iterations for link 1 are as

$$\text{follows: } {}^1\dot{\omega}_1 = \ddot{\theta}_1 {}^1\hat{Z}_1 = \begin{bmatrix} 0 \\ 0 \\ \ddot{\theta}_1 \end{bmatrix} \quad (C.80)$$

$${}^1\dot{v}_1 = \begin{bmatrix} c_1 & s_1 & 0 \\ -s_1 & c_1 & 0 \\ 0 & 0 & 1 \end{bmatrix} \begin{bmatrix} 0 \\ g \\ 0 \end{bmatrix} = \begin{bmatrix} gs_1 \\ gc_1 \\ 0 \end{bmatrix} \quad (C.81)$$

$$\begin{aligned} {}^1\dot{v}_{C_1} &= \begin{bmatrix} 0 \\ l_1\ddot{\theta}_1 \\ 0 \end{bmatrix} + \begin{bmatrix} -l_1\dot{\theta}_1^2 \\ 0 \\ 0 \end{bmatrix} + \begin{bmatrix} gs_1 \\ gc_1 \\ 0 \end{bmatrix} \\ &= \begin{bmatrix} -l_1\dot{\theta}_1^2 + gs_1 \\ l_1\ddot{\theta}_1 + gc_1 \\ 0 \end{bmatrix} \end{aligned} \quad (C.82)$$

$${}^1F_1 = \begin{bmatrix} -m_1l_1\dot{\theta}_1^2 + m_1gs_1 \\ m_1l_1\ddot{\theta}_1 + m_1gc_1 \\ 0 \end{bmatrix} \quad (C.83)$$

$${}^1N_1 = \begin{bmatrix} 0 \\ 0 \\ 0 \end{bmatrix} \quad (C.84)$$

The outward iterations for link 2 are as follows:

$${}^2\omega_2 = +\dot{\theta}_1 + {}^1\hat{Z}_1 = \begin{bmatrix} 0 \\ 0 \\ \dot{\theta}_1 + \dot{\theta}_2 \end{bmatrix} \quad (\text{C.85})$$

$${}^2\dot{\omega}_2 = \ddot{\theta}_1 {}^1\hat{Z}_1 = \begin{bmatrix} 0 \\ 0 \\ \ddot{\theta}_1 + \ddot{\theta}_2 \end{bmatrix} \quad (\text{C.86})$$

$${}^2\dot{v}_2 = \begin{bmatrix} c_2 & s_2 & 0 \\ -s_2 & c_2 & 0 \\ 0 & 0 & 1 \end{bmatrix} \begin{bmatrix} -l_1\dot{\theta}_1^2 + gs_1 \\ l_1\ddot{\theta}_1 + gc_1 \\ 0 \end{bmatrix} = \begin{bmatrix} l_1\ddot{\theta}_1s_2 - l_1\dot{\theta}_1^2c_2 + gs_{12} \\ l_1\ddot{\theta}_1c_2 + l_1\dot{\theta}_1^2s_2 + gc_{12} \\ 0 \end{bmatrix} \quad (\text{C.87})$$

$${}^2\dot{v}_{c_2} = \begin{bmatrix} 0 \\ l_2(\ddot{\theta}_1 + \ddot{\theta}_2) \\ 0 \end{bmatrix} + \begin{bmatrix} -l_2(\dot{\theta}_1 + \dot{\theta}_2)^2 \\ 0 \\ 0 \end{bmatrix} \\ + \begin{bmatrix} l_1\ddot{\theta}_1s_2 - l_1\dot{\theta}_1^2c_2 + gs_{12} \\ l_1\ddot{\theta}_1c_2 + l_1\dot{\theta}_1^2s_2 + gc_{12} \\ 0 \end{bmatrix}$$

$${}^2\dot{v}_{c_2} = \begin{bmatrix} l_1\ddot{\theta}_1s_2 - l_1\dot{\theta}_1^2c_2 + gs_{12} - l_2(\dot{\theta}_1 + \dot{\theta}_2)^2 \\ l_1\ddot{\theta}_1c_2 + l_1\dot{\theta}_1^2s_2 + gc_{12} + l_2(\ddot{\theta}_1 + \ddot{\theta}_2) \\ 0 \end{bmatrix} \quad (\text{C.88})$$

$${}^2F_2 = \begin{bmatrix} m_2l_1\ddot{\theta}_1s_2 - m_2l_1\dot{\theta}_1^2c_2 + m_2gs_{12} - m_2l_2(\dot{\theta}_1 + \dot{\theta}_2)^2 \\ m_2l_1\ddot{\theta}_1c_2 + m_2l_1\dot{\theta}_1^2s_2 + m_2gc_{12} + m_2l_2(\ddot{\theta}_1 + \ddot{\theta}_2) \\ 0 \end{bmatrix} \quad (\text{C.89})$$

$${}^2N_2 = \begin{bmatrix} 0 \\ 0 \\ 0 \end{bmatrix} \quad (\text{C.90})$$

The outward iterations for link 3 are as follows:

$${}^3N_3 = \begin{bmatrix} 0 \\ 0 \\ 0 \end{bmatrix} \quad (\text{C.91})$$

The inward iterations for link 1 are as follows:

$${}^3f_3 = {}^3F_3$$

$${}^3n_3 =$$

$$\begin{bmatrix} 0 \\ 0 \\ m_3l_1l_3\ddot{\theta}_1c_{23} + m_3l_1l_3\dot{\theta}_1^2s_{23} + m_3l_3gc_{123} + m_3l_2l_3(\ddot{\theta}_1 + \ddot{\theta}_2) + m_3l_3^2(\ddot{\theta}_1 + \ddot{\theta}_2 + \ddot{\theta}_3) \end{bmatrix} \quad (\text{C.92})$$

$$\begin{aligned}
{}^2f_2 = & \\
& \begin{bmatrix} c_3 & -s_3 & 0 \\ s_3 & c_3 & 0 \\ 0 & 0 & 1 \end{bmatrix} \\
& \begin{bmatrix} m_3 l_1 \ddot{\theta}_1 s_{23} - m_3 l_1 \dot{\theta}_1^2 c_{23} + m_3 g s_{123} - m_3 l_2 (\dot{\theta}_1 + \dot{\theta}_2)^2 - m_3 l_3 (\dot{\theta}_1 + \dot{\theta}_2 + \dot{\theta}_3)^2 \\ m_3 l_1 \ddot{\theta}_1 c_{23} + m_3 l_1 \dot{\theta}_1^2 s_{23} + m_3 g c_{123} + m_3 l_2 (\ddot{\theta}_1 + \ddot{\theta}_2) + m_3 l_3 (\ddot{\theta}_1 + \ddot{\theta}_2 + \ddot{\theta}_3) \\ 0 \end{bmatrix} \\
& + \begin{bmatrix} m_2 l_1 \ddot{\theta}_1 s_2 - m_2 l_1 \dot{\theta}_1^2 c_2 + m_2 g s_{12} - m_2 l_2 (\dot{\theta}_1 + \dot{\theta}_2)^2 \\ m_2 l_1 \ddot{\theta}_1 c_2 + m_2 l_1 \dot{\theta}_1^2 s_2 + m_2 g c_{12} + m_2 l_2 (\ddot{\theta}_1 + \ddot{\theta}_2) \\ 0 \end{bmatrix}
\end{aligned} \tag{C.93}$$

$$\begin{aligned}
{}^2f_2 = & \\
& \begin{bmatrix} m_3 l_1 \ddot{\theta}_1 (s_{23} c_3 - c_{23} s_3) - m_3 l_1 \dot{\theta}_1^2 (c_{23} c_3 + s_{23} s_3) \\ + m_3 g (s_{123} c_3 - c_{123} s_3) - m_3 l_2 (\dot{\theta}_1 + \dot{\theta}_2)^2 \\ - m_3 l_3 (\dot{\theta}_1 + \dot{\theta}_2 + \dot{\theta}_3)^2 c_3 + m_3 l_3 (\ddot{\theta}_1 + \ddot{\theta}_2 + \ddot{\theta}_3) s_{32} l_1 \ddot{\theta}_1 s_2 \\ - m_2 l_1 \dot{\theta}_1^2 c_2 + m_2 g s_{12} - m_2 l_2 (\dot{\theta}_1 + \dot{\theta}_2)^2 \\ \\ m_3 l_1 \ddot{\theta}_1 (s_{23} s_3 + c_{23} c_3) - m_3 l_1 \dot{\theta}_1^2 (c_{23} s_3 - s_{23} c_3) \\ + m_3 g (s_{123} s_3 + c_{123} c_3) - m_3 l_2 (\dot{\theta}_1 + \dot{\theta}_2)^2 s_3 + m_3 l_2 (\ddot{\theta}_1 + \ddot{\theta}_2) c_3 \\ - m_3 l_3 (\dot{\theta}_1 + \dot{\theta}_2 + \dot{\theta}_3)^2 + m_3 l_3 (\ddot{\theta}_1 + \ddot{\theta}_2 + \ddot{\theta}_3) c_3 m_2 l_1 \ddot{\theta}_1 c_2 \\ + m_2 l_1 \dot{\theta}_1^2 s_2 + m_2 g c_{12} + m_2 l_2 (\ddot{\theta}_1 + \ddot{\theta}_2) \\ \\ 0 \end{bmatrix}
\end{aligned} \tag{C.94}$$

$$\begin{aligned}
{}^2n_2 = & \\
& \begin{bmatrix} 0 \\ 0 \\ m_3 l_1 l_3 \ddot{\theta}_1 c_{23} + m_3 l_1 l_3 \dot{\theta}_1^2 s_{23} + m_3 l_3 g c_{123} + m_3 l_2 l_3 (\ddot{\theta}_1 + \ddot{\theta}_2) + m_3 l_3^2 (\ddot{\theta}_1 + \ddot{\theta}_2 + \ddot{\theta}_3) \end{bmatrix} \\
& + \begin{bmatrix} 0 \\ 0 \\ m_2 l_1 l_2 \ddot{\theta}_1 c_2 + m_2 l_1 l_2 \dot{\theta}_1^2 s_2 + m_2 l_2 g c_{12} + m_2 l_2^2 (\ddot{\theta}_1 + \ddot{\theta}_2) \end{bmatrix} + \\
& \begin{bmatrix} 0 \\ 0 \\ m_3 l_1 l_2 \ddot{\theta}_1 (s_{23} s_3 + c_{23} c_3) - m_3 l_1 l_2 \dot{\theta}_1^2 (c_{23} s_3 - s_{23} c_3) \\ + m_3 l_2 g (s_{123} s_3 + c_{123} c_3) + m_3 l_1 l_2^2 (\dot{\theta}_1 + \dot{\theta}_2)^2 s_3 \\ + m_3 l_2^2 (\ddot{\theta}_1 + \ddot{\theta}_2) c_3 - m_3 l_2 l_3 (\dot{\theta}_1 + \dot{\theta}_2 + \dot{\theta}_3)^2 s_3 + m_3 l_2 l_3 (\ddot{\theta}_1 + \ddot{\theta}_2 + \ddot{\theta}_3) c_3 \end{bmatrix}
\end{aligned} \tag{C.95}$$

$${}^2n_2 =$$

$$\begin{bmatrix} 0 \\ 0 \\ m_3 l_1 l_3 \ddot{\theta}_1 c_{23} + m_3 l_1 l_3 \dot{\theta}_1^2 s_{23} + m_3 l_3 g c_{123} + m_3 l_2 l_3 (\ddot{\theta}_1 + \ddot{\theta}_2) \\ + m_3 l_3^2 (\ddot{\theta}_1 + \ddot{\theta}_2 + \ddot{\theta}_3) + m_2 l_1 l_2 \ddot{\theta}_1 c_2 + m_2 l_1 l_2 \dot{\theta}_1^2 s_2 + m_2 l_2 g c_{12} \\ + m_2 l_2^2 (\ddot{\theta}_1 + \ddot{\theta}_2) + m_3 l_1 l_2 \ddot{\theta}_1 (s_{23} s_3 + c_{23} c_3) - m_3 l_1 l_2 \dot{\theta}_1^2 (c_{23} s_3 - s_{23} c_3) \\ + m_3 l_2 g (s_{123} s_3 + c_{123} c_3) + m_3 l_1 l_2^2 (\dot{\theta}_1 + \dot{\theta}_2)^2 s_3 + m_3 l_2^2 (\ddot{\theta}_1 + \ddot{\theta}_2) c_3 \\ - m_3 l_2 l_3 (\dot{\theta}_1 + \dot{\theta}_2 + \dot{\theta}_3)^2 s_3 + m_3 l_2 l_3 (\ddot{\theta}_1 + \ddot{\theta}_2 + \ddot{\theta}_3) c_3 \end{bmatrix} \quad (\text{C.96})$$

$${}^1f_1 = \begin{bmatrix} c_2 & -s_2 & 0 \\ s_2 & c_2 & 0 \\ 0 & 0 & 1 \end{bmatrix}$$

$$\begin{bmatrix} m_3 l_1 \ddot{\theta}_1 (s_{23} c_3 - c_{23} s_3) - m_3 l_1 \dot{\theta}_1^2 (c_{23} c_3 + s_{23} s_3) + m_3 g (s_{123} c_3 - c_{123} s_3) \\ - m_3 l_2 (\dot{\theta}_1 + \dot{\theta}_2)^2 c_3 - m_3 l_2 (\ddot{\theta}_1 + \ddot{\theta}_2) s_3 - m_3 l_3 (\dot{\theta}_1 + \dot{\theta}_2 + \dot{\theta}_3)^2 c_3 \\ + m_3 l_3 (\ddot{\theta}_1 + \ddot{\theta}_2 + \ddot{\theta}_3) s_3 m_2 l_1 \ddot{\theta}_1 s_2 - m_2 l_1 \dot{\theta}_1^2 c_2 + m_2 g s_{12} - m_2 l_2 (\dot{\theta}_1 + \dot{\theta}_2)^2 \\ m_3 l_1 \ddot{\theta}_1 (s_{23} s_3 + c_{23} c_3) - m_3 l_1 \dot{\theta}_1^2 (c_{23} s_3 - s_{23} c_3) + m_3 g (s_{123} s_3 + c_{123} c_3) \\ - m_3 l_2 (\dot{\theta}_1 + \dot{\theta}_2)^2 s_3 + m_3 l_2 (\ddot{\theta}_1 + \ddot{\theta}_2) c_3 - m_3 l_3 (\dot{\theta}_1 + \dot{\theta}_2 + \dot{\theta}_3)^2 s_3 \\ + m_3 l_3 (\ddot{\theta}_1 + \ddot{\theta}_2 + \ddot{\theta}_3) c_3 + m_2 l_1 \ddot{\theta}_1 c_2 + m_2 l_1 \dot{\theta}_1^2 s_2 + m_2 g c_{12} + m_2 l_2 (\ddot{\theta}_1 + \ddot{\theta}_2) \\ 0 \end{bmatrix} + \begin{bmatrix} -m_1 l_1 \dot{\theta}_1^2 + m_1 g s_1 \\ m_1 l_1 \ddot{\theta}_1 + m_1 g c_1 \\ 0 \end{bmatrix} \quad (\text{C.97})$$

$${}^1f_1 =$$

$$\begin{bmatrix} m_3 l_1 \dot{\theta}_1^2 + m_3 g (s_{123} c_{23} - c_{123} s_{23}) - m_3 l_2 (\dot{\theta}_1 + \dot{\theta}_2)^2 (c_{23} + s_{23}) \\ m_3 l_3 (\dot{\theta}_1 + \dot{\theta}_2 + \dot{\theta}_3)^2 (c_{23} + s_{23}) + m_2 g (s_{12} c_2 - c_{12} s_2) - m_2 l_2 (\dot{\theta}_1 + \dot{\theta}_2)^2 (c_2 - s_2) \\ m_3 l_1 \ddot{\theta}_1 + m_3 g (s_{123} s_{23} - c_{123} c_{23}) \\ 0 \end{bmatrix} \quad (\text{C.98})$$

$${}^1n_1 =$$

$$\begin{aligned}
& \begin{bmatrix} 0 \\ 0 \\ m_3 l_1 l_3 \ddot{\theta}_1 c_{23} + m_3 l_1 l_3 \dot{\theta}_1^2 s_{23} + m_3 l_3 g c_{123} 0 \\ + m_3 l_2 l_3 (\ddot{\theta}_1 + \ddot{\theta}_2) + m_3 l_3^2 (\ddot{\theta}_1 + \ddot{\theta}_2 + \ddot{\theta}_3) + m_2 l_1 l_2 \ddot{\theta}_1 c_2 \\ + m_2 l_1 l_2 \dot{\theta}_1^2 s_2 + m_2 l_2 g c_{12} + m_2 l_2^2 (\ddot{\theta}_1 + \ddot{\theta}_2) + m_3 l_1 \ddot{\theta}_1 \\ (2s_{23} c_3 s_3 - c_{23} (s_3^2 - c_3^2)) - m_3 l_1 \dot{\theta}_1^2 s_{23} + m_3 g (2s_{123} c_3 s_3 - c_{123} (s_3^2 - c_3^2)) \\ - m_3 l_2 (\dot{\theta}_1 + \dot{\theta}_2)^2 - m_3 l_3 (\dot{\theta}_1 + \dot{\theta}_2 + \dot{\theta}_3)^2 s_{23} (s_3^2 - c_3^2) \\ + m_2 l_1 \ddot{\theta}_1 (s_2 s_3 + c_2 c_3) + m_2 g - m_2 l_2 (\dot{\theta}_1 + \dot{\theta}_2)^2 s_3 + m_2 l_2 (\ddot{\theta}_1 + \ddot{\theta}_2) c_3 \end{bmatrix} \\
& + \begin{bmatrix} 0 \\ 0 \\ m_1 l_1^2 \ddot{\theta}_1 + m_1 l_1 g c_1 \end{bmatrix} \\
& \begin{bmatrix} 0 \\ 0 \\ m_3 l_1^2 l_3 \ddot{\theta}_1 (2s_{23} c_3 s_3 - c_{23} (s_3^2 - c_3^2)) - m_3 l_1^2 l_3 \dot{\theta}_1^2 s_{23} + m_3 l_1 l_3 g (2s_{123} c_3 s_3 \\ - c_{123} (s_3^2 - c_3^2)) - m_3 l_1 l_2 l_3 (\dot{\theta}_1 + \dot{\theta}_2)^2 - m_3 l_1 l_3^2 (\dot{\theta}_1 + \dot{\theta}_2 + \dot{\theta}_3)^2 s_{23} (s_3^2 - c_3^2) \\ + m_2 l_1^2 l_2 \ddot{\theta}_1 (s_2 s_3 + c_2 c_3) + m_2 l_1 g - m_2 l_1 l_2 l_3 (\dot{\theta}_1 + \dot{\theta}_2)^2 s_3 + m_2 l_1 l_2 l_3 (\ddot{\theta}_1 + \ddot{\theta}_2) c_3 \end{bmatrix}
\end{aligned} \tag{C.99}$$

Finally, the equation of torques will be provided like shown below:

$$\begin{aligned}
\tau_1 = & m_3 l_1 l_3 \ddot{\theta}_1 c_{23} + m_3 l_2 l_3 (\ddot{\theta}_1 + \ddot{\theta}_2) + m_3 l_3^2 (\ddot{\theta}_1 + \ddot{\theta}_2 + \ddot{\theta}_3) + m_2 l_1 l_2 \ddot{\theta}_1 c_2 \\
& + m_2 l_2^2 (\ddot{\theta}_1 + \ddot{\theta}_2) + m_3 l_1 \ddot{\theta}_1 ((2s_{23} c_3 s_3 - c_{23} (s_3^2 - c_3^2))) \\
& + m_2 l_1 \ddot{\theta}_1 (s_2 s_3 + c_2 c_3) + m_2 l_2 (\ddot{\theta}_1 + \ddot{\theta}_2) c_3 + m_1 l_1^2 \ddot{\theta}_1 \\
& + m_3 l_1^2 l_3 \ddot{\theta}_1 (2s_{23} c_3 s_3 - c_{23} (s_3^2 - c_3^2)) + m_2 l_1^2 l_2 \ddot{\theta}_1 (s_2 s_3 + c_2 c_3) \\
& + m_2 l_1 l_2 l_3 (\ddot{\theta}_1 + \ddot{\theta}_2) c_3
\end{aligned} \tag{C.100}$$

$$\begin{aligned}
\tau_2 = & m_3 l_1 l_3 \ddot{\theta}_1 c_{23} + m_3 l_1 l_3 \dot{\theta}_1^2 s_{23} + m_3 l_3 g c_{123} + m_3 l_2 l_3 (\ddot{\theta}_1 + \ddot{\theta}_2) + m_3 l_3^2 (\ddot{\theta}_1 \\
& + \ddot{\theta}_3) + m_2 l_1 l_2 \ddot{\theta}_1 c_2 + m_2 l_1 l_2 \dot{\theta}_1^2 s_2 + m_2 l_2 g c_{12} + m_2 l_2^2 (\ddot{\theta}_1 + \ddot{\theta}_2) \\
& + m_3 l_1 l_2 \ddot{\theta}_1 (s_{23} s_3 + c_{23} c_3) - m_3 l_1 l_2 \dot{\theta}_1^2 (c_{23} s_3 - s_{23} c_3) \\
& + m_3 l_2 g (s_{123} s_3 + c_{123} c_3) + m_3 l_1 l_2^2 (\dot{\theta}_1 + \dot{\theta}_2)^2 s_3 + m_3 l_2^2 (\ddot{\theta}_1 + \ddot{\theta}_2) c_3 - m_3 l_2 l_3 \\
& + \ddot{\theta}_2 (\dot{\theta}_1 + \dot{\theta}_2 + \dot{\theta}_3)^2 s_3 + m_3 l_2 l_3 (\ddot{\theta}_1 + \ddot{\theta}_2 + \ddot{\theta}_3) c_3
\end{aligned} \tag{C.101}$$

$$\begin{aligned}
\tau_3 = & m_3 l_1 l_3 \ddot{\theta}_1 c_{23} + m_3 l_1 l_3 \dot{\theta}_1^2 s_{23} + m_3 l_3 g c_{123} + m_3 l_2 l_3 (\ddot{\theta}_1 + \ddot{\theta}_2) \\
& + m_3 l_3^2 (\ddot{\theta}_1 + \ddot{\theta}_2 + \ddot{\theta}_3)
\end{aligned} \tag{C.102}$$

The expression of dynamic equation is:

$$\tau = M(\theta)\ddot{\theta} + V(\dot{\theta}, \ddot{\theta}) + G(\theta) \quad (3.103)$$

Where $M(\theta)$ the (n x n) mass matrix of the fingers is $V(\theta, \dot{\theta})$ is (n x 1) vector of centrifugal and Coriolis term and $G(\theta)$ is (n x 1) vector gravity. Each element of $M(\theta)$ and $G(\theta)$ is a complex function which depends on θ , the position of all the joints of the fingers. Each element of $V(\dot{\theta}, \ddot{\theta})$ is a complex function of both θ and $\dot{\theta}$. Dynamic equation of MFRH is derived in detail in *Appendix C*.

Finally, the equation of torques will be provided like shown below:

$$\begin{aligned} \tau_1 = & m_3 l_1 l_3 \ddot{\theta}_1 c_{23} + m_3 l_2 l_3 (\ddot{\theta}_1 + \ddot{\theta}_2) + m_3 l_3^2 (\ddot{\theta}_1 + \ddot{\theta}_2 + \ddot{\theta}_3) + m_2 l_1 l_2 \ddot{\theta}_1 c_2 \\ & + m_2 l_2^2 (\ddot{\theta}_1 + \ddot{\theta}_2) + m_3 l_1 \ddot{\theta}_1 (2s_{23}c_3s_3 - c_{23}(s_3^2 - c_3^2)) \\ & + m_2 l_1 \ddot{\theta}_1 (s_2s_3 + c_2c_3) + m_2 l_2 (\ddot{\theta}_1 + \ddot{\theta}_2) c_3 + m_1 l_1^2 \ddot{\theta}_1 \\ & + m_3 l_1^2 l_3 \ddot{\theta}_1 (2s_{23}c_3s_3 - c_{23}(s_3^2 - c_3^2)) + m_2 l_1^2 l_2 \ddot{\theta}_1 (s_2s_3 + c_2c_3) \\ & + m_2 l_1 l_2 l_3 (\ddot{\theta}_1 + \ddot{\theta}_2) c_3 \end{aligned} \quad (3.104)$$

$$\begin{aligned} \tau_2 = & m_3 l_1 l_3 \ddot{\theta}_1 c_{23} + m_3 l_1 l_3 \dot{\theta}_1^2 s_{23} + m_3 l_3 g c_{123} + m_3 l_2 l_3 (\ddot{\theta}_1 + \ddot{\theta}_2) + m_3 l_3^2 (\ddot{\theta}_1 \\ & + \ddot{\theta}_3) + m_2 l_1 l_2 \ddot{\theta}_1 c_2 + m_2 l_1 l_2 \dot{\theta}_1^2 s_2 + m_2 l_2 g c_{12} + m_2 l_2^2 (\ddot{\theta}_1 + \ddot{\theta}_2) \\ & + m_3 l_1 l_2 \ddot{\theta}_1 (s_{23}c_3 + c_{23}c_3) - m_3 l_1 l_2 \dot{\theta}_1^2 (c_{23}s_3 - s_{23}c_3) \\ & + m_3 l_2 g (s_{123}s_3 + c_{123}c_3) + m_3 l_1 l_2^2 (\dot{\theta}_1 + \dot{\theta}_2)^2 s_3 + m_3 l_2^2 (\ddot{\theta}_1 + \ddot{\theta}_2) c_3 - m_3 l_2 l_3 \\ & + \ddot{\theta}_2 (\dot{\theta}_1 + \dot{\theta}_2 + \dot{\theta}_3)^2 s_3 + m_3 l_2 l_3 (\ddot{\theta}_1 + \ddot{\theta}_2 + \ddot{\theta}_3) c_3 \end{aligned} \quad (3.105)$$

$$\begin{aligned} \tau_3 = & m_3 l_1 l_3 \ddot{\theta}_1 c_{23} + m_3 l_1 l_3 \dot{\theta}_1^2 s_{23} + m_3 l_3 g c_{123} + m_3 l_2 l_3 (\ddot{\theta}_1 + \ddot{\theta}_2) \\ & + m_3 l_3^2 (\ddot{\theta}_1 + \ddot{\theta}_2 + \ddot{\theta}_3) \end{aligned} \quad (3.106)$$

APPENDIX D

MATLAB CODES

D1. Matlab Code

```

clear all
clc

% set each length and gravity of Index Fingers
l1=0.0605; l2=0.0375; l3=0.0245;
g=9.81;

% set the mass of Index fingers
m1=0.0100728; m2=0.00397876; m3=0.00208544;

% set the trajectory qf, q0, Tf and T0
qf=2; q0=0; Tf=10; T0=0; t=10; pi=180;

% Conversion theta in radian
qd=((qf-q0)/2)*(1-(cosd((pi/10)*10)));
qd_dot=(pi/2)*((qf-q0)/(Tf-T0));
qd_ddot=((pi^2)/2)*((qf-q0)/((Tf-T0)^2));

%set theta for finger
q1dot=qd_dot; q2dot=q1dot; q3dot=q2dot;
q1ddot=qd_ddot; q2ddot=q1dot; q3ddot=q2dot;
%setting the value of cos=c and sin=s

c1=cosd(115); c2=cosd(c1); c3=cosd(c2);

c12=c1+c2;
c23=c2+c3;
c123=c1+c2+c3;
c233=c2+c3+c3;
c21=c12;

s1=sind(115); s2=sind(s1); s3=sind(s2);

s12=s1+s2;
s23=s2+s3;
s123=s1+s2+s3;
s233=s2+s3+s3;
s21=s12;

q1=c1; q2=q1; q3=q2;

%Formula the mass
M11=((l1^2)*(m1+(m2*(s2^2)))+(c2^2)*(m3^2)+((s23^2)*m3))+(l2^2)+(l1*
m3*c23*(1+(s2*s3)))+(l2*c2*m3)+(l3*m3)+(l1*l2)*(c2-
c23+(c2*m3)+(s2*s2*m3*(1+c3))+(m2*c2)))+(l2*l3*c3)+(l1*l3*m3*s23);
M12=((l3*m3)+(l2*c3*m3)+(2*(l2^2)))+(l2*l3*c3)+(l1*l2*s2*s3*m3*(1+c3))
+(l1*l3*m3*s2*s3);
M13=(l3*m3)+(l2*l3*c3)+(l1*l3*m3*s2*s3);

```

```

M21=(2*(l2^2))+(l3*m3)+(l1*c23*m3)+(l2*c3*m3)+(l2*l3*c3)+((l1*l2)*(-
c23+c2));
M22=(l3*m3)+(l2*c3*m3)+(2*(l2^2))+(l2*l3*c3);
M23=(l3*m3)+(l2*l3*c3);

```

```

M31=(l3*m3)+(l1*c23*m3)+(l2*c3*m3);
M32=(l3*m3)+(l2*c3*m3);
M33=0;

```

```

Mx=[M11 M12 M13; M21 M22 M23; M31 M32 M33];

```

```

M1=M11*q1ddot+M12*q2ddot+M13*q3ddot;
M2=M21*q1ddot+M22*q2ddot+M23*q3ddot;
M3=M31*q1ddot+M32*q2ddot+M33*q3ddot;

```

```

M=[M1;M2;M3];

```

```

%Formula the velocity

```

```

V1=((l2*s3*m3)-((l2^2)*s3*c3)-
(l1^l2*s2*m3)+((l2^2)*s3*c3)*(q1dot*q2dot))+((l1*m3*s23*(1-
(s2*s3)))+(l1*l2*(s2-s233)))+(l1^2)*((-
s23*c23*m3)+(s23*c2*c3*m3)+(s2*c2*m2))-((l1*c2*m2*s2))*(q1dot^2))-
((l2*s2*m2)*((q1dot*q2dot)^2))-((l2*l3*s3)*(q1dot+q2dot+q3dot))-
((l1*l3*s23*m3)*((q1dot+q2dot+q3dot)^2));
V2=((l2*s3*m3)*(q1dot+q2dot))+((l1*m3*s23)+(l1*l2*(c2-
(c23*c3)+(s23*c3)))*(q1dot^2))-((l2*l3*c23*(q1dot+q2dot+q3dot)));
V3=((l2*s3*m3)*(q1dot+q2dot))+((l1*m3*s23)*(q1dot^2));
V=[V1;V2;V3];

```

```

%Formula the gravity

```

```

G1=(g*c123*m3*(1-
(s2*s3)))+(l2*c12*g)+(l2*l3*g*s123)+(l2*g*c123*c3)+(l1*m1*g*c1)+(l1*g
*c3*c2*m3*(s123+c123))+(l1*m2*s12*g*q2)+(l1*g*s3*c2*s123*m3)+(l1*m2*c
12*c2*g);
G2=(g*c123*m3)+(l2*c12*g)+(l2*l3*g*s123)+(l2*g*c123*c3);
G3=(g*c123*m3);
G=[G1;G2;G3];
G=G1+G2+G3;

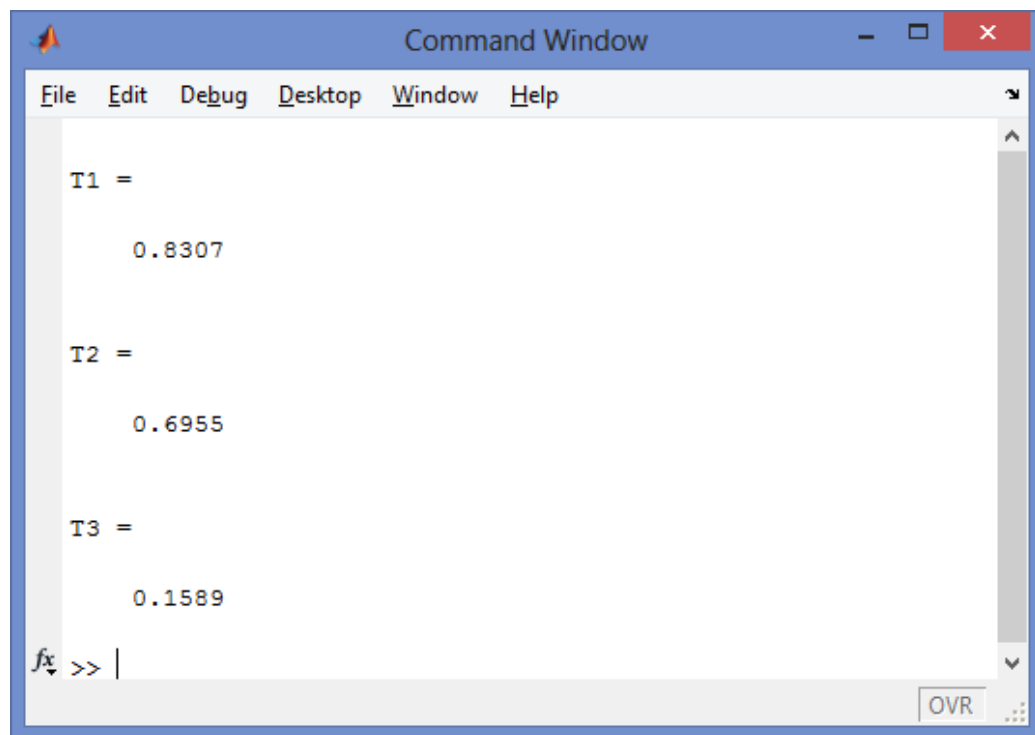
```

```

T1=(M1+V1+G1)
T2=(M2+V2+G2)
T3=(M3+V3+G3)

```

D2. Print Screen



The image shows a screenshot of a 'Command Window' application. The window has a blue title bar with the text 'Command Window' and standard window control buttons (minimize, maximize, close). Below the title bar is a menu bar with the following items: File, Edit, Debug, Desktop, Window, and Help. The main area of the window is white and contains the following text:

```
T1 =  
    0.8307  
  
T2 =  
    0.6955  
  
T3 =  
    0.1589
```

At the bottom left of the window, there is a prompt character 'fx' followed by '>>' and a vertical cursor line. At the bottom right, there is a button labeled 'OVR' and a small icon of three dots.

APPENDIX E

TECHNICAL SPECIFICATION OF DC SERVOMOTOR



DC-Micromotors

Technical Information

General information

The lifetime, depending on the application type, may exceed the 10 000 hours. Higher speeds cause accelerated mechanical wear, resulting in reduced lifetime. Also excessively high current and temperature shortens the lifetime. On the average, lifetime of up to 1 000 hours for metal brushes, and more than 3 000 hours for graphite brushes can be expected when the motors are operated within recommended values indicated on the data sheet. These values do not influence each other. It is advisable that the current under load in continuous operation should not be higher than one third of the stall current. In motors with graphite brushes the relationship between stall current and current under load depends on the delivered power and frame size. The motors should not be operated at the stall torque M_H , otherwise after a short period of time, the commutation or the windings could be damaged.

The motor develops its maximum power $P_{2\max}$ at exactly half the stall torque M_H which also corresponds to half the speed. For reasons of life performance, this working point should only be selected for intermittent periods. For exceptional long life performance, brushless DC-Motors are available.

Unspecified tolerances:

Tolerances in accordance with ISO 2768 medium.

≤ 6 = ± 0,1 mm

≤ 30 = ± 0,2 mm

≤ 120 = ± 0,3 mm

Motors with tighter tolerances and tolerances of values not specified are given on request.

Bearing options:

– Standard: Unless otherwise stated, vacuum impregnated sintered bearings are used

– Optional: Shielded ball bearings

Motor shaft:

All dimensions with shaft pushed against motor.

Motor choice:

The listed motor types represent standardised executions. However, a variety of further coil possibilities are available.

DC-Micromotors

Precious Metal Commutation

Series 0615 ... S

1	Nominal voltage	U_N
2	Terminal resistance	R
3	Output power	$P_{2\max}$
4	Efficiency	η_{\max}
5	No-load speed	n_0

Notes on technical data

All values at 22 °C.

All values at nominal voltage, motor only, without load.

Nominal voltage U_N [Volt]

The nominal voltage at which all other characteristics indicated are measured.

Terminal resistance R [Ω] ±12%

The resistance measured across the motor terminals. The value is directly affected by the coil temperature (temperature coefficient: $\alpha_{22} = 0,004 \text{ K}^{-1}$).

Output power $P_{2\max}$ [W]

The maximum obtainable mechanical power achieved at the nominal voltage.

$$P_{2\max} = \frac{R}{4} \left(\frac{U_N}{R} - I_0 \right)^2$$

Efficiency η_{\max} [%]

The max. ratio between the absorbed electrical power and the obtained mechanical power of the motor. It does not always correspond to the optimum working point of the motor.

$$\eta_{\max} = \left(1 - \sqrt{\frac{I_0 R}{U_N}} \right)^2 \cdot 100$$

No-load speed n_0 [rpm] ±12%

Describes the maximum speed under no-load conditions at steady state and 22 °C ambient temperature. If not otherwise defined the tolerance for the no-load speed is assumed to be ±12%.

$$n_0 = (U_N - I_0 \cdot R) \cdot k_n$$

No-load current I_0 [A] ±50%

Describes the current consumption of the motor without load at an ambient temperature of 22 °C after reaching a steady state condition. The tolerance is given at ±50%.

The no-load current is speed and temperature dependent. Changes in ambient temperature or cooling conditions will influence the value. In addition, modifications to the shaft, bearing, lubrication, and commutation system or combinations with other components such as gearheads or encoders will all result in a change to the no-load current of the motor.

Stall torque M_H [mNm]

The torque developed by the motor at zero speed and nominal voltage. This value is greatly influenced by temperature.

$$M_H = k_M \cdot \left(\frac{U_N}{R} - I_0 \right)$$

Friction torque M_f [mNm]

Torque losses caused by the friction of brushes, bearings and commutators. This value is influenced by temperature.

$$M_f = k_M \cdot I_0$$

Speed constant k_n [rpm/V]

The speed variation per Volt applied to the motor terminals at constant load.

$$k_n = \frac{n_0}{U_N - I_0 \cdot R} = \frac{1000}{k_E}$$

Back-EMF constant k_E [mV/rpm]

The constant corresponding to the relationship between the induced voltage in the rotor at the speed of rotation.

$$k_E = \frac{2\pi \cdot k_M}{60}$$

Torque constant k_M [mNm/A]

The constant corresponding to the relationship between the torque developed by the motor and the current drawn.

Current constant k_i [A/mNm]

The constant between the current in the motor torque developed.

$$k_i = \frac{1}{k_M}$$

Slope of n-M curve $\Delta n / \Delta M$ [rpm/mNm]

The ratio of the speed variation to the torque variation. The smaller the value, the more powerful the motor.

$$\frac{\Delta n}{\Delta M} = \frac{30000}{\pi} \cdot \frac{R}{k_M^2}$$

Rotor inductance L [μ H]

The inductance measured on the motor terminals at 1 kHz.

Mechanical time constant τ_m [ms]

The time required for the motor to reach a speed of 63% of its final no-load speed, from standstill.

$$\tau_m = \frac{100 \cdot R \cdot J}{k_M^2}$$

Rotor inertia J [gcm²]

Rotor's mass dynamic inertia moment.

Angular acceleration α_{max} [$\cdot 10^3$ rad/s²]

The acceleration obtained from standstill under no-load conditions and at nominal voltage.

$$\alpha_{max} = \frac{M_H \cdot 10}{J}$$

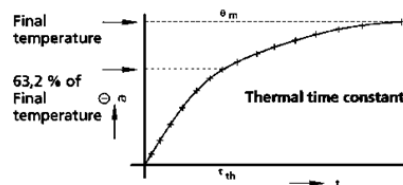
Thermal resistance R_{th1}/R_{th2} [K/W]

R_{th1} corresponds to the value between the rotor and housing. R_{th2} corresponds to the value between the housing and the ambient air.

R_{th2} can be reduced by enabling exchange of heat between the motor and the ambient air (for example using a heat sink or forced air cooling).

Thermal time constant τ_{w1}/τ_{w2} [s]

The thermal time constant specifies the time needed for the rotor and housing to reach a temperature equal to 63% of final value.



Operating temperature range [°C]

Indicates the min. and max. motor operating temperature, as well as the maximum permitted rotor temperature.

Shaft bearings

used for the DC-Micromotors.

Output shaft load M_{out} [N]

The output shaft load at a specified shaft diameter for the primary output shaft. For motors with ball bearings the load and lifetime are in accordance with the values given by the bearing manufacturers. This value does not apply to second, or rear shaft ends.

Shaft play [mm]

The shaft play on the bearings, measured at the bearing exit.

Housing material

The housing material and the surface protection.

Weight [g]

The average weight of the basic motor type.

DC-Micromotors

Technical Information

Direction of rotation

The direction of rotation is viewed from the front face. Positive voltage to the + terminal gives clockwise rotation of the motor shaft. All motors are designed for clockwise (CW) and counterclockwise (CCW) operation; the direction of rotation is reversible.

Recommended values

The maximum recommended values for continuous operation to obtain optimum life performance are listed below. The values are independent of each other. The values will be reduced with thermal insulation and elevated temperature but can be increased with forced cooling.

Speed $n_{re,max}$ [rpm]

The maximum recommended operating speed.

Torque $M_{re,max}$ [mNm]

The maximum recommended torque rating.

Current $I_{e,max}$ [A]

The maximum allowable current, based on the thermal limits of the max. permissible standard rotor temperature at 22 °C ambient.

How to select a DC-Micromotor

This section reviews a step-by-step procedure on how to select a DC-Micromotor. The procedure allows calculation of the parameters in order to produce a graph of the characteristics and permitting the definition of the motor's behaviour. To simplify the calculation, in this example continuous operation and optimum life performance are assumed and the influence of temperature and tolerances has been omitted.

Application data:

The basic data required for any given application are:

Required torque	M	[mNm]
Required speed	n	[rpm]
Duty cycle	δ	[%]
Available supply voltage, max.	U	[V DC]
Available current source, max.	I	[A]
Available space, max.	diameter/length	[mm]
Shaft load	radial/axial	[N]

The assumed application data for the selected example are:

Output torque	M	= 3	mNm
Speed	n	= 5 500	rpm

Duty cycle	δ	= 100	%
Supply voltage	U	= 20	V DC
Current source, max.	I	= 0,5	A
Space max.	diameter	= 25	mm
	length	= 50	mm
Shaft load	radial	= 1,0	N
	axial	= 0,2	N

Preselection

The first step is to calculate the power the motor is expected to deliver:

$$P_2 = M \cdot n \cdot \frac{\pi}{30 \cdot 1000} \quad [W]$$

$$P_2 = 3 \cdot 5\,500 \cdot \frac{\pi}{30 \cdot 1000} = 1,73 \quad W$$

A motor is then selected from the catalogue which will give at least 1,5 to 2 times the output power [$P_{2,max}$] than the one obtained by calculation, and where the nominal voltage is equal to or higher than the one required in the application data.

The physical dimensions (diameter and length) of the motor selected from the data sheets should not exceed the available space in the application.

$$P_{2,max} \geq P_2 \quad U_N \geq U$$

The motor selected from the catalogue for this particular application, is series **2233 T 024 S** with the following characteristics:

Nominal voltage	U_N	= 24	V DC	
Output power, max.	$P_{2,max}$	= 2,47	W	
Frame size:	diameter	\emptyset	= 22	mm
	length	L	= 33	mm
Shaft load, max.:	radial	= 1,2	N	
	axial	= 0,2	N	
No-load current	I_0	= 0,005	A	
No-load speed	n_0	= 8 800	rpm	
Stall torque	M_{st}	= 10,70	mNm	


Caution:

Should the available supply voltage be lower than the nominal voltage of the selected DC-Micromotor, it will be necessary to calculate [$P_{2,max}$] with the following equation:

$$P_{2,max} = \frac{R}{4} \cdot \left(\frac{U_N}{R} - I_0 \right)^2 \quad [W]$$

$$P_{2,max} (20 V) = \frac{57}{4} \cdot \left(\frac{20}{57} - 0,005 \right)^2 = 1,70 \quad W$$

DC servomotor specification for MFRH is using Faulhaber data sheet below and regarding to the specification of the length of MFRH.



DC-Micromotors

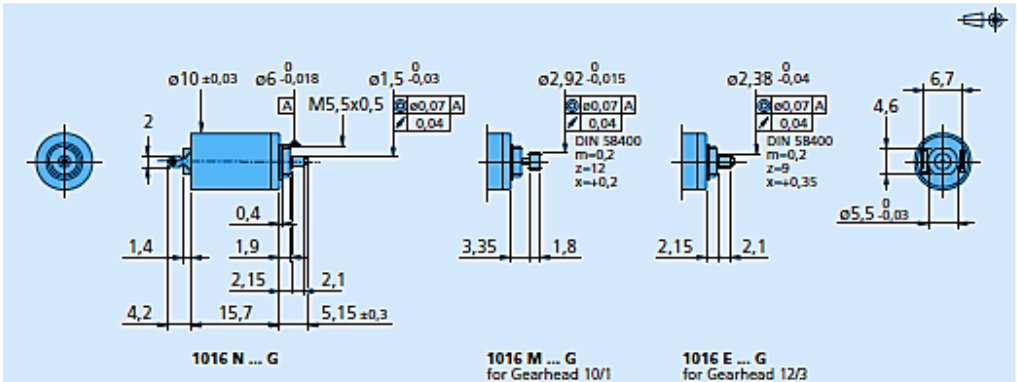
Precious Metal Commutation

0,48 mNm

For combination with
Gearheads:
10/1, 12/3
Encoders:
308, HEM3-256-W, PA2-100

Series 1016 ... G

	1016 N	003 G	006 G	012 G		
1 Nominal voltage	U _N	3	6	12	V	
2 Terminal resistance	R	8,7	20,1	95	Ω	
3 Output power	P _{2 max}	0,24	0,42	0,36	W	
4 Efficiency, max.	η _{max}	63	67	68	%	
5 No-load speed	n ₀	14 200	18 400	16 500	rpm	
6 No-load current (with shaft ø 0,8 mm)	I ₀	0,015	0,01	0,004	A	
7 Stall torque	M _{st}	0,64	0,87	0,82	mNm	
8 Friction torque	M _f	0,03	0,03	0,03	mNm	
9 Speed constant	k _s	4 948	3 173	1 419	rpm/V	
10 Back-EMF constant	k _t	0,202	0,315	0,705	mV/rpm	
11 Torque constant	k _M	1,93	3,01	6,73	mNm/A	
12 Current constant	k _i	0,518	0,332	0,149	A/mNm	
13 Slope of n-M curve	Δn/ΔM	22 304	21 185	20 029	rpm/mNm	
14 Rotor inductance	L	28	60	310	μH	
15 Mechanical time constant	T _m	9	13	10	ms	
16 Rotor inertia	J	0,04	0,06	0,05	gcm ²	
17 Angular acceleration	α _{max}	159	145	165	·10 ⁴ rad/s ²	
18 Thermal resistance	R _{th1} / R _{th2}	26 / 56			KW	
19 Thermal time constant	T _{th1} / T _{th2}	3,1 / 260			s	
20 Operating temperature range:						
- motor		-30 ... +85 (optional version	-30 ... +125)		°C	
- rotor, max. permissible		+85 (optional version	+125)		°C	
21 Shaft bearings		sintered bearings (standard)	ball bearings (optional version)			
22 Shaft load max.:						
- with shaft diameter		0,8	1		mm	
- radial at 3 000 rpm (1,5 mm from bearing)		0,5	5		N	
- axial at 3 000 rpm		0,1	0,5		N	
- axial at standstill		20	5		N	
23 Shaft play						
- radial	≤	0,03	0,02		mm	
- axial	≤	0,2	0,2		mm	
24 Housing material		steel, nickel plated				
25 Weight		6,5			g	
26 Direction of rotation		clockwise, viewed from the front face				
Recommended values - mathematically independent of each other						
27 Speed up to	n _{0 max}		13 000	13 000	13 000	rpm
28 Torque up to	M _{2 max}		0,48	0,48	0,48	mNm



1016 N ... G
1016 M ... G
for Gearhead 10/1
1016 E ... G
for Gearhead 12/3

DC-Micromotors

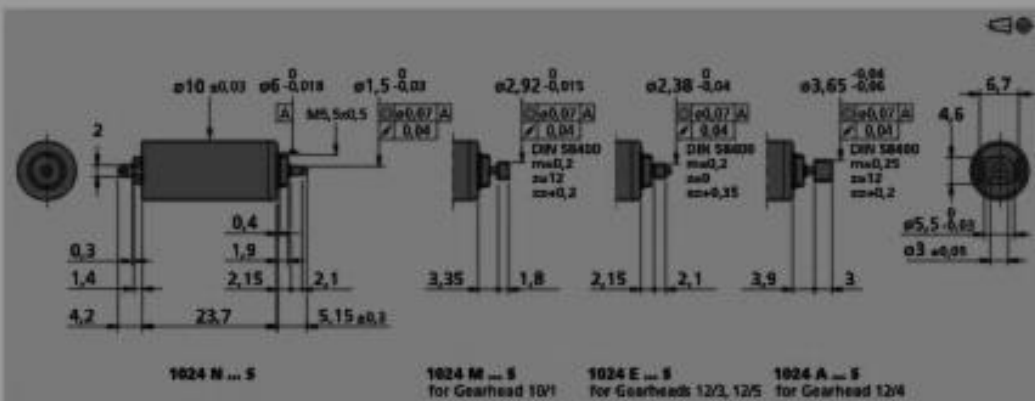
Precious Metal Commutation

1,28 mNm

For combination with
Gearheads:
10/1, 12/3, 12/4, 12/5
Encoders:
308, HEM3-256-W, PA2-100

Series 1024 ... S

	1024 N	1024 S	1024 E	1024 A	
1 Nominal voltage	U _N	3	6	12	V
2 Terminal resistance	R	2,3	10,8	31,6	Ω
3 Output power	P _{out}	0,97	0,81	1,11	W
4 Efficiency max.	η _{max}	79	78	79	%
5 No-load speed	n ₀	13 800	13 200	14 700	rpm
6 No-load current (with shaft ø 1 mm)	I ₀	0,016	0,008	0,004	A
7 Stall torque	M _s	2,69	2,34	2,89	mNm
8 Friction torque	M _f	0,03	0,03	0,03	mNm
9 Speed constant	k _n	4 658	2 231	1 240	rpm/V
10 Back-EMF constant	k _e	0,215	0,448	0,806	mV/rpm
11 Torque constant	k _t	2,05	4,28	7,7	mNm/A
12 Current constant	k _i	0,488	0,234	0,13	A/mNm
13 Slope of n-M curve	Δn/ΔM	5 135	5 630	5 090	rpm/mNm
14 Rotor inductance	L	26	100	340	μH
15 Mechanical time constant	T _m	6	7	6	ms
16 Rotor inertia	J	0,12	0,12	0,12	gcm ²
17 Angular acceleration	α _{max}	224	195	241	10 ³ rad/s ²
18 Thermal resistance	R _{th1} / R _{th2}	14 / 41			K/W
19 Thermal time constant	T _{th1} / T _{th2}	5 / 209			s
20 Operating temperature range:					
- motor		-30 ... +85 (optional version	-30 ... +125)		°C
- rotor, max. permissible		+85 (optional version	+125)		°C
21 Shaft bearings		sintered bearings			
22 Shaft load max.:					
- with shaft diameter		1			mm
- radial at 3 000 rpm (1,5 mm from bearing)		0,5			N
- axial at 3 000 rpm		0,1			N
- axial at standstill		20			N
23 Shaft play:					
- radial	c	0,03			mm
- axial	ε	0,2			mm
24 Housing material		steel, black coated			
25 Weight		8,8			g
26 Direction of rotation		clockwise, viewed from the front face			
Recommended values - mathematically independent of each other					
27 Speed up to	n _{max}	12 000	12 000	12 000	rpm
28 Torque up to	M _{max}	1,27	1,21	1,28	mNm



APPENDIX F

SYSTEM PERFORMANCE METRIC

The output of step response is to obtain value of the rise time (T_r), settling time (T_s) and percent overshoot (% O_s) as shown in Figure E-1. Where, Rise time (T_r) is the time required for waveform between the ranges 0.1 to 0.9 of the final value. The time required for transient's damped oscillations to reach and stay within $\pm 2\%$ of steady state value is called as settling time. Percent overshoot is totality the waveform overshoots the steady state and expressed as a percentage of the steady state value. The value of percent overshoots at peak time (T_p); T_p is the time required to reach the higher amplitude.

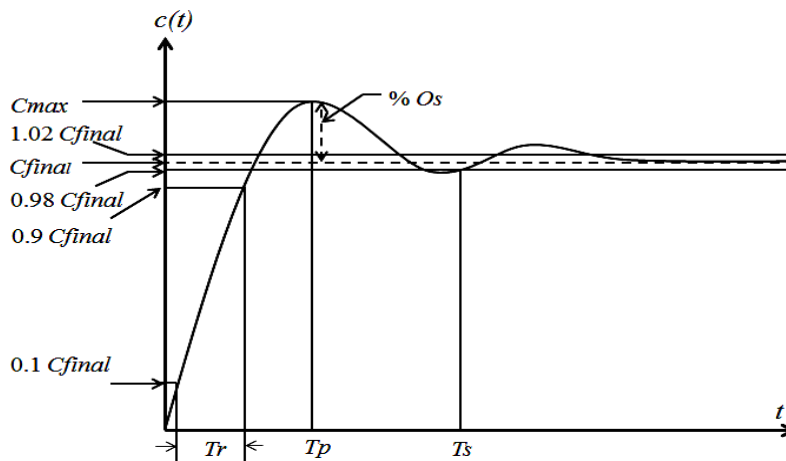


Figure E-1: Step Response of Simulation

APPENDIX G
ADDITIONAL RESULTS

E1. Comparison Of Pid From -20% To +20% Using Ziegler Nichols

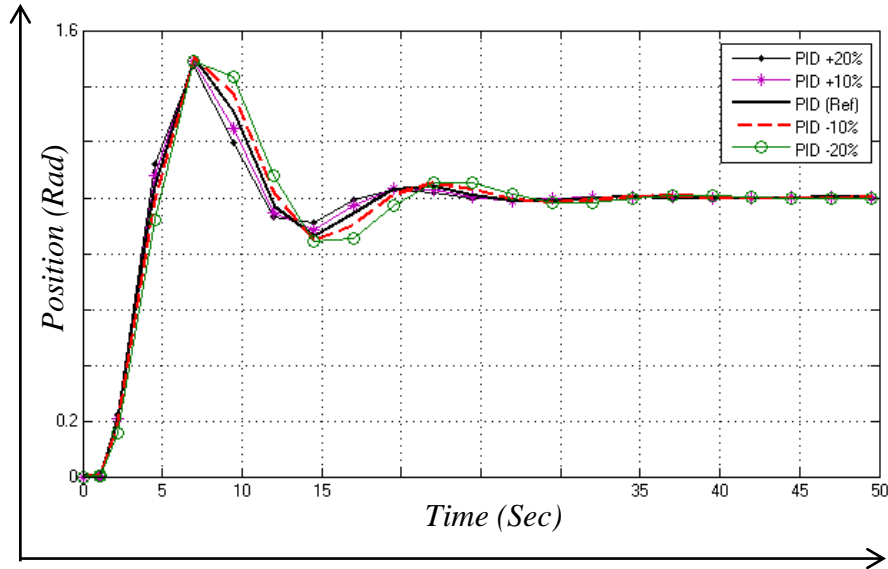


Figure E1: Pid Controller using Ziegler Nichols (from -20% to +20%)

Table E1: Result of PID (from -20% to +20%)

Controller (PID)	Rise Time (T_r)	Settling Time (T_s)	Cmax	Overshoot (%)	Error
-20 %	4.6	24.3	1.45	45	0.45
-10 %	4.4	24.0	1.45	45	0.45
Z-N (Ref)	4.2	23.8	1.45	45	0.45
+20 %	4.0	23.5	1.45	45	0.45
+10 %	3.8	23.2	1.45	45	0.45

Figure E1 shows the pid controller are compared from -20% to +20% using Ziegler Nichols as references. The results of +20% is better than others as shown in Table E1. Due is when the gain of PID are increase, the rise time (T_r), settling time a (T_s) nd Maximum amplitude (Cmax) are decrease. But the steady state error (Error) is still the same either the gains are increase or decrease.

E2. MFRH using Four Types of Memberships Function

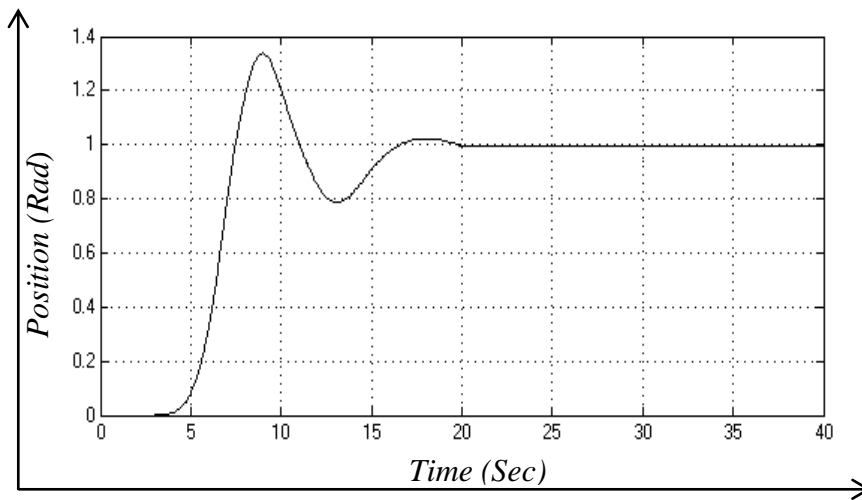


Figure E2: Two Memberships Function

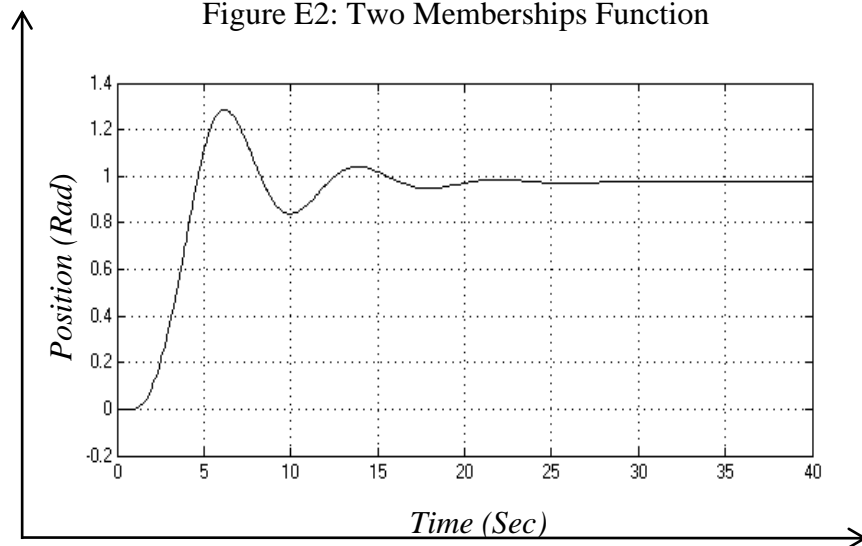


Figure E3: Three Memberships Function

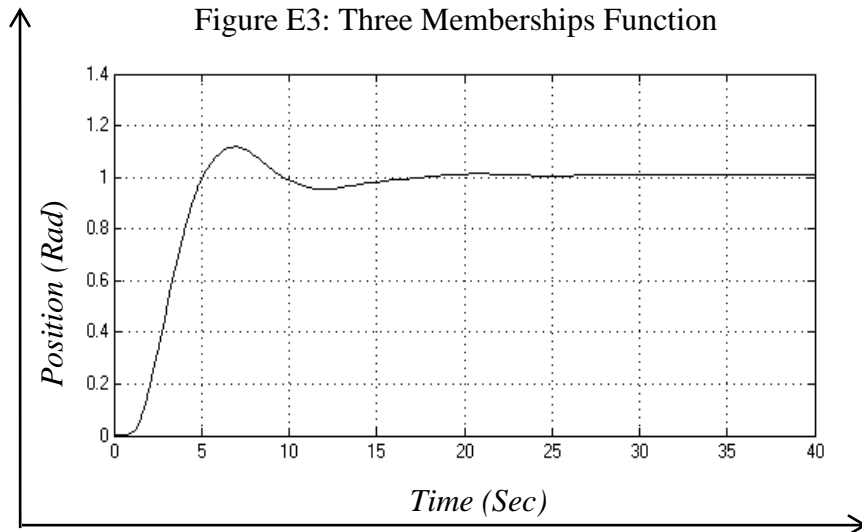


Figure E4: Five Memberships Function

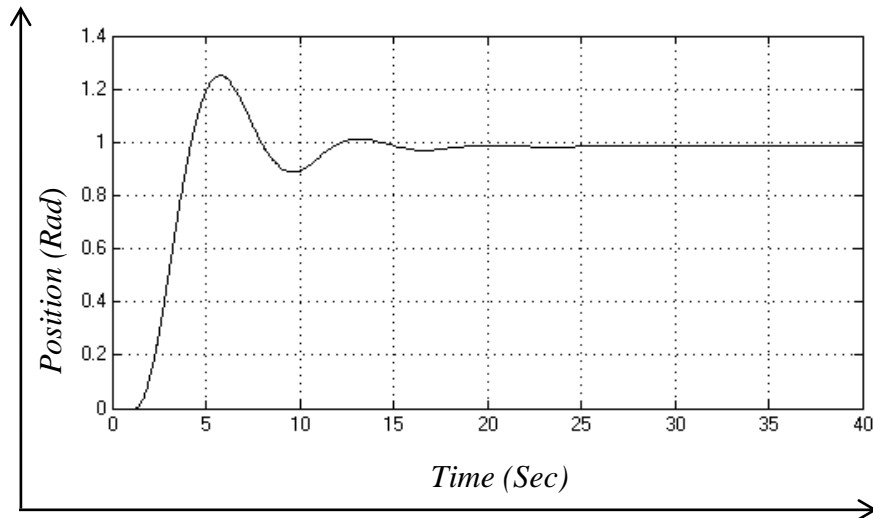


Figure E5: Seven Memberships Function

Regarding the Figure E2 –E5, Fuzzy controller using five memberships function are produce the better system response in term of rise time, settling time and small error.

Table E2: Results of Joint 1 using four types of memberships function

Controller (Fuzzy)	Rise Time (T_r)	Settling Time (T_s)	Cmax	Overshoot (%)	Error
Two memberships function	7.3	17.8	1.36	36	0.36
Three memberships function	4.82	14.4	1.28	28	0.28
Five memberships function	4.80	13.5	1.1	10	0.1
Seven memberships function	4.92	13.8	1.24	24	0.24

Where the result of five memberships function are $T_r = 4.80$, $T_s = 13.5$ and Error 0.1 as indicated in Table E2.

E3. PSO PID with Different Parameter

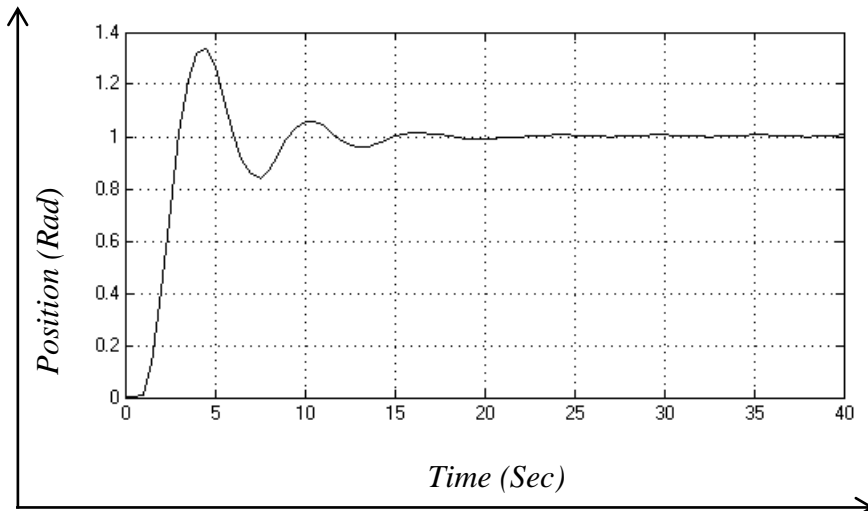


Figure E6: Parameter 1 of PSO PID

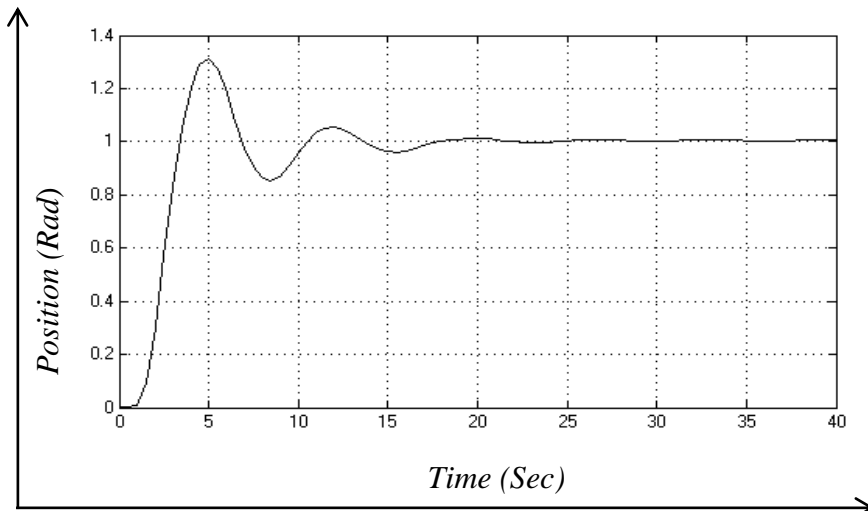


Figure E7: Parameter 2 of PSO PID

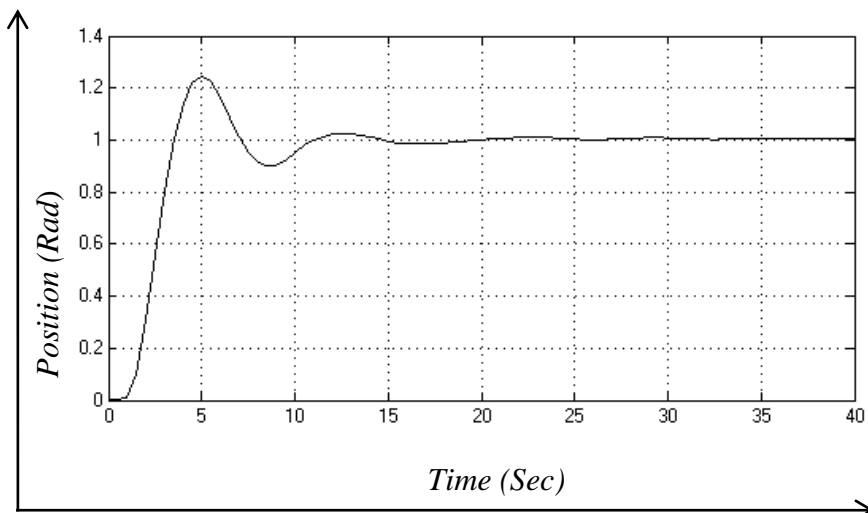


Figure E8: Parameter 3 of PSO PID

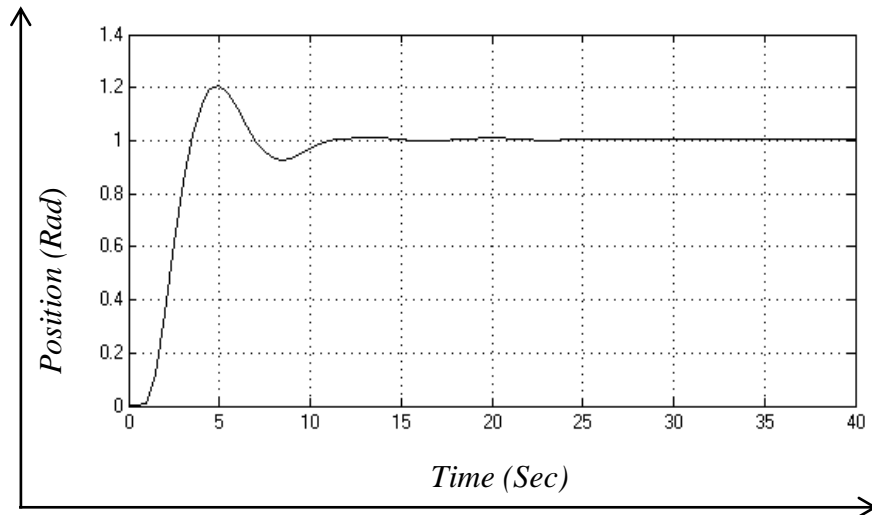


Figure E9: Parameter 4 of PSO PID

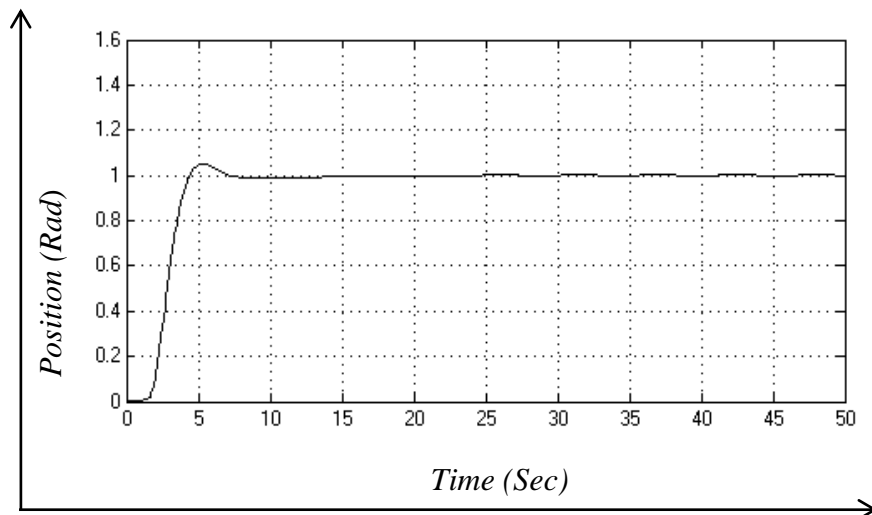


Figure E10: Parameter 5 of PSO PID

Figure E6-E10 show the step response of PSO PID using five parameters. The parameter 5 is the best parameter for particle swarm optimization (PSO) combining with PID because its can run more output response.

Table E3: Results of PSO PID

Controller (PSO PID)	Rise Time (T_r)	Settling Time (T_s)	Cmax	Overshoot (%)	Error
Parameter 1	4.85	14.8	1.36	36	0.36
Parameter 2	4.82	15.2	1.3	30	0.30
Parameter 3	4.80	12.5	1.24	24	0.24
Parameter 4	4.73	11.5	1.20	20	0.20
Parameter 5	4.70	9.6	1.07	3	0.30

. The best selection of parameter 5 like shown in Figure E10 and Table E3. Where the result of parameter 5 are $T_r=4.7$, $T_s=1.03$ and Error 0.3.

Overall, the results that are indicated in Figure E1-E10 for joint 1. Similar results were obtained joints 2 and 3.

GLOSSARY

Closed-loop system: A system that monitors its output and corrects for disturbances. It is characterized by feedback path from signal.

Controller: The subsystem that generates the input to the plant or process.

Error: The difference between the input and output of a system

Forward Kinematics: To determine the position and orientation of MFRH to determine the position and orientation of the robot hand relative to the robot base coordinate system.

Fuzzy Logic: A system developed for representing conditions that cannot be easily described by the binary term 'true' and 'false'. The concept was introduced by Lotfi Zadeh in 1965. Unlike Boolean logic, Fuzzy logic is multi-valued and handles the concept of partial truth (truth value between 'completely true' and 'complete false'). Also referred to as Fuzzy set theory.

Genetic Algorithm: A type of evolutionary computation inspired by Darwin's theory evolution. A genetic algorithm generates a population of possible solution encoded as chromosomes, evaluates their fitness, and creates a new population by applying genetic operations – crossover and mutation. By repeating this process over many generations. In genetic algorithm breeds an optimal solution to the problem.

Intelligent: The ability to learn and understand, to solve problems and to make decisions. A machine is thought intelligent if it can achieve human-level performance in some cognitive task.

Particle swarm optimization (PSO): A new variation of the algorithm used by researchers to find the optimum solution or approach optimal in a large search space.

Percentage Overshoot, %Os: The amount that the under damped step response to reach the first, maximum, peak.

PID Controller: A controller that feeds forward to the plant a proportion of the actuating signal plus its integral plus its derivative for the purpose of improving the transient response and steady-state error of closed loop system.

Plant or Process: The subsystem whose output is being controlled by the system.

Rise time, T_r : The time required for the step response to go from 0.1 of the final value to 0.9 of the final value.

Robot Hand: Described as that can mimic the movements of a human hand in operation.

Settling Time, T_s : The amount of time required for the step response to reach and stay within $\pm 2\%$ of the steady state value. Strictly speaking, this is definition of the 2% settling time.

Slip: The measurement and detection of the movement of an object relative to the sensor.

Stability: That characteristic of system defined by a natural response that decays to zero as time approaches infinity.

Tactile Sensing: The detection and measurement of the spatial distribution of forces perpendicular to a predetermined sensory area, and the subsequent interpretation of the spatial information.

Touch Sensing: The detection and measurement of a contact force at a defined point.